

# Covalent triazine frameworks as a hive for rhodium complexes

*A reusable catalyst for transfer hydrogenation*

Cato Vanleysen

Student number: 01808957

Promotor: Prof. dr. ir. Chris Stevens

Tutor: Ir. Jonas Everaert

Master's Dissertation submitted to Ghent University in partial fulfilment of the requirements for the degree of  
Master of Science in Bioscience Engineering: Chemistry and Bioprocess Technology

Academic year: 2019 – 2020







### Copyright declaration

The author and the promotor give permission to use this Master's dissertation for consultation and to copy parts of it for personal use. Every other use is subject to the copyright laws, more specifically the source must be extensively specified when using results from this thesis.

### Melding van auteursrecht

De auteur en de promotor geven de toelating deze Master thesis voor consultatie beschikbaar te stellen en delen ervan te kopiëren voor persoonlijk gebruik. Elk ander gebruik valt onder de beperkingen van het auteursrecht, in het bijzonder met betrekking tot de verplichting de bron te vermelden bij het aanhalen van resultaten uit deze scriptie.

Ghent, august 2020

The promotor,  
Prof. dr. ir. C. Stevens

The tutor,  
Ir. J. Everaert

The author,  
C. Vanleysen



# Acknowledgments

---

Two years ago, I arrived at Campus Coupure, in the beautiful city of Ghent. I was allowed to discover a new environment, new professors and new friends. The last year was the famous thesis year. I had to work hard but it was all worth the effort. Not only did I explore the world of CTFs and the organic chemistry behind, also patience and responsibility were one of the few things that I have learned. During this journey many people have helped and supported me, and I would like to thank some of them in particular.

I would like to start by thanking professor Stevens, my promoter, for guiding me through this thesis and for correcting my final work. During the monthly COF meetings, you carefully listened to my work and gave me critical remarks and insights. Thank you for your commitment, not only to me, but to the whole SynBioC Research Group.

Next, I am very grateful to Jonas, my tutor, who has always been there for me and helped me to the end. Although in the beginning, I might have been clumsy sometimes, you kept your patience and made sure that I did a good job. And even if you were very busy, you took the time to answer my enormous list of questions. You truly have the gift of explaining chemistry in a clear and understandable way! I couldn't thank you enough for passing on your knowledge, for the many corrections on my writing and for the valuable feedback and interesting ideas.

Furthermore, I would like to thank 'het COFschip' (Jonas, Flore, Maarten and Dalia) and Melike for the warm welcome, for the encouragements and the nice talks. Also, thank you to the rest of the SynBioC Research Group for creating such a pleasant work environment and for all the help. On top of that, thank you to all the thesis students for the relaxing coffee breaks and lunches, the good vibes and laughs.

Finally, I would like to express my gratitude to my mother, Bobby and my sisters for offering a listening ear, for tolerating me during the exams and for all your care and love.

Cato Vanleysen, August 2020





# Preamble

---

*This preamble was drawn up in consultation between the author and the promoter and was approved by both.*

Laboratory activities, including experimental research and analyses, were intended to continue until May 2020. However, they had to be terminated as of March 19<sup>th</sup> 2020 due to SARS-CoV-2 measures in order to avoid further spreading of the virus. As a consequence, some of the planned activities could not be accomplished:

- Optimization of the following building block synthesis:
  - Direct synthesis of 2,2'-biquinoline-6,6'-dicarbonitrile from 6-cyanoquinoline-*N*-oxide.
  - Synthesis of quinoline-2,6-dicarbonitrile.
- CTF characterization, including several nitrogen sorption analyses, elemental analyses, PXRD and XRF.
- Reactions in the context of the catalytic transfer hydrogenation:
  - Reaction optimization of the Rh@bipyCTF catalyzed transfer hydrogenation, including pH, temperature, solution concentration and catalyst loading.
  - Assessment of the recyclability and the heterogeneity of the Rh@bipyCTF catalyst.
  - The follow-up of the homogeneous reaction to compare with the heterogeneous variant.
  - Rh@bipyCTF catalyzed transfer hydrogenation of 3-methylquinoxalin-2(1*H*)-one to make a comparison with the bpyPMO catalyst reported in the literature.
  - Implementation of the Rh@bipyCTF in a continuous flow reactor to perform the transfer hydrogenation reaction in flow.

As experiments are fundamental to this Master's thesis, the intention was to resume laboratory activities during July and August 2020. Nevertheless, the university policy did not approve even after explicit questioning the dean's office and the university safety department. Therefore, the experimental findings and data already obtained were used to draw up this thesis and an additional chapter on future works and perspectives (chapter 4) was appended.



# Abstract

---

Chemistry has an essential role in the improvement of the human life standard through the development of pharmaceuticals, fertilizers and detergents, to mention just a few. However, pollution represents a major downside of chemistry and today's climate crisis urges the industry to develop more sustainable products and processes. To this end, the 12 principles of Green Chemistry were established as a guideline. The ninth principle concerns the preferential use of catalysts over stoichiometric reagents. Heterogeneous catalysts are here of particular importance, as they can be reused in the process. To date, zeolites, a type of porous inorganic catalyst, dominate the chemical industry. However, these materials have reached maturity and more tunable alternatives are searched for. Highly promising substitutes are covalent triazine frameworks (CTFs), tunable porous organic materials with remarkable thermal and chemical stability. The aim of this Master's thesis was to develop new catalytic CTFs and demonstrate their use in the catalytic transfer hydrogenation of N-heterocycles, a widely employed reaction enabling the efficient synthesis of a large number of chemicals. To achieve this goal, the thesis was organized in three parts: (1) synthesis of nitrogen-containing aromatic building blocks, (2) CTF development and catalyst immobilization, and (3) the transfer hydrogenation of N-heterocycles.

During the first part, three building blocks were synthesized, i.e. 2'-bipyridine-5,5'-dicyanitrile, 2,2'-biquinoline-6,6'-dicyanitrile and quinoline-2,6-dicyanitrile. In the second part, the bipyridine and quinoline building block were used in the preparation of CTFs via the ionothermal synthesis method employing  $\text{ZnCl}_2$  at elevated temperature (400 °C and above). The structure of the materials was investigated using several analytical methods such as nitrogen sorption analysis, PXRD, FTIR and elemental analysis. As a result, two amorphous black materials were obtained, on one hand, bipyCTF with a specific surface area of 654  $\text{m}^2/\text{g}$  and a total pore volume of 0.25  $\text{cm}^3/\text{g}$ , and on the other hand, quinCTF with a specific surface area of 1087  $\text{m}^2/\text{g}$  and a total pore volume of 0.49  $\text{cm}^3/\text{g}$ . To acquire CTFs with enhanced porosity, the salt templated CTF synthesis method was explored, using NaCl or KCl in addition to  $\text{ZnCl}_2$ . The largest increases in specific surface area and in total pore volume were obtained by using NaCl, reaching respectively 790  $\text{m}^2/\text{g}$  and 0.31  $\text{cm}^3/\text{g}$ . However, the effect of the alkali

salts on the porosity was concluded to be insignificant, as these increases were minor compared to literature values of conventional prepared bipyCTF.

Next, the bipyCTF was decorated with a rhodium complex, yielding the Rh@bipyCTF catalyst with a metal load of 22.9 g Rh/kg (0.22 mmol Rh/g). In the last part, Rh@bipyCTF was found to be highly active in the transfer hydrogenation of 2-methylquinoxaline with HCOONa/HCOOH as hydrogen donor. The heterogeneous catalyst proved to be air stable and 0.25 mol% of rhodium was sufficient to yield complete conversion within circa two hours.

Though the recyclability of the CTF-based catalyst has not been demonstrated yet, this work shows that covalent triazine frameworks are promising materials in the development of heterogeneous catalysts and may contribute to the optimization of chemical processes in line with the Principles of Green Chemistry.

# Abstract

---

Chemie heeft een cruciale rol in het verbeteren van onze levensstandaard door het ontwikkelen van bijvoorbeeld farmaceutische producten, meststoffen en detergents. Echter, de chemische industrie kampt met een behoorlijk groot probleem, namelijk vervuiling. Om de klimaat crisis tegen te gaan, moet de industrie meer duurzame producten en processen ontwikkelen. In dit kader werden 12 richtlijnen opgesteld die bekend staan als de 12 principes van de Groene Chemie. Het negende principe benadrukt het preferentiële gebruik van katalysatoren boven stoichiometrische reagentia. Hierbij zijn heterogene katalysatoren uitermate belangrijk aangezien deze hergebruikt kunnen worden. Op de dag van vandaag, worden voornamelijk zeolieten, een soort poreuze anorganische katalysator, gehanteerd in de chemische industrie. Desondanks, zijn deze materialen gelimiteerd in diversiteit en wordt er gezocht naar meer flexibele, op maat gemaakte alternatieven. Een aantrekkelijk alternatief zijn de zogenaamde *covalent triazine frameworks* (CTFs), afstembare poreuze organische materialen met uitstekende thermische en chemische stabiliteit. Het doel van deze Master thesis was het ontwikkelen van nieuwe katalytische CTFs en het aantonen van hun gebruik in de katalytische transfer hydrogenatie van N-heterocyclus. Deze reactie laat immers de efficiënte synthese van een groot aantal chemicaliën toe. Om naar het doel toe te werken, werd de thesis onderverdeeld in drie delen: (1) synthese van stikstof bevattende aromatische bouwstenen, (2) CTF-ontwikkeling en immobilisatie van de katalysator, en (3) de transfer hydrogenatie van N-heterocyclus.

Tijdens het eerste deel werden er drie bouwstenen gesynthetiseerd, namelijk 2,2'-bipyridine-5,5'-dicarbonitril, 2,2'-bichinoline-6,6'-dicarbonitril en chinoline-2,6-dicarbonitril. Tijdens het tweede deel, werden de bipyridine en chinoline bouwstenen gebruikt voor het maken van CTFs via de ionothermale synthese methode met  $\text{ZnCl}_2$  op hoge temperatuur (400 °C en hoger). De structuur van de bekomen CTFs werd onderzocht met behulp van verschillende analysemethoden zoals stikstofsorptie analyse, PXRD, FTIR en elementanalyse. Er werden twee amorfe zwarte materialen bekomen. Enerzijds werd bipyCTF met een specifiek oppervlak van 654  $\text{m}^2/\text{g}$  en totaal porievolume van 0.25  $\text{cm}^3/\text{g}$  verkregen, en anderzijds quinCTF met een specifiek oppervlak van 1087  $\text{m}^2/\text{g}$  en totaal porievolume van 0.49  $\text{cm}^3/\text{g}$ . Om de porositeit van de CTFs te verhogen, werd een alternatieve synthese methode

gehanteerd, de zout templaat methode, waarbij naast  $\text{ZnCl}_2$  ook NaCl of KCl wordt toegevoegd. Het gebruik van NaCl resulteerde in de grootste toename van specifiek oppervlak en totaal porievolume met respectievelijk  $790 \text{ m}^2/\text{g}$  en  $0.31 \text{ cm}^3/\text{g}$ . Er werd echter geconcludeerd dat het effect van de alkali zouten op de porositeit niet significant was, omdat de toename slechts gering was in vergelijking met de waarden in de literatuur voor de conventioneel gesynthetiseerde bipyCTF.

Hierna werd een rhodium complex geïmmobiliseerd op de bipyCTF wat resulteerde in een Rh@bipyCTF katalysator met een metaal lading van  $22.9 \text{ g Rh/kg}$  ( $0.22 \text{ mmol Rh/g}$ ). In het laatste deel, vertoonde Rh@bipyCTF een hoge activiteit in de transfer hydrogenatie van 2-methylchinoxaline met HCOONa/HCOOH as waterstof donor. De heterogene katalysator bleek luchtstabil te zijn en  $0.25 \text{ mol\%}$  rhodium was voldoende om binnen circa twee uur een volledige omzetting te geven.

Hoewel de recycleerbaarheid van de CTF-gebaseerde katalysator nog niet bewezen werd, toont dit werk dat *covalent triazine frameworks* veelbelovende materialen zijn voor het ontwikkelen van heterogene katalysatoren en kunnen bijdragen tot de optimalisatie van chemische processen in overeenstemming met de principes van de Groene Chemie.

# Table of contents

---

<b>1</b>	<b>Scope and goal</b> .....	<b>1</b>
1.1	Scope .....	1
1.2	Goal .....	5
<b>2</b>	<b>Literature review</b> .....	<b>7</b>
2.1	Introduction to Covalent Organic Frameworks.....	7
2.1.1	Diversity in COF design .....	8
2.1.2	Synthetic strategies for CTFs.....	12
2.1.2.1	Cyclotrimerization strategy.....	12
2.1.2.2	Polycondensation strategy.....	14
2.1.2.3	Cross-coupling strategy.....	16
2.1.3	CTFs as heterogeneous catalysts .....	17
2.2	Catalytic transfer hydrogenation .....	19
2.2.1	Typical H-donors for catalytic transfer hydrogenation.....	20
2.2.1.1	Isopropanol .....	20
2.2.1.2	Formic acid .....	20
2.2.2	Mechanism behind transition metal catalyzed transfer hydrogenation.....	21
2.2.2.1	Dihydric route .....	21
2.2.2.2	Monohydric route .....	22
2.2.3	Catalytic transfer hydrogenation of N-heterocycles .....	23
2.2.3.1	Homogeneous catalytic transfer hydrogenation in aqueous HCOONa.....	24
2.2.3.2	Heterogeneous catalytic transfer hydrogenation in aqueous HCOONa.....	25
<b>3</b>	<b>Results and discussion</b> .....	<b>28</b>
3.1	Synthesis of nitrogen-containing aromatic building blocks .....	29
3.1.1	Synthesis of 2,2'-bipyridine-5,5'-dicyanitrile <b>1</b> .....	29
3.1.2	Synthesis of 2,2'-biquinoline-6,6'-dicyanitrile <b>2</b> .....	31
3.1.3	Synthesis of quinoline-2,6-dicyanitrile <b>3</b> .....	37
3.2	CTF synthesis and post-synthetic metalation .....	39
3.2.1	Synthesis of the 2,2'-bipyridine-5,5'-dicyanitrile-based CTF <b>13</b> .....	39
3.2.2	Synthesis of the quinoline-2,6-dicyanitrile-based CTF <b>14</b> .....	44
3.2.3	Post-synthetic metalation of the 2,2'-bipyridine-5,5'-dicyanitrile-based CTF.....	47
3.3	Catalytic transfer hydrogenation of N-heterocycles .....	49

<b>4</b>	<b>Future work and perspectives</b> .....	<b>52</b>
4.1	Synthesis of nitrogen-containing aromatic building blocks .....	52
4.2	CTF synthesis and post-synthetic metalation.....	54
4.3	Catalytic transfer hydrogenation of N-heterocycles .....	55
<b>5</b>	<b>Conclusion</b> .....	<b>57</b>
<b>6</b>	<b>Materials and methods</b> .....	<b>61</b>
6.1	General analytical methods and laboratory equipment .....	61
6.2	Safety aspects .....	63
6.3	Synthesis procedures and characterization data .....	65
6.3.1	Synthesis of nitrogen-containing aromatic linkers .....	65
6.3.2	Synthesis of CTFs and post-synthetic metalation .....	70
6.3.3	Catalytic transfer hydrogenation of N-heterocycles.....	71
<b>7</b>	<b>Appendix</b> .....	<b>73</b>
<b>8</b>	<b>References</b> .....	<b>78</b>



# List of abbreviations

---

AIBN	azobisisobutyronitrile
BET	Brunauer–Emmett–Teller
C	BET constant
COF	covalent organic framework
Cp*	cyclopentadienyl
CTF	covalent triazine framework
DCC	dynamic covalent chemistry
DCM	dichloromethane
DMSO	dimethyl sulfoxide
$E_a$	activation energy
EPA	Environmental Protection Agency
eq	equivalent
MOF	metal organic framework
MPV	Meerwein-Ponndorf-Verley
MW	microwave
P	saturation pressure
$P_0$	equilibrium pressure
$pa_1$	cross section of an adsorbed gas molecule
R	gas constant
rt	room temperature
$S_{BET}$	BET specific surface area
STP	standard temperature and pressure
T	temperature
TH	transfer hydrogenation
THF	tetrahydrofuran
$V_{m,STP}$	volume of a gas needed to form a monolayer under STP conditions
$V_{p,tot}$	total pore volume
$V_{STP}$	volume of a gas adsorbed under STP conditions
$\Delta$	reflux temperature



# 1 Scope and goal

## 1.1 Scope

In 1991, the term *Green Chemistry* was coined by the Environmental Protection Agency (EPA), supporting the bigger picture of a more sustainable society. Green Chemistry aims to minimize the use and formation of waste and hazardous substances throughout the lifecycle of chemical products and processes.<sup>1,2</sup> In 1998, Paul Anastas and John Warner established 12 principles representing the most important guidelines in the design of environmentally benign chemicals and processes (Figure 1).<sup>3</sup> Among other projects, the SynBioC research group contributes to these green chemistry principles through the development of renewable based products and catalysts. The latter, representing the ninth principle, are preferably used over stoichiometric reagents.<sup>3</sup> Catalysts are used for the production of more or less 90% of the industrial chemicals including polymers, commodity, specialty and fine chemicals, petrochemicals and pharmaceuticals.<sup>4-6</sup> To understand its importance, one needs to take a closer look at the concept of catalysis.



**Figure 1. The 12 principles of Green Chemistry. The use of catalysts is encouraged by the 9<sup>th</sup> principle.**

Catalysis is a cyclic process in which a substance, the catalyst, increases the rate of a thermodynamically feasible reaction after which it returns to its original state.<sup>7</sup> Hence, the catalyst is not consumed during the reaction but reused in a next cycle, therefore the catalyst is only required in small quantities. The potential energy diagram of an uncatalyzed and a catalyzed reaction can help to visualize this phenomenon (Figure 2). During the catalytic cycle, reagent X first binds to the catalyst. Subsequently, the X-catalyst complex reacts with Y and forms the product Z which dissociates from the catalyst. In this way, the catalyzed reaction provides an alternative, more complex pathway, but with a lower overall activation energy ( $E_a$ ).<sup>8</sup>

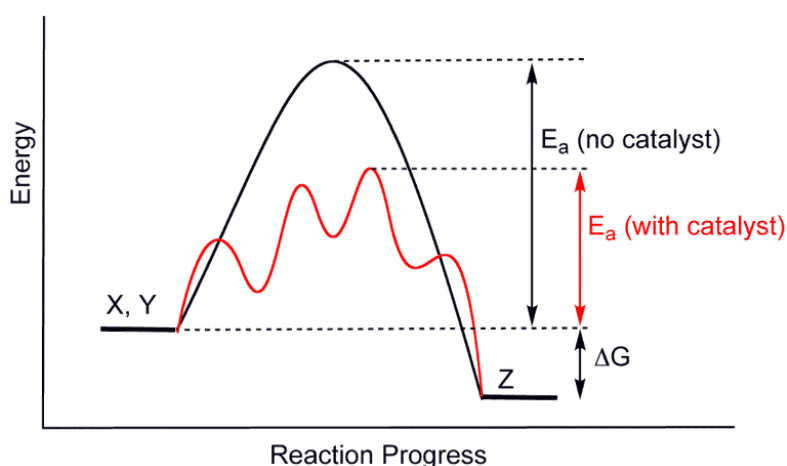


**Figure 2. Potential energy diagram of a catalyzed and uncatalyzed reaction.**

In general, the environmental and economic importance of catalysis can be explained by two properties: activity and selectivity. Activity is determined by the reaction rate. The higher the activity of the catalyst, the higher the reaction rate. As a result, highly active catalysts are only needed in small amounts. Higher activities also lead to higher productivities, smaller reactor volumes and milder reactions conditions.<sup>8</sup> Therefore, catalysts contribute to higher energy efficiencies, representing the sixth principle of Green Chemistry, and lower investment costs.<sup>3</sup> Selectivity is the extent to which reagents are converted into the desired product without the formation of undesired products.<sup>8</sup> Thus, a highly selective catalyst can reduce the production of waste and the use of derivatives, representing respectively the first and the eighth principle of Green Chemistry.<sup>3</sup> Again, this results in lower investment costs since, for example, no additional separation processes are required.

Catalysis can be divided into three domains: heterogeneous, homogeneous and enzymatic catalysis or biocatalysis. Among other differences, they occur in distinct phases. Enzymes can be dissolved (homogeneous) as well as immobilized (heterogeneous). Homogeneous catalysts are soluble in the reaction phase. In contrast to heterogeneous catalysis, homogeneous catalytic systems are often better understood regarding the active site and reaction mechanism. This is because organometallic molecules are well-defined species and hence more straightforward to be studied. They usually provide higher activity and selectivity than heterogeneous catalysts, as these parameters can be easily tuned via ligand modification. However, the major disadvantage of homogeneous catalysts is the rather complicated separation from the reaction medium, generating additional waste.<sup>7</sup> Also, homogeneous catalysts do not lend themselves easily for continuous operations.

Heterogeneous catalysts, usually solids, are in a phase different from the reactants and/or products. As a result, they can be easily isolated (e.g. via filtration) and recycled.<sup>8</sup> In heterogeneous catalysis, reaction of the substrate molecules only occurs on the surface of the solid catalyst. In order to increase the catalytic activity, the goal is to maximize the catalyst surface by means of small catalyst particles. The ultimate frontier in particle size is a single atom. Unfortunately, single metal atoms are unstable and have the tendency to aggregate into clusters or nanoparticles reducing the surface area.<sup>9</sup> Anchoring metal atom or metal complexes on a support material is therefore an attractive strategy to stabilize the metal atoms. In that case, single-site heterogeneous catalysts (SSHC), single-atom catalysts (SAHC) or surface organometallic catalyst (SOMC) are generated.<sup>10-12</sup>

A support material has three main requirements. Firstly, thermal, chemical and mechanical stability is needed. Secondly, the support material should have interaction sites at which metal particles can attach. Finally, high surface area and open porosity are required for the access of reagents at the catalytically active sites.<sup>8</sup> It should be pointed out that in order to have well-defined and uniform catalytic active sites, the support material should have well-defined and uniform coordination sites as well. Therefore, development of methodologies for precise synthesis of support materials with high accuracy at molecular level is desired.

A popular family of microporous support materials are zeolites, with pore diameter up to 1 nm.<sup>13</sup> In general, they comprise an open crystalline 3D network of inorganic SiO<sub>4</sub> and AlO<sub>4</sub> tetrahedra, called aluminosilicates (Figure 3).<sup>14</sup> Zeolites can be applied as solid acid catalysts

which are widely employed in petrochemical processes, such as fluid catalytic cracking.<sup>7</sup> However, as zeolites are deprived of a high degree of functionality-tuning and have limited pore sizes, their use as heterogeneous catalysts has reached maturity. To this end, other porous materials such as metal organic frameworks (MOFs) and covalent organic frameworks (COFs) have been developed (Figure 3). MOFs are 2D or 3D structured networks formed by polyatomic inorganic metal-containing clusters linked to rigid organic molecules.<sup>15-17</sup> COFs arise from linking rigid organic building blocks by strong covalent bonds.<sup>18-20</sup> Both types of organic frameworks profit from flexibility in geometry, size and functionality design of the building blocks while maintaining a high surface area and pore volume. However, COFs display substantial higher thermal and chemical stability due to covalent instead of coordination bonding. Thereby, they are attractive to be used in a variety of applications such as gas adsorption and storage, electrochemical energy storage and heterogeneous catalysis for example.<sup>21</sup>

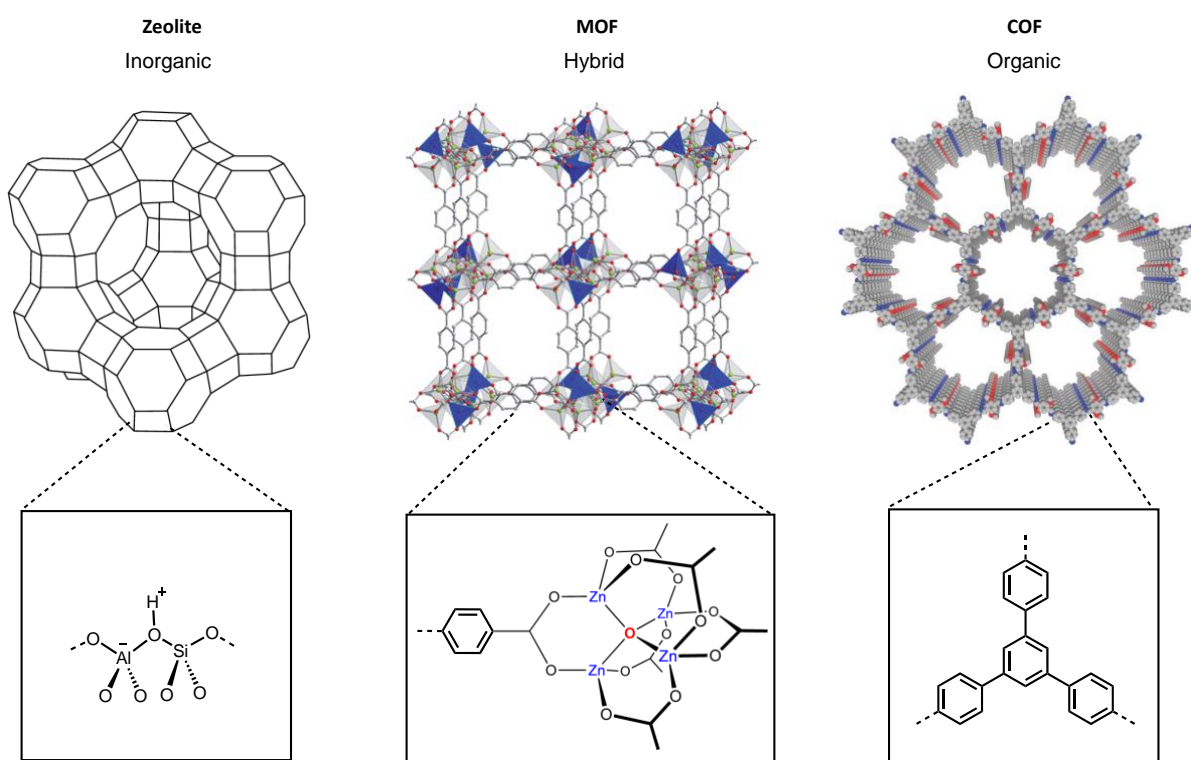


**Figure 3. Examples of porous support materials: zeolite, MOF and COF.**

In 2008, Antonietti and co-workers pioneered a new class of COFs: the covalent triazine frameworks (CTFs). Here, building blocks are connected through triazine moieties formed by the cyclotrimerization of cyano-groups. CTFs exhibit high specific surface areas and porosities, but most interestingly, they outperform many other organic frameworks by their remarkable high chemical and thermal stability.<sup>22,23</sup> Moreover, the strong electron donating property of the nitrogen-containing triazine moieties gives rise to a coordination site for metals.<sup>24</sup> For these reasons, they represent excellent candidates for heterogeneous catalysis.<sup>25</sup>

## 1.2 Goal

The main goals of this Master thesis are (1) to develop new CTFs, and (2) to use these CTFs as support material for the heterogenization of transition metal catalysts applicable in chemical reactions. The heterogenization of the catalyst facilitates the separation and enables its reuse or use in continuous flow reactions. For the first goal synthetic methodologies will be developed for the synthesis of nitrogen-containing building blocks such as 2,2'-bipyridine-5,5'-dicarbonitrile **1**, 2,2'-biquinoline-6,6'-dicarbonitrile **2** and quinoline-2,6-dicarbonitrile **3** (Figure 4).

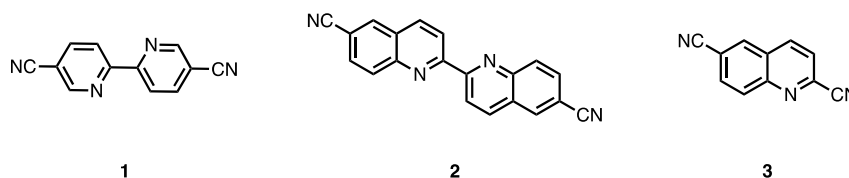


**Figure 4. Nitrogen-containing building blocks for CTF synthesis.**

The use of these building blocks in CTF synthesis will result in new CTFs with distinct pore sizes, surface areas and properties (Figure 5). In a first approach to synthesize the CTFs, the conventional ionothermal method will be applied. Since porosity is the result of interparticle space as well as induced by templated synthesis, the latter method will also be taken into account.

The linkers that constitute the framework can serve as bidentate ligands to coordinate transition metal complexes and give rise to stable anchored heterogenized catalysts. To

establish the second goal, the framework will be decorated with a rhodium(III) complex (Figure 5) and further applied as a heterogeneous catalyst in the transfer hydrogenation reaction of N-heterocycles. The catalyst will be first evaluated in batch reactions, after which integration of the solid catalyst into a continuous flow reactor will be considered.

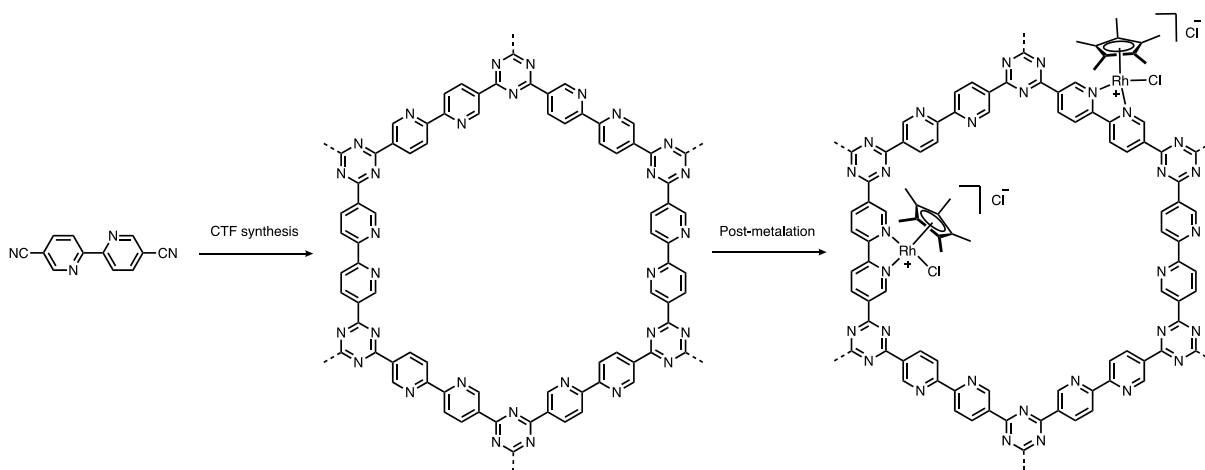


**Figure 5. CTF synthesis and post-metalation with a rhodium(III) complex.**



## 2 Literature review

---

COFs, and CTFs in particular, represent a new and promising platform for the development of heterogeneous catalysts. In the first part of this chapter, these materials will be further introduced, and an overview will be given of the chemical reactions accelerated by CTF-based catalysts. In the second part, the transfer hydrogenation of N-heterocycles, the reaction central to this Master thesis will be discussed in more detail.

### 2.1 Introduction to Covalent Organic Frameworks

Porous inorganic materials such as zeolites have a long history as adsorbents and catalysts in our chemical industries. In the quest for more tailorable materials, the field of porous materials became revolutionized at the end of the 20th century by the introduction of *reticular chemistry*. In this type of chemistry, molecular building blocks are linked together by strong bonds to yield ordered extended structures and is therefore considered as chemistry beyond the molecule.<sup>16</sup> This concept has led to the rapidly expanding development of two classes of extended structures: metal organic frameworks (MOFs) and covalent organic frameworks (COFs). Covalent organic frameworks or COFs are porous ordered extended solids in which organic molecules are stitched together into 2D or 3D networks. In contrast to MOFs, which are hybrid materials constructed from metal ions and organic buildings blocks hold together by weaker coordination bonds, the building blocks of COFs are entirely composed of light elements such as H, C, B, O, N (and Si), and are linked through strong covalent bonds. Therefore, COF materials are characterized as light weighted, yet strong materials displaying high thermal and chemical stability.<sup>17,19,20</sup> Owing to these favorable properties, COFs can be used in a broad range of applications. For instance, they have been applied in gas separation and storage (CO<sub>2</sub>, H<sub>2</sub>, NH<sub>3</sub> and CH<sub>4</sub>)<sup>26,27</sup>, energy storage<sup>28</sup>, catalysis<sup>29</sup>, chemical sensing<sup>30</sup> and temperature sensing<sup>31</sup>.

The concept of reticular chemistry allows for the synthesis of porous extended structures in a targeted manner and has led to the development of more than 100 COFs. According to Yaghi

and Diercks, the reticulation process is a top-down approach and can be divided into 5 steps.<sup>19</sup> Figure 6 provides an example of a reticulation process for a particular COF, namely CTF-1.

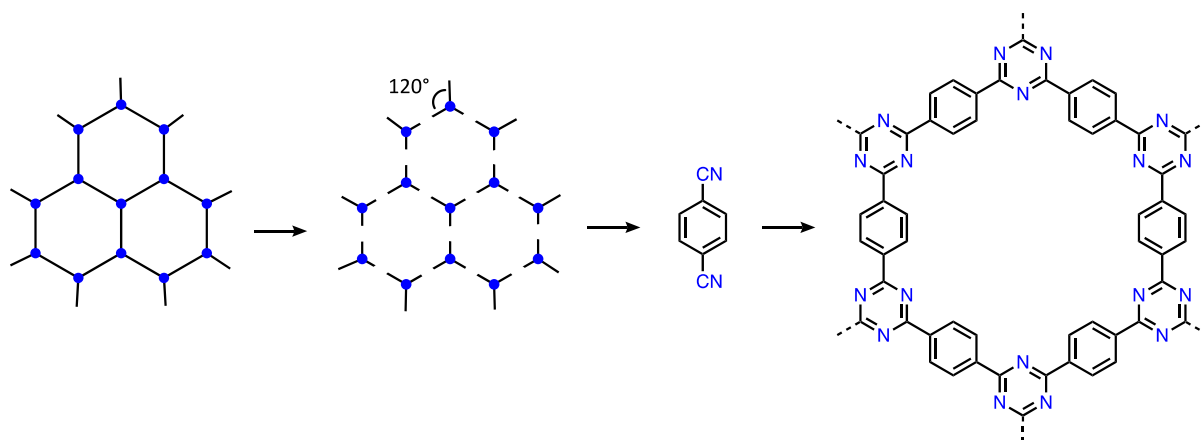


**Figure 6. Reticulation process for CTF-1.**

Firstly, a target framework topology is selected e.g. a 3-connected topology with hexagonal shaped pores. Secondly, the framework topology is deconstructed into its underlying geometric units. In the example, the angle between the geometric units is equal to  $120^\circ$ . Thirdly, molecular equivalents of the geometric units are searched for. Note that multiple building blocks (or linkers) with the same geometry can be used to form a framework with a specific topology. For instance,  $120^\circ$  angles are found in triazine linkages which can be formed by cyclotrimerization of 1,4-dicyanobenzene building blocks. Fourthly, bonds between the building blocks (or linkages) are created for the crystallization of the COF material. For linkage formation, the choice of reaction conditions is important in order to create reversibility.<sup>18,32</sup> Finally, the structure of the expected framework is confirmed by characterization.

### 2.1.1 Diversity in COF design

The orientation of the linkages is highly directed by the linkage-groups of the building blocks. So, the directionality of the covalent bonds allows us to predict how a building block is incorporated in the framework. Therefore, the building blocks can be designed, according to the envisaged application.<sup>33,34</sup> Depending on the size and constitution of the building blocks, frameworks with different pore sizes and shapes are obtained (Figure 7).<sup>18,35–37</sup> Also, a

different chemical environment within the pores is achieved through variation of the monomer. Hence, remarkable diversity and flexibility can be achieved in the design of COFs.

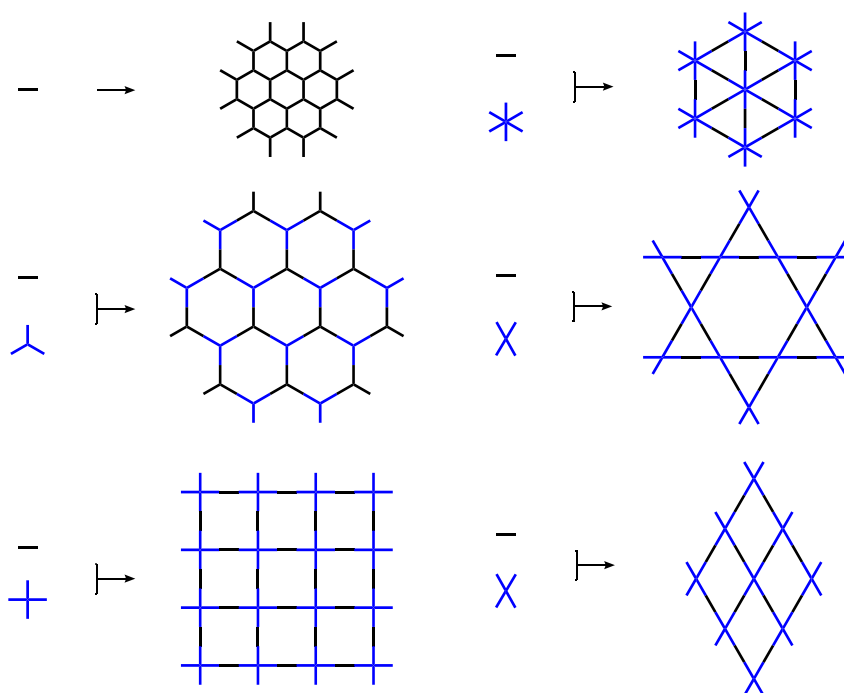


**Figure 7. Different building block combinations resulting in COF structures with diverse pore sizes and shapes.**

However, the crystallization of organic extended materials, which are generally insoluble, is challenging. Linking of molecular building blocks by strong covalent bonds often yields amorphous or poorly ordered materials. Organic chemists were able to overcome this crystallization problem through the principles of dynamic covalent chemistry (DCC).<sup>34,38</sup> In order to obtain an ordered extended solid, the formation of linkages should be reversible. In this way, structural defects can be repaired through back reaction and bond reformation.<sup>39</sup>

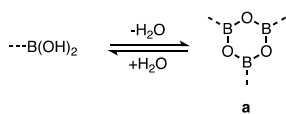
Over the past decades, several reversible bond formation reactions have been used for the synthesis of COFs.<sup>40</sup> An overview is given in Figure 8. The reactions are classified based on the type of linkage between the building blocks.<sup>41</sup> The synthetic difficulty in achieving crystalline organic frameworks initially led to the reliance on the highly reversible self-condensation reaction of boronic acid into boroxine **a** (or boronate anhydride) which was used for the synthesis of the first COF, COF-1, made by Yaghi and co-workers in 2005.<sup>18</sup> Here, the trade-off

between the degree of crystallinity and the chemical stability of the resulting material was in favor of the former, thus limiting its applications. Later, numerous other types of linkage chemistries have been introduced, often relying on condensation reactions and providing stronger materials.

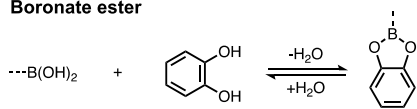
Reaction conditions have to be selected carefully to achieve thermodynamic control in which bonds are reversibly formed. For most of the types of listed reactions, this can be achieved by solvothermal synthesis at elevated temperatures (< 200°C) in presence of an acid or a base.<sup>41</sup> However, for the particular case of covalent triazine frameworks **k** other synthetic methods and reaction conditions are applied as will be discussed in the following section.

### B-O linkages

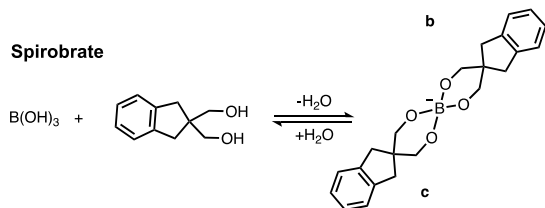
#### Boroxine



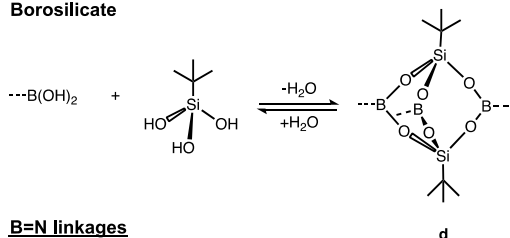
#### Boronate ester



#### Spiroborate

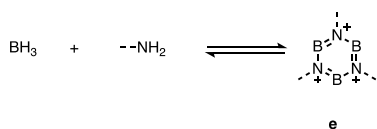


#### Borosilicate



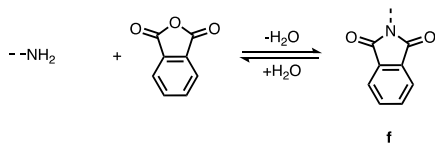
### B=N linkages

#### Borazine

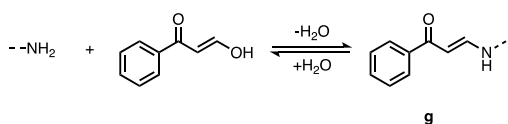


### C-N linkages

#### Imide

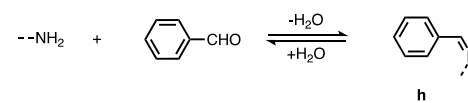


#### $\beta$ -ketoenamine

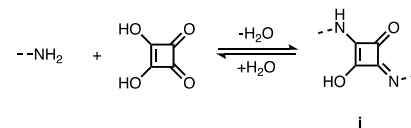


### C=N linkages

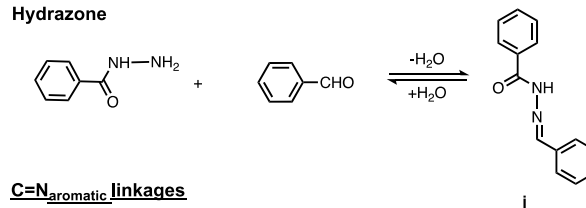
#### Imine



#### Squaraine

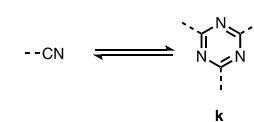


#### Hydrazone

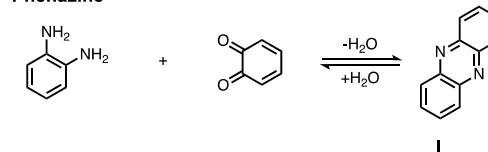


### C=N<sub>aromatic</sub> linkages

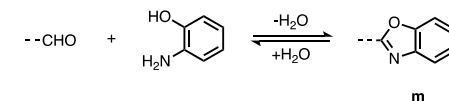
#### Triazine



#### Phenazine

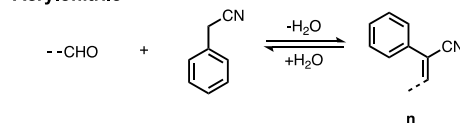


#### Benzoxazole



### C=C linkages

#### Acrylonitrile



### N=N linkages

#### Azodioxy

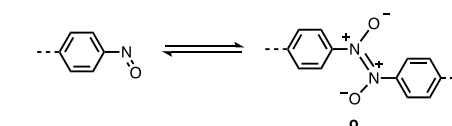


Figure 8. Different reversible covalent bond formation reactions.

## 2.1.2 Synthetic strategies for CTFs

The building blocks in covalent triazine frameworks (CTFs) are connected by aromatic C=N bonds in the form of triazine units. There are three main synthetic strategies for the formation of CTFs: (1) the cyclotrimerization of aromatic nitriles,<sup>42,43</sup> (2) the polycondensation strategy<sup>44,45</sup> and (3) cross-coupling of triazine moieties<sup>46,47</sup>. Several reaction conditions are possible for each strategy. Selection of the best synthetic method is not clear-cut and will mostly depend on its downstream application.

### 2.1.2.1 Cyclotrimerization strategy

The cyclotrimerization of aromatic nitriles generally gives rise to amorphous materials because of the low reversibility of the triazine linkage formation reaction. Four possible methods have been reported.<sup>48</sup> The first synthesis of a CTFs was achieved via cyclotrimerization of nitriles. It was carried out in sealed quartz ampules under ionothermal conditions in which 1,4-dicyanobenzene was reacted at 400 °C for 40-48 h in the presence of ZnCl<sub>2</sub>. The latter acts here both as Lewis acid catalyst and solvent. ZnCl<sub>2</sub> causes polarization of the C≡N triple bond facilitating a nucleophilic attack of a second nitrile group on the positively polarized carbon atom (Figure 9). The resulting carbenium ion undergoes a subsequent attack by a third nitrile group yielding the triazine ring. High temperatures are required to ensure reversibility in the reaction system, nevertheless CTFs generally lack a high degree of crystallinity. Using 1 equivalent ZnCl<sub>2</sub>, this method yielded CTF-1 as a black, rather amorphous solid with a specific surface area of 791 m<sup>2</sup> g<sup>-1</sup> and a total pore volume of 0.40 cm<sup>3</sup> g<sup>-1</sup>.<sup>42</sup> By increasing the temperature or the amount of ZnCl<sub>2</sub>, higher specific surface areas as well as higher porosities were achieved. By adding 5 equivalents of ZnCl<sub>2</sub>, a specific surface area of 920 m<sup>2</sup> g<sup>-1</sup> and a total pore volume of 0.47 cm<sup>3</sup> g<sup>-1</sup> were obtained for CTF-1. On the other hand, increasing the temperature to 500 °C for 20 h resulted in a specific surface area of 1600 m<sup>2</sup> g<sup>-1</sup> and a total pore volume of 1 cm<sup>3</sup> g<sup>-1</sup> for CTF-1.<sup>49</sup> Nonetheless, the temperature is characterized by an optimum. At temperatures below 400 °C, the polymerization of the nitrile functionalities is not ensured. On the other hand, at temperatures above 400 °C, partial decomposition of the nitrile functionalities can occur leading to nitrogen loss and structural defects.<sup>48,50</sup> The remaining ZnCl<sub>2</sub> can be partly removed through reflux with an aqueous solution of HCl. Subsequent washing with organic solvents like THF and acetone removes the

unreacted building blocks.<sup>42</sup> Although  $\text{ZnCl}_2$  could not be removed completely at present, the ionothermal conditions are easy to handle and can be applied on a variety of linkers.<sup>48</sup>

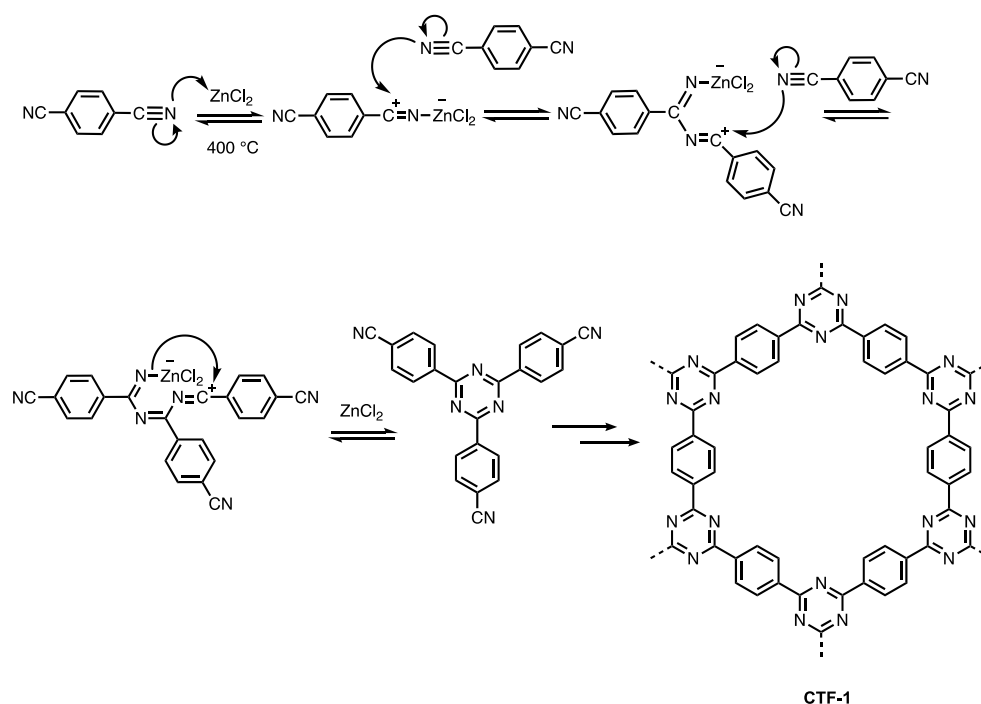


**Figure 9. Cyclotrimerization of aromatic nitriles.**

A second method is similar to the previous one but was carried out in a microwave (MW) for 10-60 min at different MW outputs. Generation of high porosities, easy scale-up and short reaction times are the main advantages of this protocol. For example, a specific surface area of  $1526 \text{ m}^2 \text{ g}^{-1}$  and total pore volume of  $2.25 \text{ cm}^3 \text{ g}^{-1}$  for CTF-1 was already achieved by MW-synthesis at 280 W for 30 min.<sup>51</sup> Yet, again partial decomposition is likely to occur due to the fast reaction rate and high temperatures used.

A third approach is provided by the salt-templated synthesis in which  $\text{ZnCl}_2$  is mixed with an alkali chloride (LiCl, KCl or NaCl).<sup>52</sup> After initiating the oligomerization at 300 °C for 60 h, polymerization proceeded at 400 °C for 5 h. As a result, higher specific surface areas and mesopore volumes were obtained. This method gave CTF-1 with a specific surface area of  $1130 \text{ m}^2 \text{ g}^{-1}$  and a total pore volume of  $0.53 \text{ cm}^3 \text{ g}^{-1}$  with a  $V_{\text{micro}}/V_{\text{meso}}$  ratio of 4.40.<sup>52</sup>

In a last method the cyclotrimerization is catalyzed by a strong Brønsted acid, such as triflic acid, and allows the reaction to proceed at room temperature, with  $\text{CHCl}_3$  as solvent.<sup>43</sup> Contrary to the previous methods, slightly colored crystalline powders are obtained by using a significantly lower temperature. This expands the scope of CTFs as potential photocatalysts.

By using the last protocol, cyclotrimerization of 1,1'-biphenyl-4,4'-dicyanitrile has been achieved resulting in DCBP-CTF which has a specific surface area of  $776 \text{ m}^2 \text{ g}^{-1}$  and a total pore volume of  $0.45 \text{ cm}^3 \text{ g}^{-1}$ .<sup>43</sup> Unfortunately, this mild approach is not suitable for every linker, especially not for heteroaromatic nitriles. Additionally, these conditions result in a lower surface area compared to methods using  $\text{ZnCl}_2$ . Even no porosity was observed for CTF synthesis from 1,4-dicyanobenzene.<sup>43,48</sup>

### 2.1.2.2 Polycondensation strategy

Alternatively, triazine moieties can be introduced in the framework structure by means of the polycondensation strategy. A first method involves the condensation of aromatic amides around  $400 \text{ }^\circ\text{C}$  in presence of a  $\text{P}_2\text{O}_5$  catalyst (Figure 10). High specific surface areas and total pore volumes were obtained with this method. pCTF-1 with a specific surface area of  $2034.1 \text{ m}^2 \text{ g}^{-1}$  and a total pore volume of  $1.04 \text{ cm}^3 \text{ g}^{-1}$  has been reported.<sup>45</sup> Another polycondensation reaction is carried out between an aldehyde and amidine at  $120 \text{ }^\circ\text{C}$  in DMSO with  $\text{Cs}_2\text{CO}_3$  as a base (Figure 11).<sup>44</sup> The aldehyde can also be generated *in situ* by oxidation of the alcohol in air. Initially, the temperature must be below the boiling point of DMSO to achieve slow oxidation of the alcohol into the aldehyde monomer. Afterwards, the temperature must increase to the boiling point for the polymerization to occur.<sup>53</sup> CTF-HUST-1 shows a specific surface area of  $663 \text{ m}^2 \text{ g}^{-1}$  and a total pore volume of  $0.32 \text{ cm}^3 \text{ g}^{-1}$ .<sup>44</sup> In comparison with the previous method, the values are significantly lower. However, the use of milder reaction conditions and the *in situ* oxidation resulted in colored powders with enhanced crystallinity and are advantageous for scale-up.<sup>48</sup>



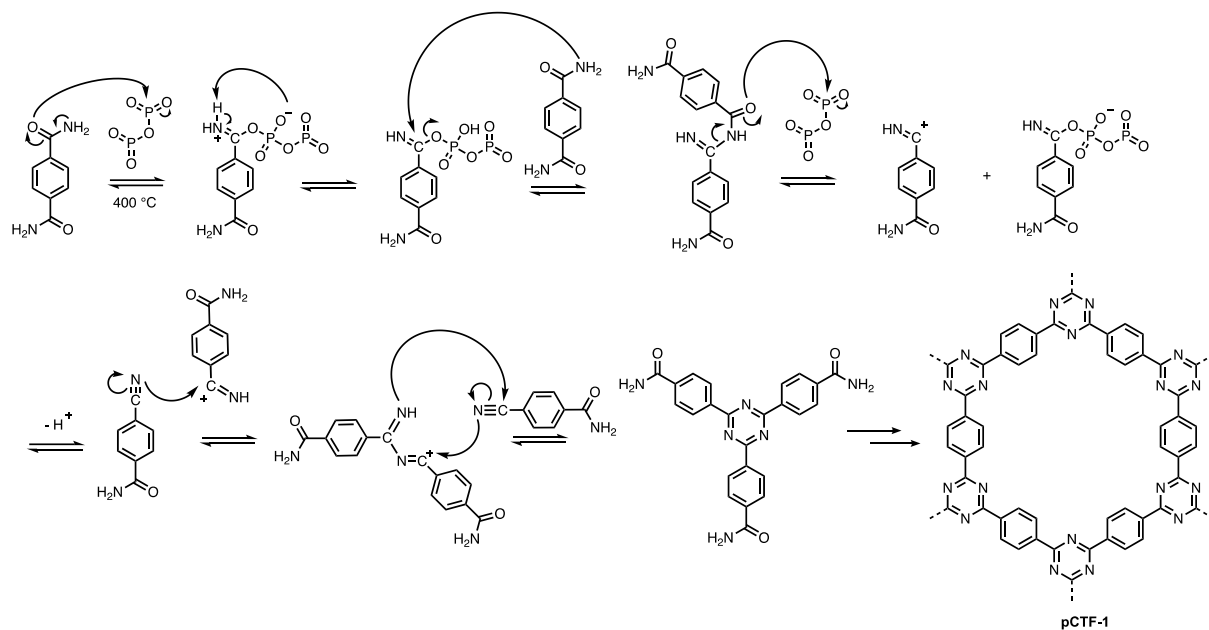


Figure 10. Polycondensation strategy through direct condensation of aromatic amides.

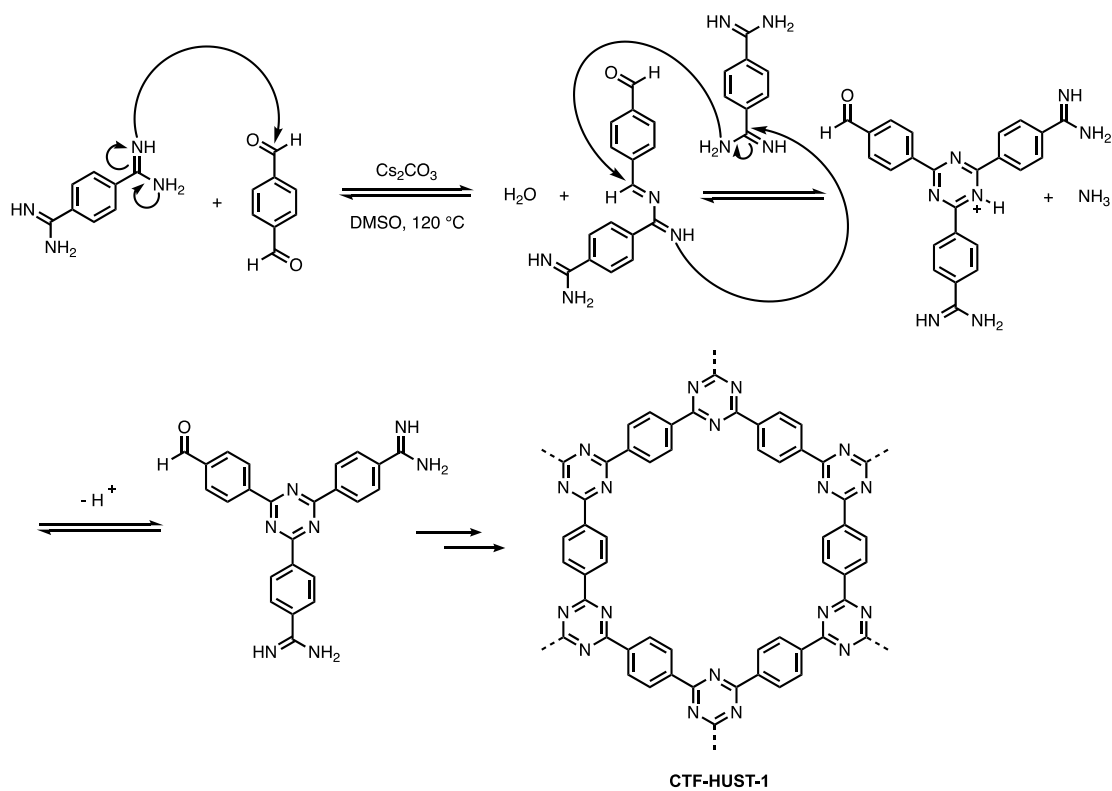


Figure 11. Polycondensation strategy through condensation with an amidine and an aldehyde.

### 2.1.2.3 Cross-coupling strategy

In a last synthetic strategy, the triazine unit is introduced using triazine as building block, such as cyanuric chloride. Accordingly, aromatic compounds and cyanuric chloride were reacted via the Friedel-Crafts cross-coupling in presence of a Lewis acid catalyst  $\text{AlCl}_3$  under reflux in DCM (Figure 12).<sup>46</sup> Due to steric hindrance, the substitution reaction mainly occurs at the *para*-position of the aromatic compounds. Again, a colored powder was obtained. For example, a 1,1'-biphenyl building block can be cross-coupled with cyanuric chloride yielding a specific surface area of  $1220 \text{ m}^2 \text{ g}^{-1}$ .<sup>54</sup> Although frameworks with high specific surface areas are yielded and multiple aromatic building blocks can be used, this method results in low crystallinity due to the irreversibility of the substitution reaction.<sup>48</sup> Materials obtained by this method are therefore sometimes classified as covalent triazine polymers (CTPs).<sup>54</sup>

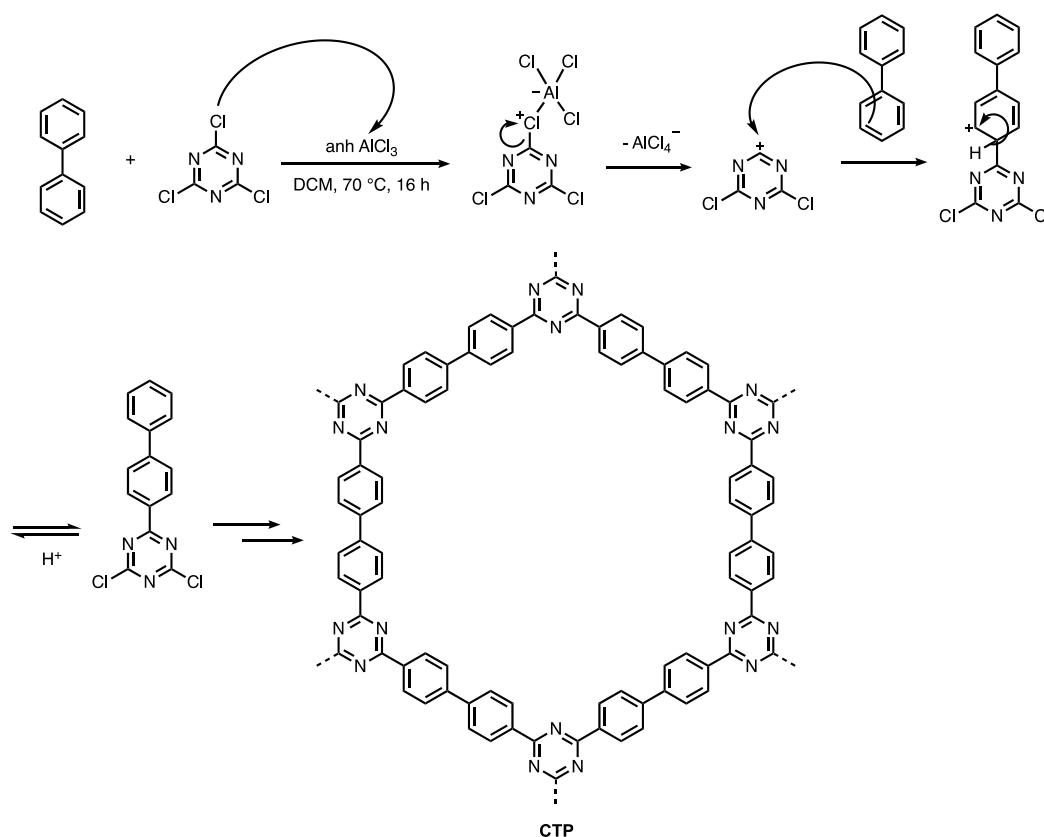


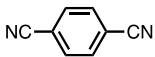
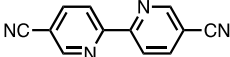
Figure 12. Cross-coupling of cyanuric chloride and an aromatic compound.

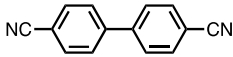
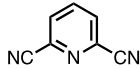
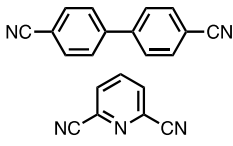
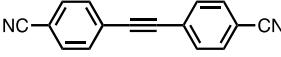
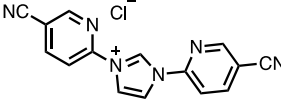
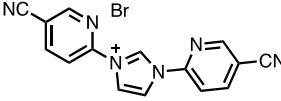
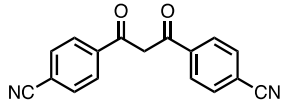
### 2.1.3 CTFs as heterogeneous catalysts

CTFs are excellent candidates for heterogeneous catalysis for many reasons. The strong electron donating nitrogen species in the triazine moieties provide a good coordination site for metals.<sup>24</sup> Moreover, due to the principles of reticular chemistry, the building blocks can be functionalized according to the type of reaction to be catalyzed. Also, CTFs can obtain high specific surface areas and porosities which are important for the accessibility of the catalytic active site.<sup>22</sup> Another important reason is their rigidity, thermal and chemical stability which are of great use in the harsh conditions required for some catalytic reactions.<sup>23</sup>

To date, several metal complexes have been successfully anchored onto CTF materials and subsequently deployed in different types of catalytic transformations.<sup>48</sup> A summary is given in Table 1 to give an idea of which CTF can be used for which transformation. The type of building block, catalyst and reaction are mentioned.

**Table 1. CTFs as heterogeneous catalysts for several organic transformation reactions.** Adapted from Tahir *et al.*<sup>48</sup>

Building block	Catalyst	Type of reaction	Ref
	Pd/CTF	Oxidation of glycerol to glyceric acid	55
		Oxidation of benzyl alcohol	56
		Hydrogenation of N-heterocycles	57
		Selective double carbonylation of aryl iodides	58
	Ru/CTF-c	Oxidation of 5-hydroxymethylfurfural to 2,5-furandicarboxylic acid	59
		Hydrogenolysis of xylitol	60
	Rh@CTF-c	Hydroformylation of 1-octene	61
	Bpy-CTF-(IrCp*Cl)Cl	Hydrogenation of CO <sub>2</sub> to formate	62
	Bpy-CTF-Ru(acac) <sub>2</sub> Cl	Hydrogenation of CO <sub>2</sub> to formate	63
	Bpy-CTF-RuCl <sub>3</sub>	Hydrogenation of CO <sub>2</sub> to formate	64
	Bpy-CTF(RhCp*Cl)Cl	Transfer hydrogenation of carbonyl compounds	65

	Bpy-CTF(IrCp*Cl)Cl	Transfer hydrogenation of carbonyl compounds	65
	Bpy-CTF-Al(OTf) <sub>2</sub> Co(CO) <sub>4</sub>	Carbonylation of epoxides into β-lactones	66
	Ir(I)@bpyCTF	C-H borylation of 1,2-dichlorobenzene	67
	Ir@CTF	Isomerization of 1-octen-3-ol to 3-octanone	68
	Pt-CTF	Oxidation of methane to methanol	69
	CTF-Ir	Dehydrogenation of formic acid	70
	Ir@meso-CTF@monolith	Dehydrogenation of formic acid	71
	Ir@meso-CTF	Hydrogenation of CO <sub>2</sub> to formate	72
	CTF-CDE-Ag	Carbonylation of terminal alkynes	73
	Rh-bpim-CTF	Carbonylation of methanol	74
	Imidazolium-CTF-Co(CO) <sub>4</sub>	Direct synthesis of methyl-3-hydroxybutyrate from propylene oxide	75
	Ir0.68-NHC-CTF	Hydrogenation of CO <sub>2</sub> to formate	76
	V@acacCTF	Mannich reaction between 2-naphtol and N-mythylmorpholine N-oxide	77

As illustrated by this part, covalent organic frameworks are highly diverse porous materials established through the principles of reticular chemistry. Reticular chemistry uses modular designed building blocks. Upon connection of these building blocks different types of linkages can be formed. A particular type of linkage, the triazine linkage, yields covalent triazine frameworks. There are different synthetic strategies possible to obtain these materials. The cyclotrimerization strategy using ionothermal conditions (ZnCl<sub>2</sub> at 400 °C for 40-48 h) is the most commonly used. Although this synthesis yields amorphous black materials, generally

high specific surface areas and pore volumes are achieved. CTFs are promising materials for the development of heterogeneous catalysts owing to their insolubility, functionality tailoring possibility, high porosity, chemical and thermal stability. To date, different types of reactions have been catalyzed using CTFs as solid support. For this Master Thesis the transfer hydrogenation reaction is of particular interest and will therefore be further elaborated in the next part of this chapter.

## 2.2 Catalytic transfer hydrogenation

One of the reactions wherein CTF-based catalysts have been studied is the transfer hydrogenation reaction.<sup>65</sup> However, the scope of substrates was limited to acetophenone derivatives only. This Master thesis has the aim to expand the substrate scope towards N-heterocycles. Hence, the catalytic transfer hydrogenation reaction will be more elaborated here.

A variety of unsaturated compounds are reduced by means of hydrogenation reactions. Carbonyl compounds can be transformed to alcohols, olefins to alkanes, nitrobenzene to aniline and imines to amines, to mention a few. Hence, its industrial application ranges from fine chemicals and pharmaceuticals to petrochemicals.<sup>78</sup> Catalytic transfer hydrogenation (TH) is a reduction reaction at which an organic molecule, the hydrogen donor, transfers a proton and a hydride to an organic substrate, the hydrogen acceptor, all facilitated by a catalyst. The advantage of transfer hydrogenation, with an H-donor as the hydrogen source, compared to direct hydrogenation, with molecular H<sub>2</sub> as the hydrogen source, is twofold. TH avoids the use of hazardous pressurized H<sub>2</sub> gas, which is flammable and can explode in presence of a heat source. Thereby, special equipment such as pressure vessels are not needed. Advantages of catalytic TH over methodologies that use lithium or boron hydrides are that the H-donors are cheaper, less hazardous and easily manageable.<sup>79-81</sup>

Today, catalytic TH can be carried out by different kinds of catalysts including Meerwein-Ponndorf-Verley (MPV) catalysts, transition metal (TM) catalysts, bases, enzymes and other organocatalytic compounds. In particular, transition metal catalysts gained attention over the past decades due to their high selectivity and activity.<sup>82</sup>

## 2.2.1 Typical H-donors for catalytic transfer hydrogenation

In theory, an H-donor can be any organic compound from which one hydrogen can be transferred as a proton and the other as a hydride. Moreover, in order to carry out the transfer hydrogenation under mild reaction conditions, the H-donor needs to have low oxidation potential.<sup>81</sup> Selection of the most suitable H-donor is not clear-cut. Some H-donors may be more compatible with a specific type of catalyst and substrate than others.<sup>79,82</sup> Availability, activity, selectivity and environmentally benign are important criteria to consider within the context of Green Chemistry. Frequently used H-donors are isopropanol (2-PrOH) and formic acid (HCOOH).<sup>83</sup>

### 2.2.1.1 *Isopropanol*

Generally, secondary alcohols like isopropanol are better H-donors than primary alcohols since they have a higher inductive donating effect due to the presence of an additional alkyl group.<sup>79</sup> Nonetheless, often strong bases like metal hydroxides and alkoxides are still needed to promote hydrogen removal from the H-donor. In isopropanol, the  $\alpha$ -hydrogen is transferred to the substrate and the hydroxyl group is transformed into acetone. The latter, being a hydrogen acceptor, can reversibly be reduced to isopropanol and therefore competes with the substrate. By means of distillation, acetone can easily be removed to shift the thermodynamic equilibrium towards the product side. Another option is using isopropanol as the solvent in order for the hydrogen donor to be in excess. Isopropanol is an attractive candidate as hydrogen donor for a broad range of substrates because it's cheap, readily available, easy to handle and environmentally friendly.<sup>79,83,84</sup>

### 2.2.1.2 *Formic acid*

On the other hand, formic acid or its salts can also serve as an H-donor. The transfer of hydrogens is promoted by weak bases such as triethylamine. After donating two hydrogens, formic acid is decomposed into carbon dioxide.<sup>83,84</sup> Carbon dioxide has a large negative enthalpy of formation ( $\Delta_f H^\circ_{298} = -393.51$  kJ/mol) contributing to enhanced reactivity of the transfer hydrogenation reaction.<sup>79</sup> This renders the reaction irreversible and under kinetic control. The transfer hydrogenation reaction can be performed in aqueous solvents.

Moreover, carbon dioxide is volatile and therefore does not require additional separation. The major drawback of formic acid is its inherent acidity causing decomposition or loss of catalytic activity in some catalysts.<sup>83–85</sup>

## 2.2.2 Mechanism behind transition metal catalyzed transfer hydrogenation

Among the various transition metals active for the transfer hydrogenation, ruthenium (Ru), rhodium (Rh) and iridium (Ir) are by far the most widely used transition metals for this purpose.<sup>82</sup> However, the abundant, cheaper and less toxic iron (Fe), cobalt (Co) and nickel (Ni) gain interest in the search for greener alternatives.

In general, transition metal catalysts make use of the hydridic pathway, involving a metal hydride as an important intermediate.<sup>86–88</sup> The metal hydride can either carry one or two hydrogens resulting in, respectively, a monohydridic or dihydridic route. Rhodium and iridium catalysts usually operate through the former route. Ruthenium catalysts can operate through both routes, depending on its ligands.<sup>89,90</sup>

### 2.2.2.1 Dihydridic route

In the dihydridic route, the C-H and O-H hydrogens from the H-donor lose their identity as hydride and proton in the hydrogenated substrate. This is because they are both transferred to the metal, yielding the dihydride (Figure 13).<sup>83</sup>

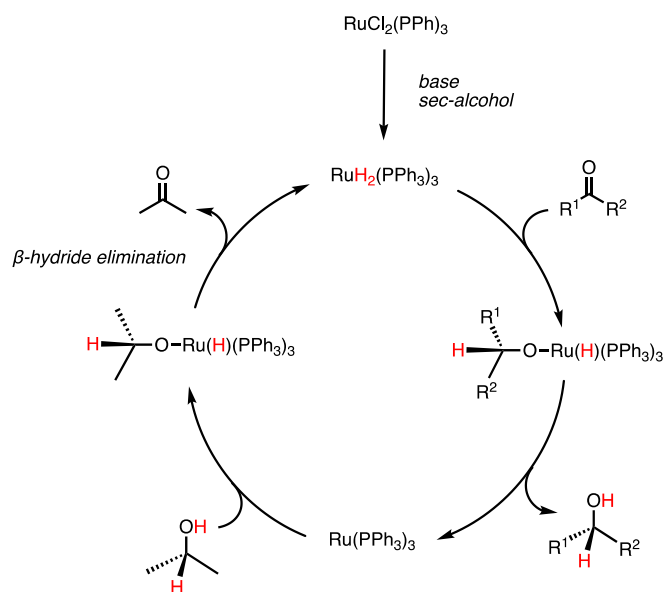


**Figure 13. Dihydridic route (inner-sphere mechanism).**

#### 2.2.2.2 Monohydridic route

In the monohydridic route, the two hydrogens preserve their identity since only the C-H from the H-donor is transferred to the metal. The O-H hydrogen is transferred as a proton to the ligand. The monohydridic route can proceed via an inner- or outer-sphere mechanism, depending on whether the H-donor or the substrate coordinates to the metal.<sup>83</sup> If the H-donor or the substrate directly coordinate to the metal, as for the dihydridic route, the inner-sphere mechanism will take place. The metal and hydrogen donor form then an alkoxide intermediate which is converted to the metal hydride after  $\beta$ -elimination. The outer-sphere mechanism occurs when the H-donor or substrate do not directly coordinate to the metal. The latter can be accomplished in a one-step concerted process (Figure 14) or a two-step process in which the hydride transfer occurs after protonation of the substrate.<sup>90</sup> The outer-sphere mechanism is characteristic for transition metal-ligand bifunctional catalysts, a term introduced by Noyori.<sup>91,92</sup> These catalysts contain a basic ligand which can interact with the proton. As a result, hydride transfer is facilitated and promoters like metal hydroxides, alkoxides or triethylamine are no longer necessary.<sup>90</sup>



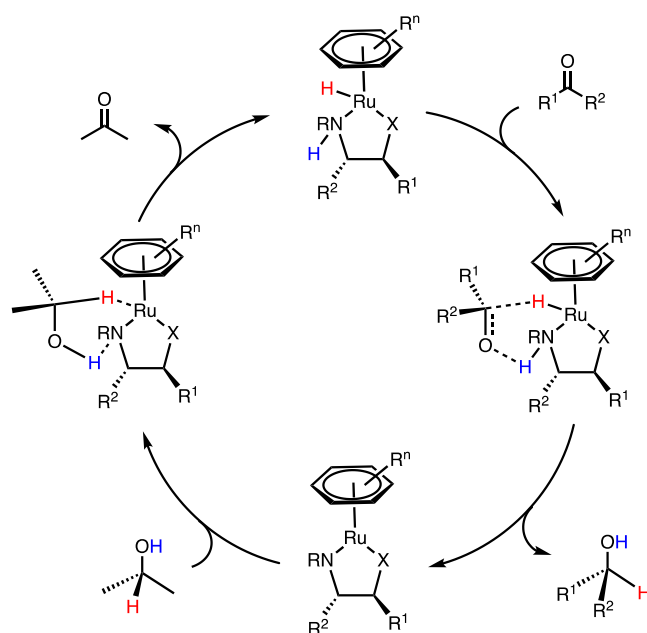


**Figure 14. Monohydric route (outer-sphere mechanism) through one-step concerted process.**

### 2.2.3 Catalytic transfer hydrogenation of N-heterocycles

N-heterocycles represent an essential class of compounds for the synthesis of pharmaceuticals, agrochemicals and other fine chemicals.<sup>93–96</sup> Among others, functionalized 1,2,3,4-tetrahydroquinoxalines and 3,4-dihydroquinoxalinones are biologically active core structures or crucial intermediates for the latter purposes. For example, they could inhibit a specific lectin that viruses like HIV, Ebola and hepatitis C use to spread out more easily.<sup>96,97</sup> For the synthesis of these hydrogenated compounds, transfer hydrogenation of the corresponding quinoxalines and quinoxalinones appears to provide a simple and efficient method. The area of transfer hydrogenation of N-heterocycles still offers many opportunities. A number of specific approaches, using different H-donors and catalysts, have already been reported.<sup>98</sup> The use of formic acid as H-donor seems to be the best choice from an environmental point of view. It is non-toxic, safe, abundant and has a high energy density.<sup>99,100</sup> Additionally, it allows to carry out the TH in water as the solvent. Besides being environmentally benign, the use of aqueous HCOONa provides another benefit. By regulating the pH, the selectivity and reaction rate can be optimized.<sup>101</sup> To achieve high catalytic activity for the TH in presence of aqueous HCOONa, previous work implied bidentate N,N-ligands were crucial.<sup>102–106</sup> Among other transition metal–N,N-ligand complexes, a rhodium-2,2'-bipyridine

complex has been reported as efficient catalyst for the TH of N-heterocycles. For the latter catalyst, homogeneous as well as heterogeneous variants have been applied.<sup>107,108</sup> In this Section, examples will be discussed in more detail as they are essential for this Master thesis.

### 2.2.3.1 Homogeneous catalytic transfer hydrogenation in aqueous HCOONa

Zhang and co-workers applied the homogeneous catalyst (pentamethylcyclopentadienyl)rhodium-2,2'-bipyridine ( $[\text{Cp}^*\text{Rh}(\text{bpy})\text{Cl}]\text{Cl}$ ) in the aqueous TH of several N-heterocycles with formate as H-donor.<sup>107</sup> The authors suggest the TH proceeds through the monohydridic route via an inner sphere mechanism since formic acid is directly coordinated to rhodium (Figure 15). In order to find the most effective catalyst, the authors tested several bipyridine and phenanthroline analogues in complexation with rhodium. 2,2'-bipyridine represented the best ligand in terms of yield, cost and availability. Additionally, rhodium was replaced by ruthenium and iridium but these were not performant under the same reaction conditions. The complex was efficient for the TH of a broad range of substrates such as quinolines, quinoxalines, quinoxalinones and indoles. The regulation of the pH, depending on the substrate, is the key to obtain high reaction rates and selectivities. For the model substrate 2-methylquinoxaline, pH 4.4 proved to be the optimal pH. As illustrated in Figure 15, acidic conditions activate the substrate via protonation which causes a decrease in the substrate's LUMO energy and therefore an increase in the reaction rate. However, when the pH drops below its optimal level, the rhodium hydride would decompose leaving less catalytically active complexes and consequently reducing the reaction rate. In order to control pH fluctuations, a 2 M HCOOH/HCOONa buffer solution is used for the TH of 2-methylquinoxaline. With this catalytic system, 2-methyl-1,2,3,4-tetrahydroquinoxaline was obtained after 3 hours at 80 °C with a 96% yield and a substrate to catalyst ratio up to 10 000. The reaction could be performed in air. Moreover, two control experiments were carried out which confirmed the TH only proceeded in presence of  $[\text{Cp}^*\text{Rh}(\text{bpy})\text{Cl}]\text{Cl}$ . In the first control experiment  $[\text{Cp}^*\text{RhCl}_2]_2$  was used. In the second control experiment no rhodium species was added.

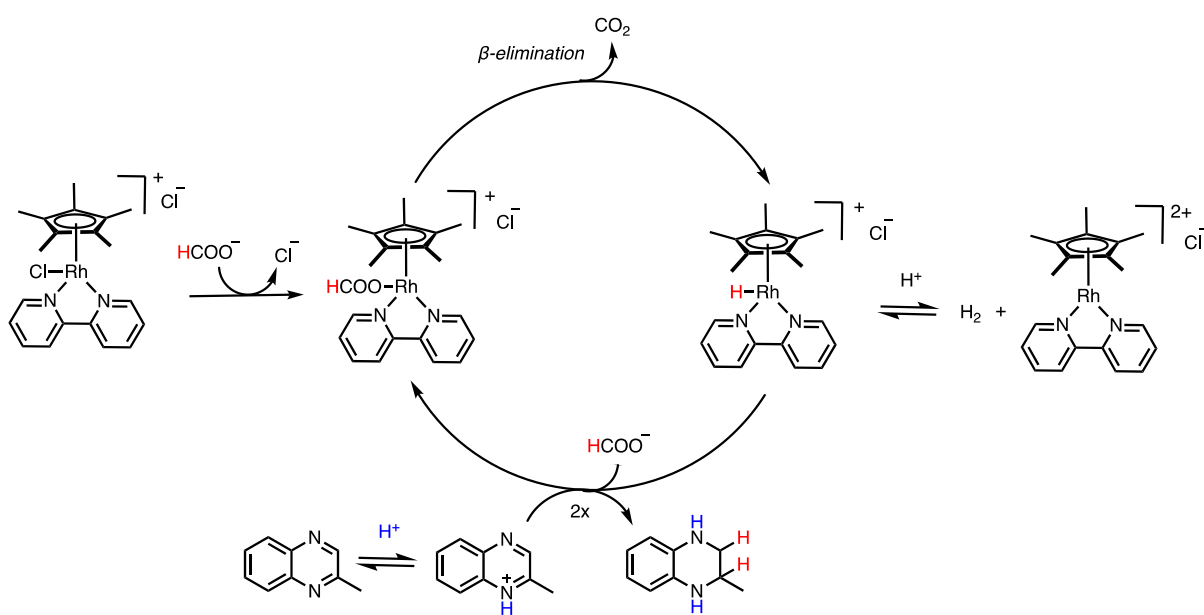


**Figure 15.** Aqueous transfer hydrogenation of 2-methylquinoxaline with  $[\text{Cp}^*\text{Rh}(\text{bpy})\text{Cl}]\text{Cl}$  as homogeneous catalyst and formic acid as H-donor.

### 2.2.3.2 Heterogeneous catalytic transfer hydrogenation in aqueous $\text{HCOONa}$

Inspired by the previous work and the increasing demand for heterogeneous catalysts, Matsui and co-workers aimed to immobilize the rhodium catalyst on a bipyridine-periodic mesoporous organosilica ( $\text{Rh@Bpy-PMO}$ ), illustrated in Figure 16.<sup>108</sup> The catalyst loading was targeted at a Rh/Bpy-PMO molar ratio of 0.06 (0.20 mmol/g). Nitrogen adsorption analysis revealed a BET surface area of  $298 \text{ m}^2/\text{g}$ , a total pore volume of  $0.127 \text{ cm}^3/\text{g}$  and a pore diameter of 3.1 nm.

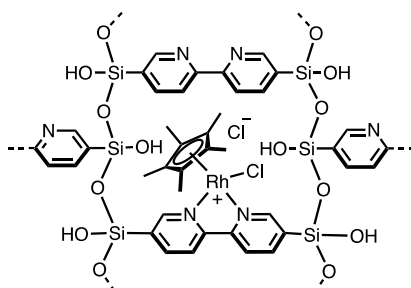


**Figure 16.**  $\text{Rh@Bpy-PMO}$ .

As for its homogeneous counterpart, Rh@BPy-PMO could efficiently catalyze the TH of several N-heterocycles such as quinolines, quinoxalines, quinoxalinone, indolines, indolenines and benzodiazepines. The model substrate used for this work was 3-methylquinoxalin-2(1*H*)-one, a crystalline solid forming a suspension in the reaction medium. The TH reaction was carried out with 0.5 mol% [Rh] in a 0.6 M HCOOH/HCOONa aqueous buffer solution at pH 4.1 resulting in a 98% yield after 2 hours at 80 °C. The same yield was obtained if only 0.2 mol% [Rh] was applied. The reaction was performed under argon. A control experiment with Bpy-PMO alone afforded no product. Measuring the Rh-concentration in the reaction filtrate after filtering off the heterogeneous catalyst revealed a small amount of leached catalyst (<1.2 ppm). The authors suggested this was due to leaching of [Cp\*RhCl<sub>2</sub>]<sub>2</sub> residues which were adsorbed on the silanol groups during immobilization. However, upon addition of fresh substrate to the filtrate and further heating of the mixture no increase in product yield was found. This confirmed the TH reaction occurred at the catalytic site on the pore surface of Rh@BPy-PMO. Furthermore, catalyst recycling experiments were carried out (Figure 17). The catalyst remained highly active for about four reaction cycles after which the yield decreased gradually to 71%. According to previous work, this decrease could be due to the hydride transfer from the rhodium to the cyclopentadienyl ligand. This causes slippage to η<sup>4</sup>-cyclopentadiene coordination which could lead to ligand dissociation.<sup>109,110</sup> However, the rhodium species lacking the Cp\* ligand showed also catalytical activity since conversion of the substrate was still observed.<sup>108</sup>

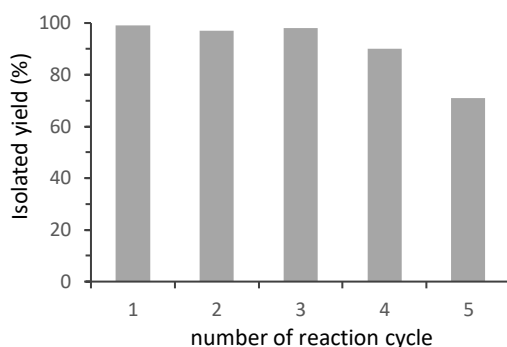


**Figure 17. Results from catalyst recycling experiments. Yield in function of reaction cycle.**

By comparing the latter examples several differences could be observed between the homogeneous and heterogeneous catalyzed TH. As Matsui *et al.* did not test the TH for 2-methylquinoxaline, 3-methylquinoxalin-2(1*H*)-one was used for the comparison. The main differences are highlighted in Table 2.

**Table 2. Comparison homogeneous and heterogeneous TH of 3-methylquinoxalin-2(1*H*)-one.**

	pH	Concentration HCOOH/HCOONa solution (M)	Reaction time (h)	Yield (%)	[Rh] amount (mol %)	Air/argon	Ref
Zhang <i>et al.</i>	4	5	3	99	0.5	air	107
Matsui <i>et al.</i>	4.1	0.6	2	98	0.2	argon	108

Since the TH reaction in both reseaches was carried out in aqueous medium, several of the used N-heterocycles were insoluble. For example, the model substrate used by Zhang *et al.* is an oily liquid leading to the formation of a biphasic reaction medium. Yet, this had no negative effect on the reaction rate of the homogeneous catalyzed TH. This has also been observed for aromatic ketones which are generally water insoluble.<sup>111</sup> Matsui *et al.* tested likewise some substrates with poor solubility in water, such as 3-isopropylquinoxalin-2(1*H*)-one. However, for the heterogeneous catalyzed TH a reduced reaction rate was observed under optimal conditions. Therefore, they applied 2-propanol as co-solvent to complete the TH.

This part clarified the general principle of transfer hydrogenation in which an organic donor molecule passes on its hydrogen atoms to an organic substrate. Isopropanol and formic acid are commonly employed H-donors. The TH reaction is often catalyzed by transition metals involving the formation of a metal-hydride intermediate. Depending on the type of metal, the TH follows either the dihydridic route, with two hydrogens on the metal-hydride, or monohydridic route, with one hydrogen on the metal hydride. As for rhodium complexes, the TH proceeds through the monohydridic route. Both the homogeneous and heterogeneous variant of the rhodium-2,2'-bipyridine complex were able to efficiently catalyze the TH of a broad range of N-heterocycles in aqueous HCOONa.

## 3 Results and discussion

---

In this Master's thesis, the development of a CTF as heterogeneous support for the catalytic transfer hydrogenation of N-heterocycles is divided into three parts. During the first part (section 3.1), nitrogen-containing aromatic building blocks with cyano end groups are synthesized. Keeping in mind the envisaged application as catalytic support, the building blocks must be rigid and contain strong binding sites for the coordination of the metal. By selecting building blocks with aromatic moieties, the first requirement is met. By introducing nitrogen atoms in the structure, these building blocks can serve as bidentate or tridentate ligands fulfilling the other requirement. Further, in the second part (section 3.2), the formed building blocks are connected into CTFs. To this end, a synthetic strategy compatible with heteroaromatic nitriles and yielding high specific surface areas and porosities must be selected. Therefore, the ionothermal cyclotrimerization synthesis with  $\text{ZnCl}_2$  is chosen. In a first approach, the conventional ionothermal method is performed. In a second approach, the salt templated ionothermal method is carried out in order to investigate whether specific surface areas and porosities can be improved to provide higher accessibility of the future catalytic sites. Afterwards, the CTF is decorated with a rhodium complex. The potential of rhodium-based catalysts for the transfer hydrogenation of different N-heterocycles has been shown in the literature review. Therefore, in the third part (section 3.3), the rhodium containing support ( $\text{Rh@CTF}$ ) is applied in the catalytic transfer hydrogenation reaction with 2-methylquinoxaline as model substrate. The latter N-heterocycle has also been used as model substrate in the work of Zhang *et al.*<sup>107</sup>, discussed in the literature review, and could therefore serve as a guideline for the reaction conditions. Nevertheless, the reaction conditions must be fine-tuned in order to optimize the catalytic system. However, due to SARS-CoV-2 measures all laboratory activities were interrupted. Therefore, the intended optimization of reaction parameters as pH, temperature, catalyst loading, and solution concentration could not be performed and will therefore be further elaborated in the chapter about Future work and perspectives (chapter 4). The same holds for the evaluation of recyclability and heterogeneity as well as the integration of the catalytic system in a continuous flow reactor set-up.

### 3.1 Synthesis of nitrogen-containing aromatic building blocks

The goal was to synthesize the following nitrogen-containing aromatic building blocks: 2,2'-bipyridine-5,5'-dicyanitrile **1**, 2,2'-biquinoline-6,6'-dicyanitrile **2** and quinoline-2,6-dicyanitrile **3** (Figure 18). These building blocks will give rise to CTFs with a similar chemical pore environment, but different pore sizes and shapes.

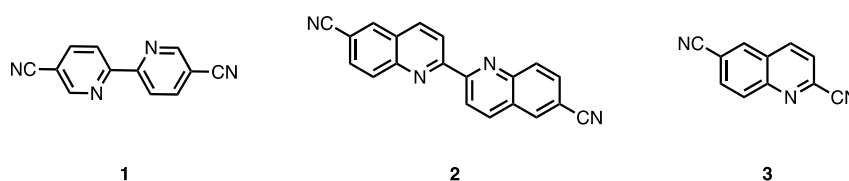


**Figure 18. Nitrogen-containing aromatic building blocks.**

#### 3.1.1 Synthesis of 2,2'-bipyridine-5,5'-dicyanitrile **1**

2,2'-bipyridine-5,5'-carbonitrile **1** was chosen as first building block, since bipyridines are widely used ligands with strong coordination of the transition metal.<sup>112</sup> An elegant synthetic approach for bipyridine **1** has been reported by Duan and co-workers and proceeds through the nickel-catalyzed reductive homocoupling of 2-halopyridines.<sup>113</sup> While the nickel complex in reductive coupling reactions is generally accompanied by high loadings of additional ligand, such as triphenylphosphine, bipyridines or phenanthrolines, Duan and co-workers noticed that the addition of an external ligand was not required for efficient coupling of 2-bromopyridines into 2,2'-bipyridines. This results from the fact that the formed 2,2'-bipyridine itself functions as ligand.

In this work, a slightly adapted procedure was employed, which was earlier developed within the research group (Figure 19).<sup>67</sup> Herein, 5 mol% of nickel(II), added as  $\text{NiCl}_2 \cdot 6\text{H}_2\text{O}$ , was used to catalyze the reductive homocoupling of 2-bromo-5-cyanopyridine **4**. In order to maintain the reducing activity of nickel, 1.2 equivalents zinc granules as reducing agent and 1 equivalent LiCl were added.

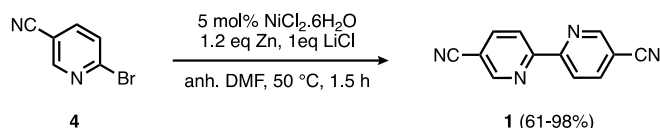


**Figure 19. Synthesis of 2,2'-bipyridine-5,5'-dicarbonitrile 1.**

The proposed catalytic cycle by Duan *et al.* (Figure 20) contains successive oxidative additions and reductive eliminations.<sup>113</sup> Through an oxidative addition step pyridine **4** joins the nickel complex. Afterwards, zinc eliminates bromide from the complex in a reductive elimination step, accelerated by means of LiCl.<sup>114</sup> Hereby, ZnBr<sub>2</sub> is formed.<sup>115</sup> In general, 2,2'-bipyridine is proved to act as a good ligand to coordinate nickel for the catalysis of couplings reactions.<sup>116–118</sup> However, initially no bipyridine is formed yet. Therefore, the addition of iodine is crucial as it acts as an interchangeable ligand. Moreover, since bipyridine effectively binds nickel, high concentrations cause product inhibition of the catalyst.<sup>119</sup> Therefore, in order to control the concentration of bipyridine **1** around nickel, ZnBr<sub>2</sub> also forms a complex with bipyridine **1**. In this way, the formation of **1** is autocatalyzed by the *in situ* formed nickel complex without inhibition, nor the need for external ligands as PPh<sub>3</sub> or high catalyst loadings. Consequently, this procedure is in line with the first and ninth principle of Green Chemistry.

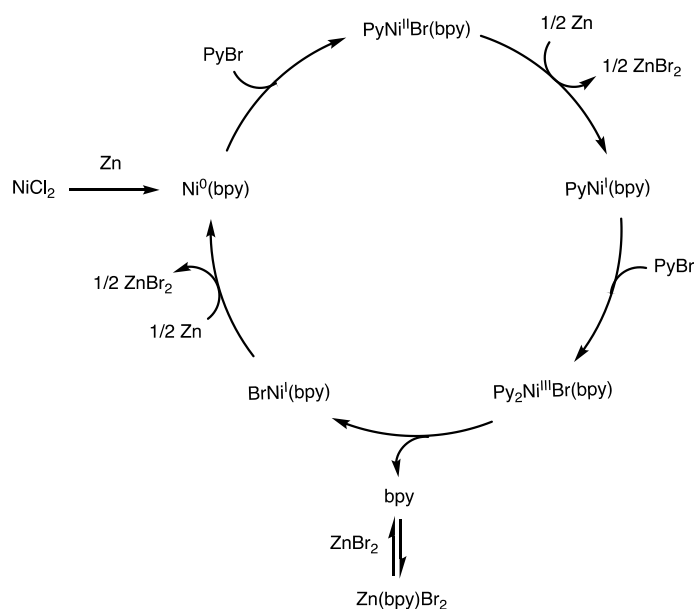


**Figure 20. Proposed mechanism by Duan *et al.* for the Ni-catalyzed reductive homocoupling of bromopyridines.**



As the mechanism suggests, maintaining the reducing activity of nickel is important for the coupling of **4**. Therefore, the reaction was carried out in anhydrous DMF under argon atmosphere. However, some attempts resulted in a complex reaction mixture, wherein 2,2'-bipyridine-5-carbonitrile was identified as major side-product. The inconsistency in reaction outcome could be avoided by carefully maintaining the reaction temperature under 60 °C and thoroughly washing the zinc granules with diluted HCl prior to use. Upon activation of zinc with HCl, zinc oxides are removed from the surface and reactive sites are created.<sup>120</sup> With the adapted method, complete conversion of starting materials was obtained after about 1.5 h reaction, which is shorter than described by Duan *et al.*<sup>118</sup> (3 h), but longer than described by Tahir *et al.*<sup>72</sup> (30 min). After the reaction, bipyridine **1** was isolated in a 61-98 % yield. The variation in yield can be assigned to losses during extraction. Upon extraction, a dark brown hazy mixture is formed causing a more difficult work-up. Additionally, 2,2'-bipyridine-5,5'-carbonitrile **1** showed better solubility in ethyl acetate than in chloroform, used as extraction solvents.

Furthermore, Duan *et al.* indicated that the coupling reaction was also compatible with functionalized 2-chloropyridines instead of the more expensive 2-bromopyridines.<sup>113</sup> Hence, the reaction was tested with 2-chloro-5-cyanopyridine but was more sluggish and resulted in a mixture with the formation of 2,2'-bipyridine-5-carbonitrile.

### 3.1.2 Synthesis of 2,2'-biquinoline-6,6'-dicarbonitrile **2**

In order to further extend the scope of nitrogen-containing building blocks, 2,2'-biquinoline-6,6'-dicarbonitrile **2** was chosen. The large delocalized  $\pi$  system of 2,2'-biquinolines makes them attractive ligands, especially in photochemical applications. However, no 2,2'-biquinoline based building blocks have been utilized in COF synthesis so far. The larger biquinoline **2** compared to bipyridine **1** should also result in CTFs with wider pores. For the synthesis of this new building block, different pathways were explored. All pathways required 6-cyanoquinoline-*N*-oxide **8** as starting reagent. The latter compound was synthesized according to the reaction scheme depicted in Figure 21. Quinolin-6-yl trifluoromethanesulfonate **6** was synthesized based on previous work.<sup>121-123</sup> By adding 1.3 equivalents triflic anhydride (Tf<sub>2</sub>O) and 2 equivalents pyridine in dry DCM, the hydroxyl group in quinolin-6-ol **5** is transformed into a trifluoromethanesulfonyl group. Next, the resulting

aryl triflate **6** was converted into quinoline-6-carbonitrile **7**.<sup>123,124</sup> By adding 1.2 equivalents  $\text{Zn}(\text{CN})_2$  in presence of 3 mol%  $\text{Pd}(\text{PPh}_3)_4$  catalyst in degassed DMF, the trifluoromethanesulfonyl group is replaced by a cyano group. The resulting quinoline **7** was purified by normal phase column chromatography. Hereafter, quinoline **7** was oxidized to the corresponding quinoline-*N*-oxide **8** by means of 1.3 equivalents *meta*-chloroperbenzoic acid (*m*CPBA).<sup>125–127</sup>

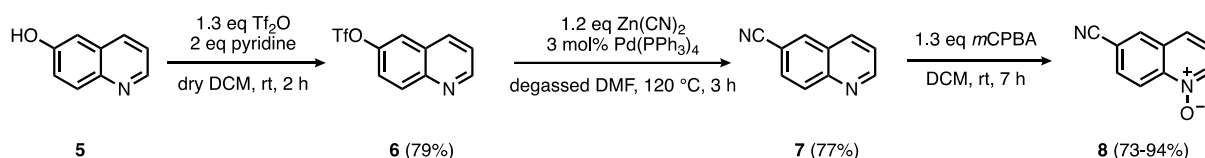


**Figure 21. Synthesis of 6-cyanoquinoline-*N*-oxide **8**.**

In a first approach to obtain biquinoline **2**, the rationale was to transform 6-cyanoquinoline-*N*-oxide **8** to a 2-haloquinoline-6-carbonitrile and subsequently perform a reductive homocoupling similar to the one described for building block **1** (section 3.1.1). To this end, 2-chloroquinoline-6-carbonitrile **9a** was synthesized according to the reaction scheme outlined in Figure 22. Quinoline-*N*-oxide **8** was treated with 2.2 equivalents phosphoryl trichloride ( $\text{POCl}_3$ ) and 0.5 equivalent anhydrous DMF in dry DCM under argon atmosphere. For the chlorination of quinoline-*N*-oxide using this method, a C2:C4 regioselectivity of about 10:1 has been reported in literature.<sup>128</sup> However, applying this method on 6-cyanoquinoline-*N*-oxide **8** resulted in a mixture of the C2 and C4 isomer in a ratio of 1:3.3 with inversed regioselectivity. By means of preparative thin layer chromatography, 2-chloroquinoline-6-carbonitrile **9a** was isolated in a 17 % yield.

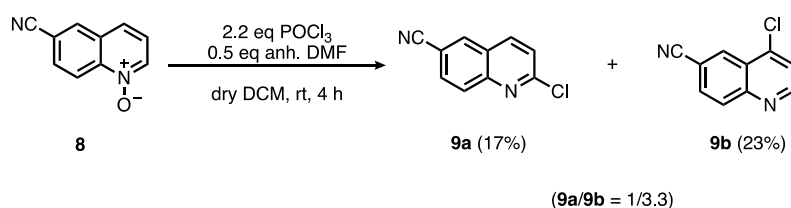


**Figure 22. Direct synthesis of 2-chloroquinoline-6-carbonitrile **9a** from 6-cyanoquinoline-*N*-oxide **8**.**

In order to find a method with improved selectivity for the chlorination reaction, intermediate 2-oxo-1,2-dihydroquinoline-6-carbonitrile **10** was synthesized (Figure 23). The latter compound **10** was formed based on a method reported by Xie *et al.*, promising no formation of regioisomers, a high yield, short reaction time and a straightforward purification.<sup>126</sup> Accordingly, 6-cyanoquinoline-*N*-oxide **8** was allowed to react with 2 equivalents of methanesulfonyl chloride (MsCl) in water. The solid product **10** was filtered off and isolated in 83 % yield. Two different procedures were examined. In the first procedure, compound **10** was dissolved in dry toluene. Hereafter, 10 equivalents of phosphoryl trichloride was added, and the mixture was refluxed under argon.<sup>129</sup> In the second procedure, compound **10** was dissolved in phosphoryl trichloride and refluxed for 30 min.<sup>130</sup> Both methods revealed selective halogenation at the C2 position. However, the second method is preferred as it is less time consuming and requires a lower amount of chemicals. 2-chloroquinoline-6-carbonitrile **9** was obtained in a 72 % yield using the second method.

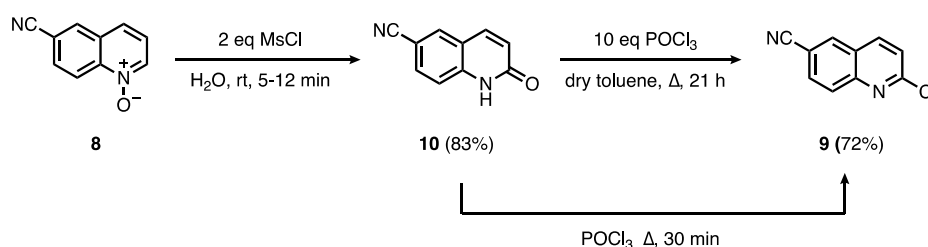


**Figure 23.** Indirect synthesis of 2-chloroquinoline-6-carbonitrile **9** from 6-cyanoquinoline-*N*-oxide **8**.

Next, 2-chloroquinoline-6-carbonitrile **9** was used to synthesize 2,2'-biquinoline-6,6'-dicarbonitrile **2** through the Ni-catalyzed reductive homocoupling previously described (section 3.1.1). The reaction scheme is depicted in Figure 24. However, the conversion of 2-chloroquinoline **9** to biquinoline **2** was sluggish, as indicated by LC-MS and full conversion could not be achieved. Instead, quinoline-6-carbonitrile **7** was formed as a side-product.

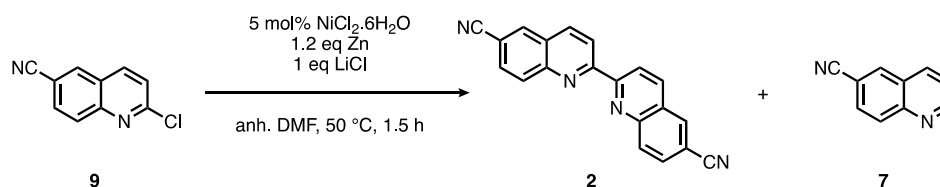


**Figure 24.** Synthesis of 2,2'-biquinoline-6,6'-dicarbonitrile **2** by the Ni-catalyzed reductive homocoupling.

As it was believed that bromo-substituted N-heterocycles displayed better activity in the Ni reductive homocoupling, the synthesis of 2-bromoquinoline-6-carbonitrile **11** was pursued (Figure 25). To this end, 2-oxo-1,2-dihydroquinoline-6-carbonitrile **10** was added to a solution of 5 equivalents *N*-bromosuccinimide (NBS) and 5 equivalents triphenylphosphine in dioxane.<sup>126</sup> However, formation of quinoline **11** could not be observed. Instead, compound **10** was transformed to quinoline-6-carbonitrile **7**.

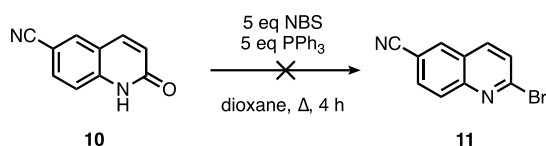


**Figure 25. Synthesis of 2-bromoquinoline-6-carbonitrile 11.**

The failed attempts to synthesize 2,2'-biquinoline-6,6'-dicarbonitrile **2**, led to another approach involving a *tert*-butoxide-mediated dimerization of 6-cyanoquinoline-*N*-oxide **8**. In previous work, this synthetic method has been applied to unsubstituted and substituted quinoline-*N*-oxides as well as pyridine-*N*-oxides, revealing moderate to high yields.<sup>131,132</sup> However, the particular dimerization of 6-cyanoquinoline-*N*-oxide **8** has not yet been performed to our knowledge. To this end, two procedures were examined (Figure 26). Following the procedure developed by Stephens *et al.*, a mixture of 6-cyanoquinoline-*N*-oxide **8** and degassed DMF was heated to 65 °C. Subsequently, 2 equivalents KO<sup>t</sup>Bu and 0.2 equivalent azobisisobutyronitrile (AIBN) were added.<sup>131</sup> However, there was no indication of biquinoline formation based on NMR and LC-MS analysis. Hereafter, the reaction was repeated using degassed 2-MeTHF instead of DMF as the solvent. The latter resulted in a mixture of 2,2'-biquinoline-6,6'-dicarbonitrile **2**, 6,6'-dicyano-2,2'-biquinoline-*N*-oxide **12**, 6-cyanoquinoline-*N*-oxide **8** and quinoline-6-carbonitrile **7**. The mole fraction of each component in the mixture is given in Table 3. The formation of quinoline-*N*-oxide and quinoline, in addition to the biquinoline, has also been reported by Stephens and co-workers, but not the formation of a biquinoline-*N*-oxide, which constituted here a large part of the mixture.

**Table 3. Composition (in mol%) of the obtained mixture in the KOtBu-mediated dimerization of 6-cyanoquinoline-*N*-oxide in 2-MeTHF, as determined by <sup>1</sup>H NMR analysis.**

Biquinoline 2	Quinoline- <i>N</i> -oxide 8	Quinoline 7	5,5'-dicyanobiquinoline- <i>N</i> -oxide 12
27	5	35	33

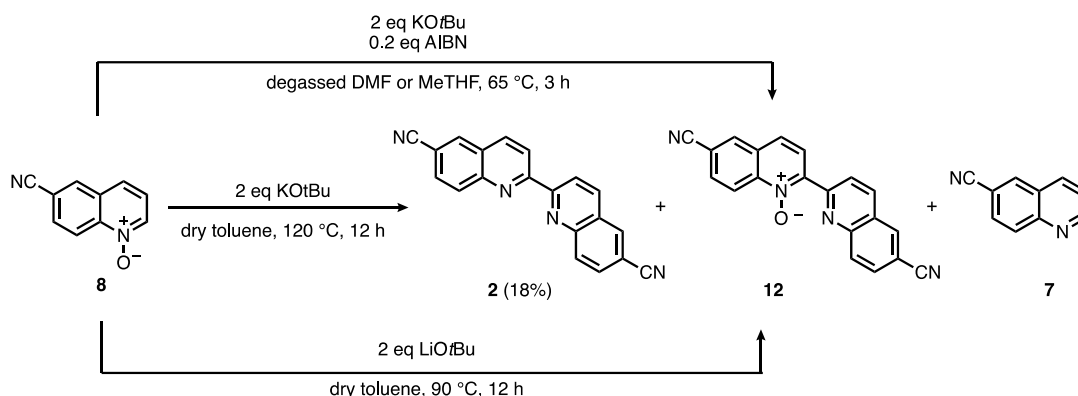


**Figure 26. Direct synthesis of 2,2'-biquinoline-6,6'-dicarbonitrile **2** from quinoline-*N*-oxide **8**.**

Figure 27 shows the mechanism proposed by Stephens and co-workers involving radical anionic intermediates. First, KOtBu deprotonates quinoline-*N*-oxide **13** and DMF **14** (or 2-MeTHF) resulting in the formation of carbanions. However, one can question if the deprotonation of DMF by KOtBu is possible as DMF is a stronger base than KOtBu. Evoniuk *et al.* suggest that, at equilibrium, a small quantity of the DMF anion is formed and stabilized by a counter cation, K<sup>+</sup>. After, the DMF anion oxidizes and forms a DMF radical accelerated by means of AIBN.<sup>133</sup> The formed carbanions act as electron donors and give rise to radical anion **15**. The latter reacts with quinoline-*N*-oxide **13** forming another radical anion **16**. This radical anion **16** is converted to biquinoline **19** via two possible routes. The first route involves the formation of anion **17** and the subsequent KOtBu mediated elimination of ROH and hydroxide. The second route proceeds through the formation of dianion **20** and subsequent KOtBu mediated elimination of hydroxide. The authors reported that quinoline may originate from either the reduction of quinoline-*N*-oxide **13** with R<sup>-</sup> or as a result of the reaction between KOtBu and quinoline-*N*-oxide **13** with the formation of *tert*-butyl peroxide. Additionally, upon

usage of 2-MeTHF as the solvent, regeneration of quinoline-*N*-oxide **13** would be possible through the deprotonation of 2-MeTHF with anionic quinoline-*N*-oxide.

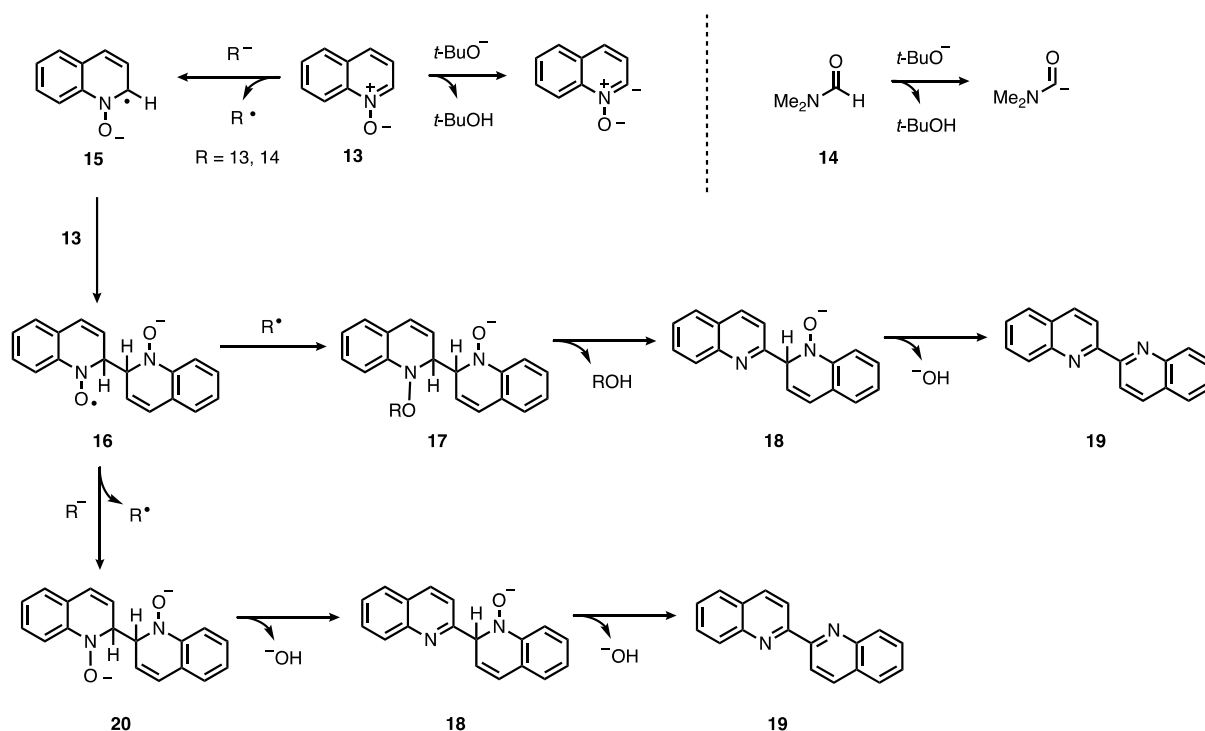


**Figure 27. Proposed mechanism by Stephens *et al.* for the *tert*-butoxide mediated dimerization of quinoline-*N*-oxides.<sup>131</sup>**

In an attempt to reduce the formation of quinoline-6-carbonitrile **7**, the procedure developed by Wang *et al.* was adapted. Herein, 6-cyanoquinoline-*N*-oxide **8** was dissolved in dry toluene at a temperature of 120 °C. Next, 2 equivalents of  $\text{KO}t\text{Bu}$  were added, under nitrogen atmosphere (Figure 26).<sup>132</sup> Similarly, the reaction was also performed with 2 equivalents of  $\text{LiO}t\text{Bu}$  at 90 °C instead of 120 °C.<sup>134</sup> Both resulted in the formation of 2,2'-biquinoline-6,6'-dicarbonitrile **2**, 6,6'-dicyano-2,2'-biquinoline-*N*-oxide **12** and quinoline-6-carbonitrile **7**. Table 4 displays the mole fraction of each component in the mixture of the  $\text{LiO}t\text{Bu}$  mediated dimerization. Finally, building block **2** was obtained as a solid and was purified by successive filtration and washing steps in a 18% yield. However, this yield may not be representative as, prior to purification, no deoxygenation was carried out to convert 6,6'-dicyano-2,2'-biquinoline-*N*-oxide **12** to 2,2'-biquinoline-6,6'-dicarbonitrile **2**.

**Table 4. Composition (in mol%) of the obtained mixture in the LiOtBu-mediated dimerization of 6-cyanoquinoline-*N*-oxide in toluene, as determined by <sup>1</sup>H NMR analysis.**

Biquinoline <b>2</b>	Quinoline- <i>N</i> -oxide <b>8</b>	Quinoline <b>7</b>	5,5'-dicyanobiquinoline- <i>N</i> -oxide <b>12</b>
59	0	25	16

In general, monitoring the synthesis of building block **2** by LC-MS proved to be difficult, as this compound showed only a weak to no signal in mass spectroscopy. This may be attributed to ion suppression, a commonly found problem in LC-MS analysis.<sup>135,136</sup> However, there is still limited knowledge on the underlying mechanisms and it is difficult to determine the particular cause of ion suppression for the biquinoline building block. In addition, <sup>1</sup>H NMR signals of quinoline **8**, biquinoline **2** and the corresponding *N*-oxides all appear in the range of 7.5-9 ppm, which made it often difficult to assign a signal to the corresponding proton.

### 3.1.3 Synthesis of quinoline-2,6-dicarbonitrile **3**

Since a synthetic route towards 6-cyanoquinoline-*N*-oxide **8** was established, this compound could give access to another building block, i.e. quinoline-2,6-dicarbonitrile **3**. Trimerization of this building block will provide a CTF with tridentate coordination sites. Having an additional coordination site compared to bipyridine ligands, terpyridine derivatives act as Pincer ligands and give rise to firmer metal complexes.<sup>137</sup>

In order to cyanate 6-cyanoquinoline-*N*-oxide **8** selectively at C2, an adapted procedure based on previous work was applied.<sup>138</sup> However, as we found that cyano-substituted *N*-heterocycles were more difficult to follow up, the reaction was first tested with unsubstituted quinoline-*N*-oxide. Accordingly, quinoline-*N*-oxide was dissolved in MeOH and was treated with 2 equivalents of KCN and benzoyl chloride. The use of cyanide may involve the evolution of poisonous hydrogen cyanide. Therefore, the headspace of the reaction flask was continuously flushed with a gentle flow of nitrogen gas and directed to two consecutive gas washing bottles containing a 1 M KOH and a 1 M Na<sub>2</sub>S<sub>2</sub>O<sub>3</sub> aqueous solution. Using benzoyl chloride as activating agent resulted in the formation of several side-products including 2-(benzoyloxy)-6-cyanoquinoline-*N*-oxide. Replacing benzoyl chloride by acetyl chloride likewise led to the formation of the side-product 2-(acetoxy)-6-cyanoquinoline-*N*-oxide. Hence both

activators delivered analogous results. Nonetheless, using acetyl chloride as activator led to a better removal of the excess and the formed acetic acid in the work-up step compared to benzyl chloride. As a result, a clearer  $^1\text{H}$  NMR spectrum was obtained. Additionally, acetyl chloride is less hazardous than benzoyl chloride. Therefore, acetyl chloride together with KCN were added to 6-cyanoquinoline-*N*-oxide **8**, forming a suspension in MeOH (Figure 28). With 2 equivalents KCN and acetyl chloride the conversion was not complete after 25 h as 6-cyanoquinoline-*N*-oxide **8** was still present. To this end, an extra equivalent of both KCN and acetyl chloride were added, which pushed the conversion to completeness after 4 more hours. Finally, water was added to the reaction, quinoline-2,6-dicarbonitrile **3** was filtered off and thoroughly rinsed with water. A yield of 58 % was obtained. In the future, recrystallization of the filtrate in MeOH could further enhance the yield.

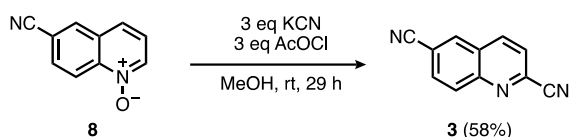


**Figure 28. Synthesis of quinoline-2,6-dicarbonitrile 3.**

Sufficient product was obtained after the reaction. Nevertheless, there is still room for optimization. A plausible reaction mechanism is depicted in Figure 29. The last step consists of a deprotonation, restoring the aromaticity. By adding a stronger base, e.g. KOtBu, deprotonation could be enhanced possibly leading to a faster conversion with less equivalents of reactants and a higher yield.

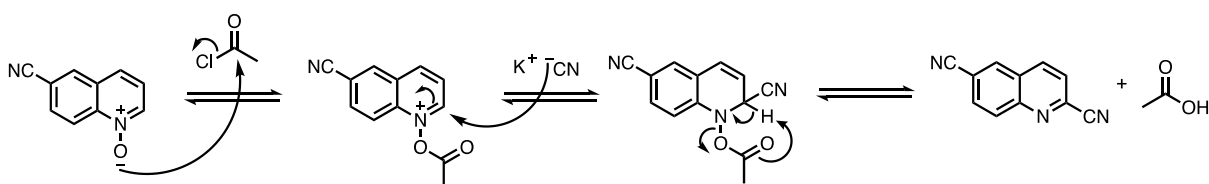


**Figure 29. Plausible mechanism for the cyanation reaction with acetyl chloride and KCN.**



## 3.2 CTF synthesis and post-synthetic metalation

Building block **1** and **3** were used to synthesize the corresponding CTFs, the 2,2'-bipyridine-5,5'-dicyanitrile-based CTF **21** (bipyCTF) and the quinoline-2,6-dicyanitrile-based CTF **22** (quinCTF) respectively. To this end, the ionothermal CTF synthesis with ZnCl<sub>2</sub> was performed. In order to investigate the structure and properties of the obtained CTFs, several types of analysis were carried out. Hereafter, rhodium was immobilized on the bipyCTF **21** to generate the heterogeneous Rh@bipyCTF catalyst.

### 3.2.1 Synthesis of the 2,2'-bipyridine-5,5'-dicyanitrile-based CTF **21**

In the literature review, the ionothermal cyclotrimerization of aromatic nitriles, along with its corresponding reaction mechanism, has been described (section 2.1.2.1). Important parameters for this method are the reaction temperature and quantities of ZnCl<sub>2</sub>. In the selection of these parameters, a trade-off has to be made between porosity of the structure and preservation of the structural integrity of the building blocks. In general, a temperature of 400 °C is applied to ensure complete polymerization and allow a certain degree of reversibility in the cyclotrimerization reaction. Nevertheless, reversibility turned out to be quite low which is evidenced by the formation of amorphous black materials. Increasing the temperature above 400 °C would increase the reversibility of triazine formation but would additionally induce irreversible side reactions leading to the partial decomposition of nitrile functionalities causing nitrogen loss and structural defects. On the other hand, this thermal decomposition is accompanied with higher specific surface areas, introduction of mesopores and higher pore volumes. Decreasing the temperature would avoid irreversible side reactions. However, at temperatures below 400 °C, the polymerization reaction is not ensured leading to the formation of aryl-triazine oligomers with low specific surface areas and pore volumes. Furthermore, ZnCl<sub>2</sub> appears to encourage the same effects as the temperature. Higher equivalents of ZnCl<sub>2</sub> come along with higher specific surface areas and pore volumes. For the CTF synthesis with 1,4-dicyanobenzene as monomer (CTF-1), 1 equivalent of ZnCl<sub>2</sub> was sufficient to yield a specific surface area of 791 m<sup>2</sup> g<sup>-1</sup> and a total pore volume of 0.40 cm<sup>3</sup> g<sup>-1</sup>, as reported by Antonietti *et al.*<sup>42</sup>

In this light, the 2,2'-bipyridine-5,5'-dicyanitrile-based CTF **21** was prepared by the ionothermal method heating building block **1** in presence of 5 equivalents  $\text{ZnCl}_2$  at  $400\text{ }^\circ\text{C}$  for 48 hours (Figure 30).<sup>22</sup> As expected, a resulting black material was obtained. Consecutive filtration and washing steps were carried out to remove  $\text{ZnCl}_2$ , unreacted building blocks and other impurities from the pores. Finally, the bipyCTF **21** was isolated in an 80-87% yield. Remarkably is the higher quantity of  $\text{ZnCl}_2$  needed than for the synthesis of CTF-1. This can be explained by the presence of nitrogen atoms in the pyridine rings.  $\text{ZnCl}_2$ , acting both as solvent and catalyst, has higher affinity for these pyridinic nitrogen atoms leaving less  $\text{ZnCl}_2$  available for the cyclotrimerization of the nitrile functionalities.

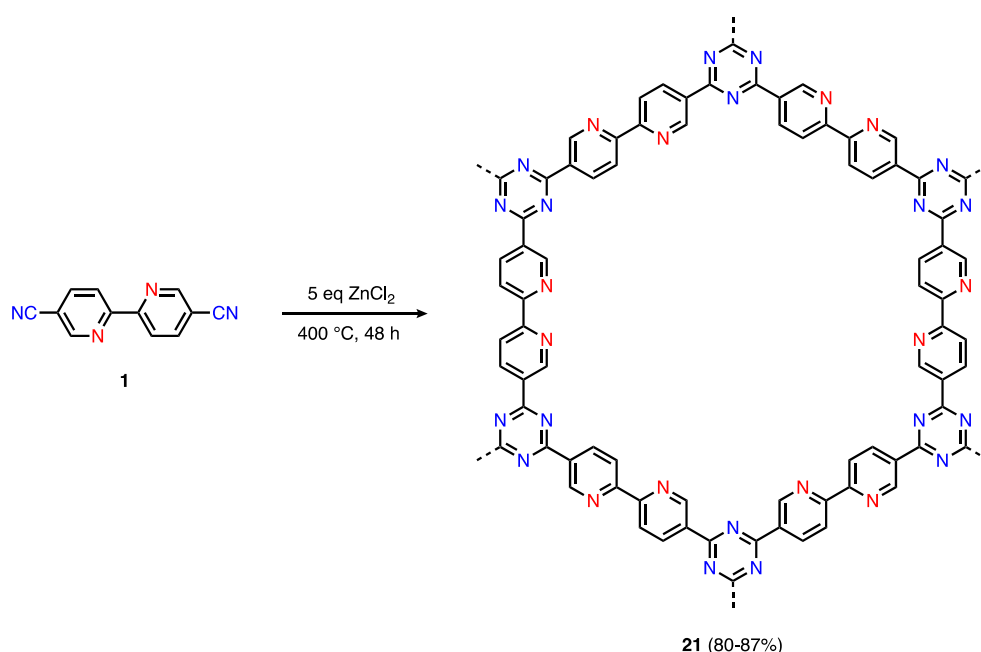


**Figure 30. Ionothermal synthesis of bipyCTF 21.**

The specific surface area and porosity of the formed bipyCTF **21** was checked by means of nitrogen sorption analysis and calculated based on the Brunauer-Emmett-Teller (BET) equation. The adsorption isotherm is depicted in Figure 31. The multiple point BET plot is given in Figure 51 in Appendix A. The adsorption isotherm shows that, at low relative pressure, the volume of  $\text{N}_2$  gas adsorbed by the bipyCTF **21** almost reaches saturation (type 1 isotherm). This type 1 isotherm indicates the formation of micropores (<2 nm) in the framework. The mean pore diameter is 1.95 nm indicating again micropore formation. The bipyCTF **21** has a BET surface area of  $531\text{ m}^2/\text{g}$  and a total pore volume of  $0.24\text{ cm}^3/\text{g}$  which are relatively low

compared to the values reported in the literature ( $787 \text{ m}^2/\text{g}$  and  $0.4 \text{ cm}^3/\text{g}$ ).<sup>139</sup> This could be due to the scale on which the bipyCTF was synthesized. Building block **1** was added at a relatively large quantity of 500 mg, resulting in a less homogeneous mixture of the monomer and  $\text{ZnCl}_2$ . Therefore, the reaction was repeated on smaller scale (180 mg) which resulted in a BET specific surface area of  $654 \text{ m}^2/\text{g}$  and a total pore volume of  $0.25 \text{ cm}^3/\text{g}$ . The multiple point BET plot is depicted in Figure 52 in Appendix A.

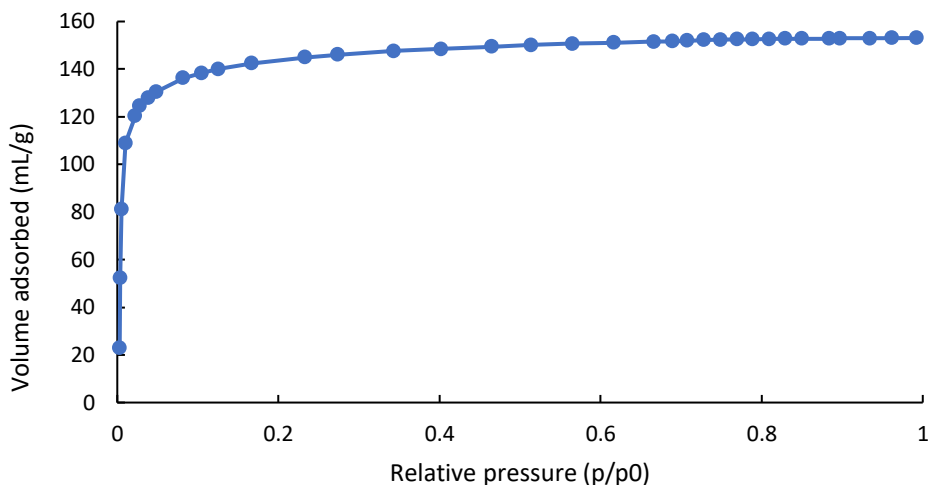


**Figure 31. Adsorption isotherm for the bipyCTF.**

On the other hand, in an attempt to further improve the porosity of the framework, bipyCTF **21** was also prepared by a salt templated method. This method makes use of alkali salts such as  $\text{NaCl}$  or  $\text{KCl}$  which have a much higher melting point than  $\text{ZnCl}_2$  and remain solid during the ionothermal synthesis. Hence, the CTF framework will polymerize around the alkali salt template. In previous work, the salt templated synthesis was performed to CTF-1 leading to the formation of mesopores, aside from micropores, and increased total pore volume in the structure. Mesoporous structures are characterized by type IV adsorption isotherms showing a typical hysteresis loop. Alternatively, synthesis at more elevated temperatures could likewise lead to mesoporosity and enhanced total pore volume. However, the salt templated method provides a milder alternative as it causes less nitrogen loss and structural defects.<sup>52</sup> Accordingly, building block **1** (80 mg) was heated in presence of 5 equivalents  $\text{ZnCl}_2$  and 2.1 equivalents  $\text{NaCl}$  or  $\text{KCl}$  first at  $350 \text{ }^\circ\text{C}$  for 48 hours and subsequently at  $450 \text{ }^\circ\text{C}$  for 15 hours or 24 hours.<sup>52</sup> Hence, the salt templated synthesis is performed at two distinct temperatures. At the first reaction temperature, oligomers are formed. At the second reaction

temperature, the oligomers are allowed to completely polymerize. Again, the bipyCTF **21** was obtained as a black material. For each reaction condition, the resulting specific surface areas and total pore volumes are shown in Table 5. The adsorption isotherms are given in Figure 32. The corresponding multiple point BET plots are depicted in Figures 53 to 56 in Appendix A.

**Table 5. Specific surface areas and pore volumes of bipyCTF for different reaction conditions in the salt templated ionothermal method.**

Entry	Time of T <sub>2</sub> <sup>a</sup> (hours)	Alkali salt	Specific surface area (m <sup>2</sup> /g)	Total pore volume (cm <sup>3</sup> /g)
Default <sup>b</sup>	48	-	654	0.25
A	15	NaCl	790	0.31
B	15	KCl	630	0.31
C	24	NaCl	524	0.20
D	24	KCl	565	0.30

<sup>a</sup> T<sub>2</sub> = 450 °C

<sup>b</sup> The conventional method, i.e. T<sub>2</sub> = T<sub>1</sub> = 400 °C, 5 eq. ZnCl<sub>2</sub>, no alkali salt.

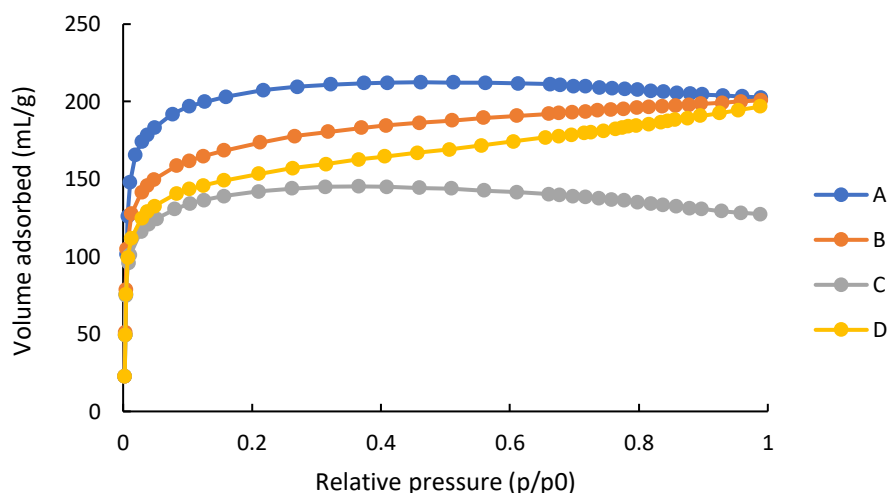


**Figure 32. Adsorption isotherms for the bipyCTF synthesized by the salt templated method at different reaction conditions.**

One can see from Table 5 that the increase in specific surface area and pore volume was not significant for the salt templated synthesis in comparison to the literature values obtained for the conventional ionothermal synthesis (787 m<sup>2</sup>/g and 0.4 cm<sup>3</sup>/g).<sup>139</sup> Additionally, type I

isotherms are obtained instead of expected type IV isotherms, indicating no formation of mesopores.

As mentioned before, aromatic heterocyclic nitriles begin to decompose at temperatures above 400°C resulting in the loss of nitrogen and leading to more structural defects. To investigate this phenomenon, an elemental analysis was carried out on the bipyCTF synthesized at 400 °C. The experimentally obtained values for C, H, N and the C/N ratio were compared to the theoretically calculated values (Table 6). The experimentally obtained N value is lower and the C/N ratio is higher than the calculated values. The latter confirms the expected partial decomposition during CTF synthesis.

**Table 6. Comparison experimental and theoretical elemental composition (in wt%) of bipyCTF.**

			wt% C	wt% H	wt% N	C/N
<b>bipyCTF</b>	<b>400 °C</b>	theoretical	69.90	2.93	27.17	2.57
		experimental	73.71	4.17	22.12	3.33

During cyclotrimerization, the cyano groups of the building blocks are transformed into triazine moieties resulting in the formation of the desired CTF. In order to evaluate this cyclotrimerization reaction, an FTIR analysis was performed on building block **1** as well as the bipyCTF **21**. Upon complete polymerization, the FTIR spectrum of the bipyCTF **21** will lack the stretching vibration band at 2234 cm<sup>-1</sup>, typical for cyano groups. This is illustrated in Figure 33, proving quasi complete polymerization of the building blocks. Nevertheless, the absorption bands corresponding to the formed triazine moieties at 1315-1352 cm<sup>-1</sup> and 1507-1535 cm<sup>-1</sup> are not visible.

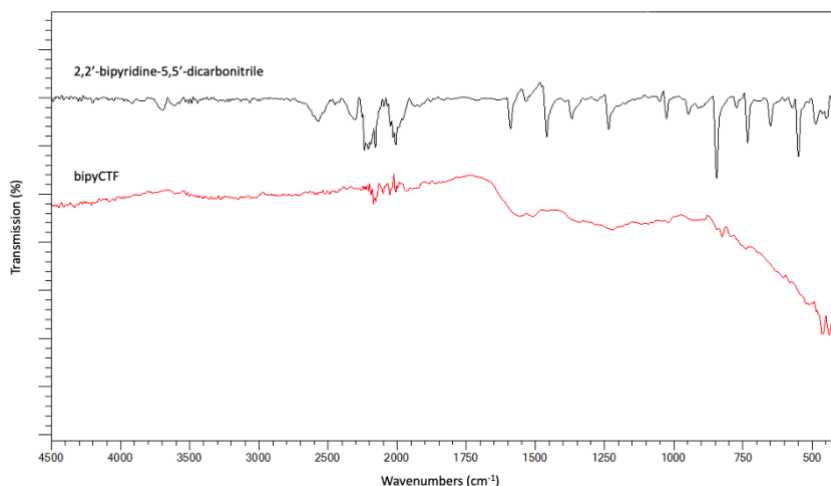


**Figure 33. FTIR analysis for building block 1 compared to bipyCTF.**

Finally, the structural ordering of the bipyCTF was evaluated by Powder X-Ray Diffraction (PXRD) analysis (Figure 34). As expected for amorphous structures, a broad diffraction pattern is obtained revealing no long-range ordering in the structure. However, at  $2\theta$  equal to  $25^\circ$ , a broad peak is formed suggesting a certain degree of 'graphitic' layer stacking.<sup>143</sup>

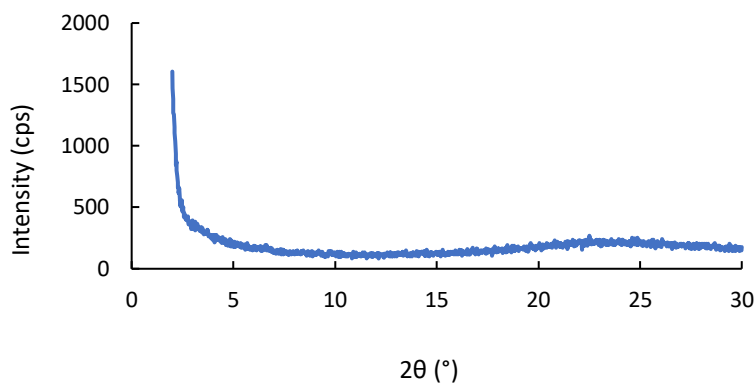


**Figure 34. Powder XRD pattern of bipyCTF.**

### 3.2.2 Synthesis of the quinoline-2,6-dicyanitrile-based CTF **22**

The quinoline-2,6-dicyanitrile-based CTF **22** was similarly prepared by the ionothermal synthesis method heating building block **3** in presence of 5 equivalents  $\text{ZnCl}_2$  at  $450^\circ\text{C}$  for 48 hours (Figure 35).<sup>22</sup> As for the bipyCTF, a resulting black material was produced.

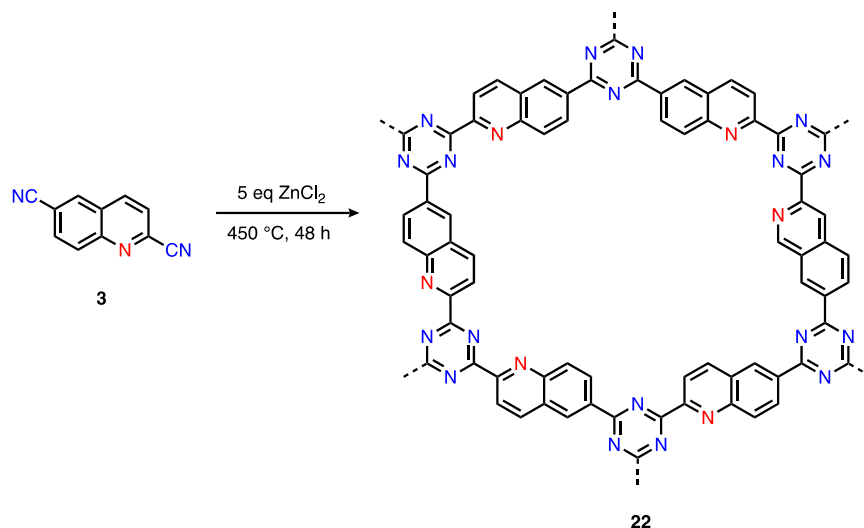


**Figure 35. Ionothermal synthesis of quinCTF 22.**

Again, an adsorption type I isotherm was obtained illustrating the formation of micropores (Figure 36). The multiple point BET plot is shown in Figure 57 in Appendix A. The BET specific surface area and total pore volume were calculated at 1087 m<sup>2</sup>/g and 0.49 cm<sup>3</sup>/g, respectively. These values are significantly higher than the values obtained for the bipyCTF synthesized at a temperature of 400 °C by the conventional ionothermal method and the bipyCTF synthesized at 450 °C by the salt templated method.

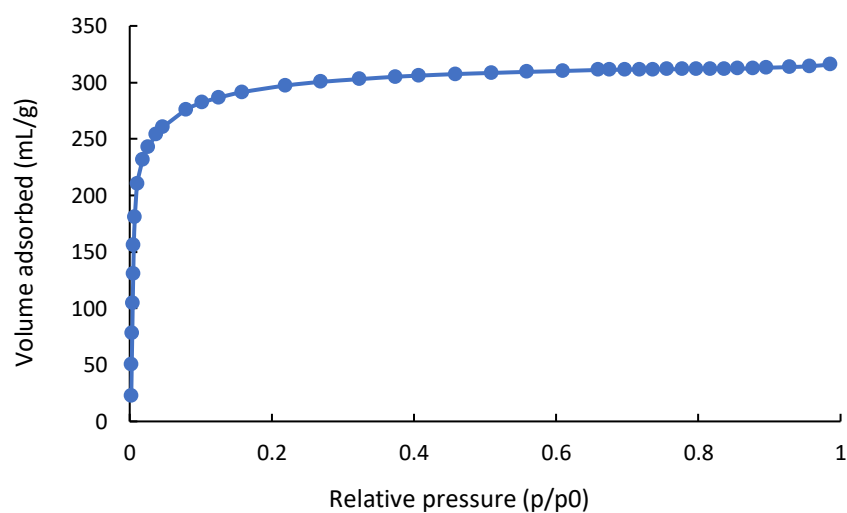


**Figure 36. Adsorption isotherm of quinCTF.**

An elemental analysis was conducted, however due to technical issues no data was obtained. A second elemental analysis was planned but couldn't proceed due to SARS-CoV-2 measures.

The comparison between the FTIR spectra of the quinCTF **22** and building block **3** unraveled the complete polymerization of the monomers (Figure 37). The stretching vibration band at  $2240\text{ cm}^{-1}$  disappeared in the spectrum of the quinCTF. However, as for the bipyCTF, the characteristic triazine absorption bands at  $1315\text{-}1352\text{ cm}^{-1}$  and  $1507\text{-}1535\text{ cm}^{-1}$  are not visible.

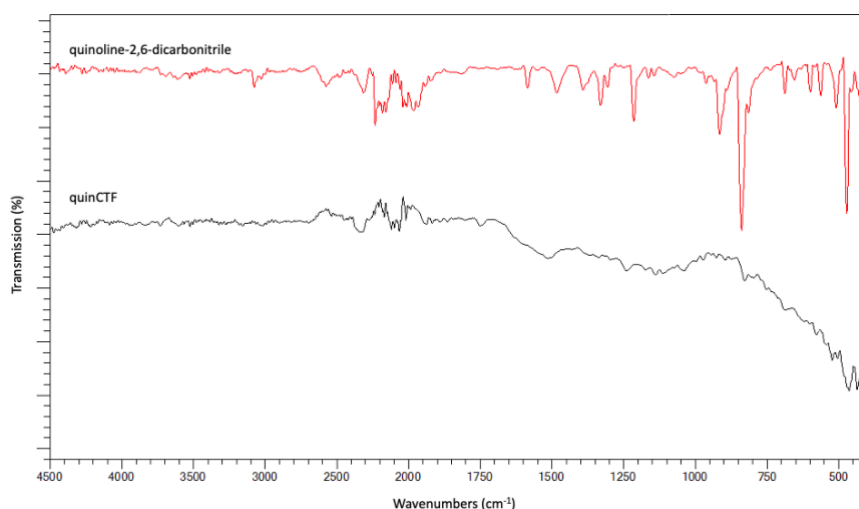


**Figure 37.** FTIR analysis for building block **2** compared to quinCTF.

The amorphous structure of the CTF, manifested through its black color, was confirmed by PXRD analysis revealing a broad diffraction pattern (Figure 38). A slightly higher intensity obtained at  $25^\circ$  indicates stacking between the different layers.



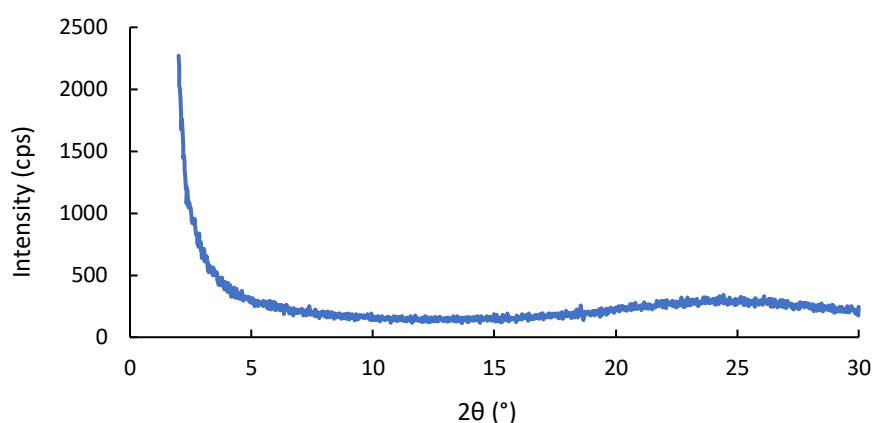


**Figure 38. Powder XRD pattern of quinCTF.**

### 3.2.3 Post-synthetic metalation of the 2,2'-bipyridine-5,5'-dicyanitrile-based CTF

Owing to their porous structure and high nitrogen content, CTFs can harbor metals for the development of heterogeneous catalysts. In previous work, the bipyCTF has been used to immobilize transition metals such as Ir, Ru and Rh for the catalytic transfer hydrogenation reaction of carbonyl compounds.<sup>63,65</sup> Herein, the bipyCTF was used to coordinate Rh for the catalytic transfer hydrogenation of N-heterocycles. To this end,  $[\text{Cp}^*\text{RhCl}_2]_2$  was added to bipyCTF **21** in dry MeOH and was refluxed for 16 hours under argon (Figure 39).<sup>141</sup> Afterwards, the obtained Rh@bipyCTF **23** was filtered and washed with MeOH,  $\text{CHCl}_3$  and  $\text{Et}_2\text{O}$  to remove non-bonded or weakly bonded rhodium complex.

The amount of added  $[\text{Cp}^*\text{RhCl}_2]_2$  was calculated to yield a loading of 25 g Rh/kg (0.24 mmol Rh/g). The actual Rh-loading on the bipyCTF was found to be only 10.9 g Rh/kg (0.11 mmol Rh/g), as determined by means of Induced Coupled Plasma Optical Emission Spectrometry (ICP-OES). This suggests that only a small part of the added  $[\text{Cp}^*\text{RhCl}_2]_2$  binds to the framework. Moreover, the adsorption isotherms of Rh@bipyCTF **23** and the previously obtained bipyCTF **21** were compared (Figure 40). The multiple point BET plot is given in Figure 58 in Appendix A. For complex **23**, the nitrogen adsorption isotherm indicates that only a low volume of  $\text{N}_2$  is adsorbed by the material. Furthermore, the BET specific surface area and total pore volume decreased from 531 to 103  $\text{m}^2/\text{g}$  and from 0.24 to 0.03  $\text{cm}^3/\text{g}$ , respectively. These

low values suggest that the pores are not only occupied with rhodium complex, but also with solvent molecules. The latter could be better removed by extending the time of vacuum drying prior to the analysis. However, due to the stop of the lab activities (SARS-CoV-2) this measurement could not be repeated.

In order to enhance the metal loading, an adapted synthesis method was applied wherein an adapted solvent mixture was used and the reflux time was prolonged. Accordingly,  $[\text{Cp}^*\text{RhCl}_2]_2$  and bipyCTF **21** were added in a 1:1 mixture of dry MeOH and  $\text{CHCl}_3$  and were refluxed for 24 hours under argon. The ICP-OES analysis revealed a loading of 22.9 g Rh/kg (0.22 mmol Rh/g) this time, indicating a significant improvement compared to the first method.

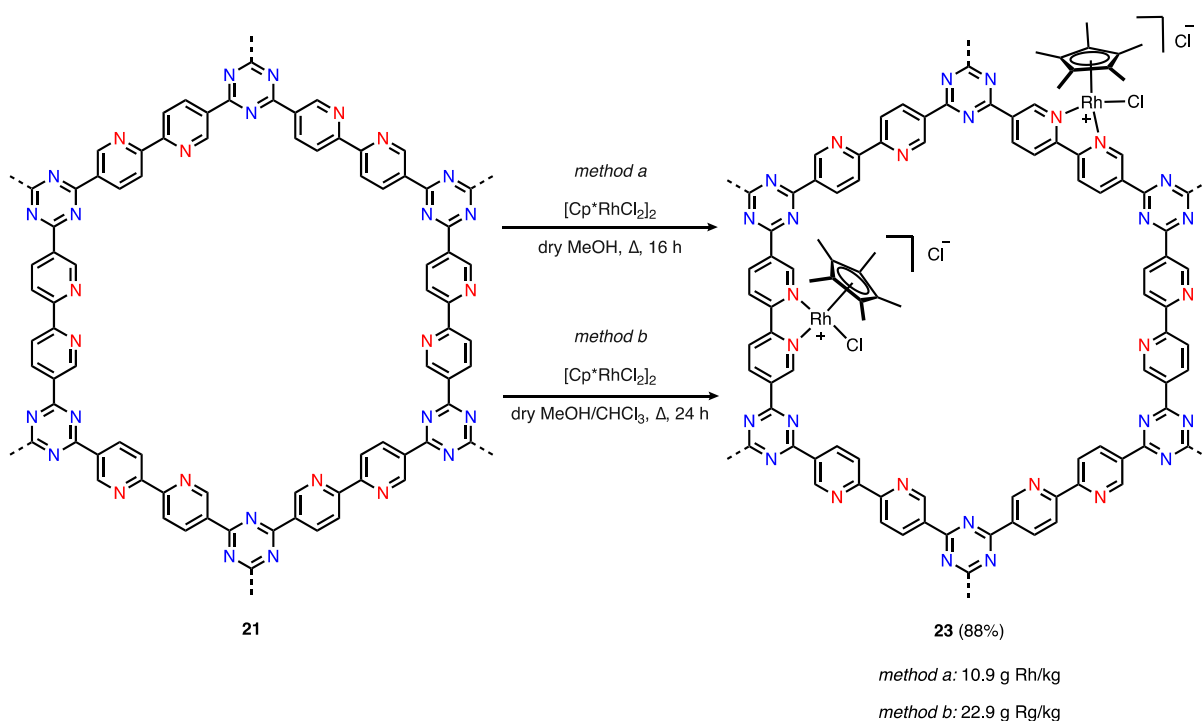


**Figure 39.** Post-synthetic metalation of bipyCTF **21** to Rh@bipCTF **23**.

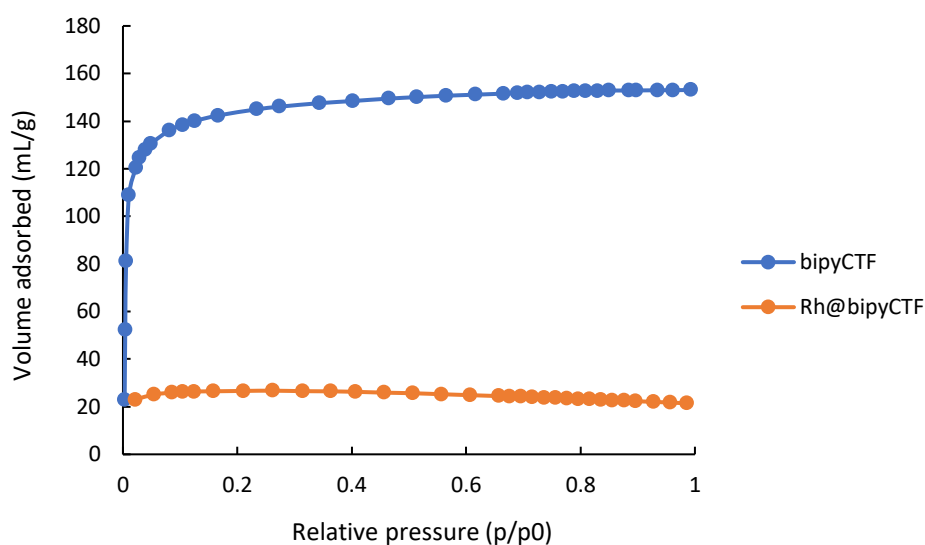


Figure 40. Adsorption isotherm of Rh@bipyCTF compared to bipyCTF.

### 3.3 Catalytic transfer hydrogenation of N-heterocycles

The hydrogenation reaction provides a simple and efficient reaction to reduce several unsaturated substrates. There are different kinds of hydrogenation reactions including direct hydrogenation and catalytic transfer hydrogenation. The latter represents a safer alternative by avoiding the use of pressurized H<sub>2</sub> gas and using an organic hydrogen donor instead. Therefore, this reaction gained increasing interest during the past years. However, most of the research was dedicated to the transfer hydrogenation of carbonyl compounds. The goal of this Master's thesis was to carry out the Rh@bipyCTF-catalyzed transfer hydrogenation reaction on N-heterocycles, which is a rather unexplored substrate class in this reaction.

First of all, the transfer hydrogenation was tested in a homogeneous mode to confirm the reported findings by Zhang *et al.*<sup>107</sup> The synthesis of the homogeneous rhodium catalyst proceeded through the addition of [Cp\*RhCl<sub>2</sub>]<sub>2</sub> in dry MeOH and subsequent treatment with 2,2'-bipyridine. The mixture was stirred for 1 hour at room temperature and the homogeneous catalyst, [Cp\*Rh(bpy)Cl]Cl, was recovered by recrystallization in diethyl ether. A yield of 84% was achieved. Hereafter, the homogeneous transfer hydrogenation reaction was performed. To this end, 0.25 mol% [Cp\*Rh(bpy)Cl]Cl and 2-methylquinoxaline **24** were added to a 2 M HCOONa/HCOOH aqueous solution at pH 4.4 and heated to 80 °C (Figure 41).

Indeed, as claimed by Zhang and co-workers, the transfer hydrogenation reaction completed after 2 h and 2-methyl-1,2,3,4-tetrahydroquinoxaline **25** was obtained in a quantitative yield. Furthermore, the air stability of the catalyst was confirmed, since the reaction was not operated under inert atmosphere.

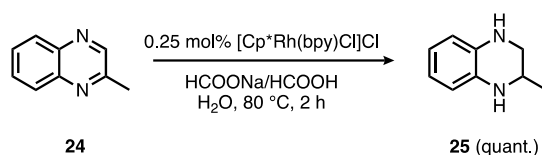


**Figure 41. Rhodium-catalyzed transfer hydrogenation of 2-methylquinoxaline **24**.**

Next, the heterogeneous Rh@bipyCTF-catalyzed transfer hydrogenation was carried out. Again, 2-methylquinoxaline **24** was used as the model substrate. The same reaction procedure as for the homogeneous rhodium catalyzed transfer hydrogenation was followed. Accordingly, Rh@bipyCTF (0.25 mol% Rh) and 2-methylquinoxaline **24** were added to a 2 M HCOONa/HCOOH solution at pH 4.4 and heated to 80 °C in air.

The transfer hydrogenation was complete after 2 h 15 min reaching a quantitative yield. Hence, a low quantity of catalyst is sufficient to complete the transfer hydrogenation reaction. In addition, the reaction turned out to be air stable. It was proven that the catalytic activity of the homogeneous complex is preserved after immobilization on the bipyCTF supporting material.

To follow up the reaction, samples were taken at different time intervals and analyzed by means of <sup>1</sup>H NMR. The kinetic profile was obtained by integrating the methyl protons of both substrate **24** ( $\delta_{\text{H}}$  2.79 ppm, s) and product **25** ( $\delta_{\text{H}}$  1.19 ppm, d), (Figure 42). To investigate the possible reversibility of the reaction and the byproduct formation, the reaction was allowed to continue for 18 h. The transfer hydrogenation of methylquinoxaline **24** was concluded to be irreversible. However, a side product, identified as 2-methyl-3,4-dihydroquinoxaline-1(2H)-carbaldehyde **26**, was observed in a 1:5 ratio with respect to the desired product after 18 h reaction. This was probably attributed to the reaction of formic acid with the generated 2-methyl-1,2,3,4-tetrahydroquinoxaline **25** (Figure 43).<sup>142</sup>

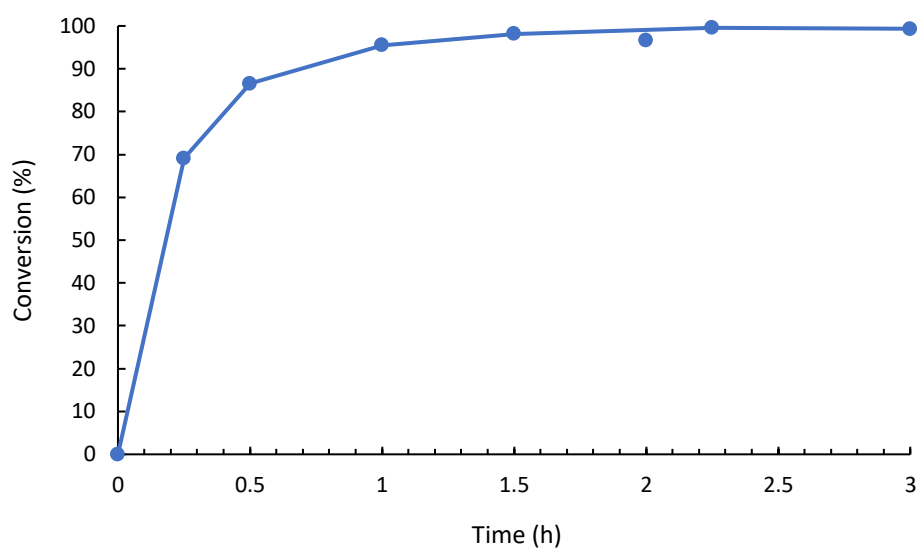


**Figure 42.** Kinetic profile for the Rh@bipyCTF-catalyzed transfer hydrogenation of 2-methylquinoxaline.

In order to ensure that only the Rh@bipyCTF resulted in the catalytic transfer hydrogenation of 2-methylquinoxaline **24**, two control experiments were carried out. For the first control experiment, the model substrate **24** was added to a 2 M aqueous HCOONa/HCOOH solution (pH 4.4) and stirred for 16 hours at 80 °C. No transfer hydrogenation occurred as was confirmed by  $^1\text{H}$  NMR. This reveals that a catalyst is required for the transfer hydrogenation to proceed. In the second control experiment, bipyCTF without rhodium was added to compound **24** in a 2 M aqueous HCOONa/HCOOH solution (pH 4.4) and stirred for 8 hours at 80 °C. Again, no hydrogenation product was formed illustrating the essential role of the anchored rhodium complex in the transfer hydrogenation reaction.

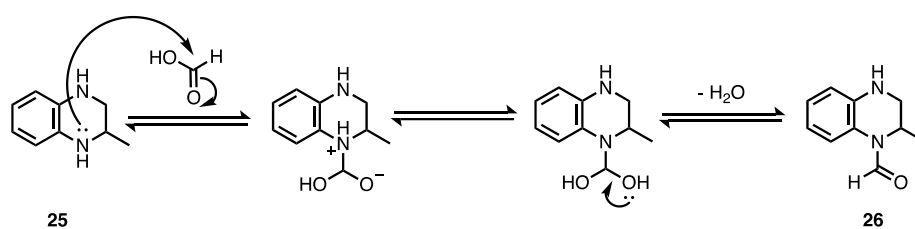


**Figure 43.** N-formylation reaction of 2-methyl-1,2,3,4-tetrahydroquinoxaline **25** with formic acid yielding 2-methyl-3,4-dihydroquinoxaline-1(2H)-carbaldehyde **26**.

## 4 Future work and perspectives

Some experiments and analyses were not completed as laboratory activities had to be terminated in view of SARS-CoV-2 measures. Nevertheless, the performed experiments and literature research allowed to gain knowledge on building block synthesis, CTF design and development, and transfer hydrogenation of N-heterocycles. The achieved know-how encountered problems and opportunities for future research will be highlighted in this chapter.

### 4.1 Synthesis of nitrogen-containing aromatic building blocks

The biquinoline building block **2** was synthesized through the LiOtBu mediated dimerization of 6-cyanoquinoline-*N*-oxide **8** (section 3.2.1). However, the overall yield was low and a considerable amount of quinoline was formed. In order to get more insight on the dimerization reaction, different reaction conditions were planned to be tested, based on the previous work of Stephens *et al.*<sup>131</sup> For each reaction condition, the yield of the formed compounds (2,2'-biquinoline-6,6'-dicarbonitrile **2**, 6,6'-dicyano-2,2'-biquinoline-*N*-oxide **12**, quinoline-6-carbonitrile **7**, 6-cyanoquinoline-*N*-oxide **8**) were to be calculated. Alternatively, biquinoline **2** could be synthesized through a different synthesis route as proposed in Figure 44.

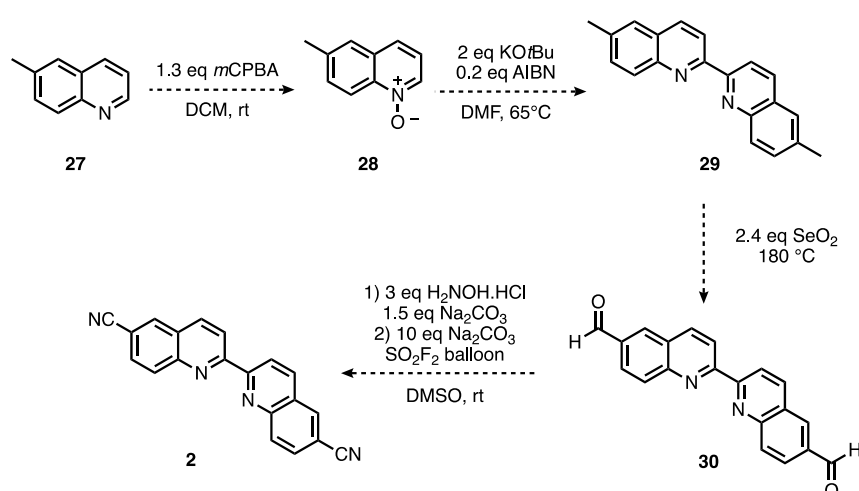
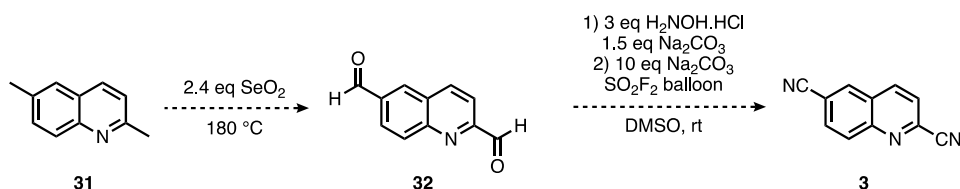


Figure 44. Alternative reaction pathway for the synthesis of 2,2'-biquinoline-6,6'-dicarbonitrile **2**.

Herein, dimerization is performed on 6-methylquinoline-*N*-oxide **28** as Stephens and co-workers achieved to synthesize 6,6'-dimethyl-2,2'-biquinoline **29** in an 85% yield.<sup>131</sup> Afterwards, the methyl groups are transformed to aldehydes through the oxidation with SeO<sub>2</sub>. The latter has been briefly tested on a small scale (100 mg) with 6-methylquinoline **27**, just before laboratory activities were stopped. First, the reaction was performed with 0.5 equivalent SeO<sub>2</sub> at 160 °C. However, there was no complete conversion and quinolin-6-ylmethanol was formed as a side-product. Hereafter, the procedure was adapted with 1.2 equivalents of SeO<sub>2</sub> at 180 °C leading to complete conversion without side-product formation. Next, the aldehydes are transformed to nitriles based on the work of Fang and Qin.<sup>143</sup> Their procedure claims high yields for a broad substrate scope including nitrogen heterocyclic aldehydes.

Furthermore, the synthesis of quinoline-2,6-dicarbonitrile **3** was intended to be optimized. As the mechanism suggests (Figure 29, section 3.1.3), adding a strong base, such as KO<sup>t</sup>Bu, could enhance deprotonation at the C2-position. On the other hand, similarly to the biquinoline building block, one could oxidize 2,6-dimethylquinoline **31** to quinoline-2,6-dicarbaldehyde **32** and subsequently obtain quinoline-2,6-dicarbonitrile **3** (Figure 45). In this way, the reaction pathway would be reduced to two steps instead of four.



**Figure 45. Alternative reaction pathway for the synthesis of quinoline-2,6-dicarbonitrile **3**.**

Upon connection of building block **3** into quinCTF **22**, the 1,3,5-triazine moiety can either be surrounded by two quinoline nitrogens, one or none, as shown in Figure 35 (section 3.2.2). However, this means that tridentate, bidentate as well as monodentate coordination sites are created within the CTF structure. Therefore, care should be taken in the design of future building blocks with respect to their functionalities and geometries in order to reduce the possibility of several CTF outcomes and to obtain materials with uniform catalytic sites. For example, to increase the amount of tridentate coordination sites within the CTF structure,

quinoline-2,6-dicarbonitrile **3** could be substituted by 1,5-naphthyridine-2,6-dicarbonitrile **33** (Figure 46).

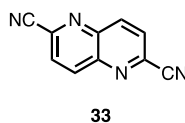


**Figure 46. Nitrogen-containing building block 1,5-naphthyridine-2,6-dicarbonitrile 33.**

Furthermore, by designing building blocks with other functionalities, one could develop CTFs that serve as organocatalysts, rather than solely a support material, avoiding the use of transition metals.

## 4.2 CTF synthesis and post-synthetic metalation

The salt templated synthesized bpyCTFs showed no significant increase in specific surface area and total pore volume in comparison to the conventional ionothermal synthesized bpyCTF at 400 °C. The nitrogen sorption analysis of bpyCTF at 450 °C would allow for a better comparison but was not carried out due to laboratory interruptions. In the future, one could test different reactions conditions by varying the reaction time, temperature and equivalents of alkali salt to further investigate the formation of mesopores in the bpyCTF, as reported in the literature.<sup>52</sup> In addition, it is important to conduct all experiments at the same scale as it is believed that it could influence the results.

Until today, three main issues in CTF synthesis remain unresolved: (1) poor to negligible crystallinity, (2) difficult scalability, and (3) difficult processability. The first issue emerges from the low reversibility of the trimerization reaction causing the need for elevated synthesis temperatures and hence the formation of amorphous CTFs. As a consequence of their amorphous insoluble character, the structural determination of CTFs is rather difficult. For example, as can be seen from the bpyCTF (Figure 30), prior to trimerization, the building blocks have a certain degree of rotational freedom. The pyridine rings will be in trans conformation with the nitrogen atoms on opposite site as a consequence of the lone pair-lone pair repulsion. Yet, as ZnCl<sub>2</sub> coordinates to the pyridine nitrogen atoms, it may be possible that the lone pair repulsion is partially lifted causing the pyridine nitrogen atoms to face each



other. However, the latter cannot be evidenced since no details are provided on the exact orientation of the pyridine nitrogen atoms. Hence, the aim is to obtain highly crystalline CTFs as they are structural definable. To this end, several milder synthetic strategies (section 2.1.2) have been proposed that slow down the crystallization process. However, these methods often provide a slight increase in crystallinity at the expense of porosity, which is nonetheless an important feature in heterogeneous catalysis to provide accessibility of the catalytic sites. The synthesis of porous crystalline CTFs thus remains a major challenge. The issue on scalability results from the method of CTF preparation, which requires sealed quartz ampules, internal reduced pressure, high temperatures and long reaction times. A closed reaction system is needed since, at the elevated synthesis temperature, the cyano substituted building blocks evaporate before  $\text{ZnCl}_2$  melts. Additionally, all residual solvent molecules and gases need to be removed by vacuum drying as  $\text{ZnCl}_2$  is hygroscopic and gases can increase the pressure possibly leading to ampule explosion.<sup>25,144</sup> However, all this makes their synthesis difficult to upscale in a reproducible manner. So, moving towards an open reaction system is desired and goes hand in hand with milder reaction temperatures and the abandon of the use of  $\text{ZnCl}_2$ . Finally, the third issue is related to their high chemical and physical stability giving rise to insoluble materials. Although these features are desired for heterogeneous catalysts, it makes them difficult to process e.g. molding in a particular shape.<sup>25</sup>

### 4.3 Catalytic transfer hydrogenation of N-heterocycles

The results from the Rh@bipyCTF catalyzed transfer hydrogenation of 2-methylquinoxaline were promising. In order to optimize the reaction, the effect of the pH,  $\text{HCOONa}/\text{HCOOH}$  solution concentration, temperature and catalyst loading on the conversion were intended to be tested. Furthermore, the turnover number, recyclability and heterogeneity of the catalytic system were to be explored. The follow-up of the homogeneous catalytic transfer hydrogenation, as reported by Zhang *et al.*<sup>107</sup>, was planned, to compare the kinetic profile of the homogeneous and heterogeneous catalyzed reaction. After the optimization in batch, the aim was to introduce the Rh@bipyCTF in a continuous flow reactor and expand the substrate scope. Some pharmaceutical important N-heterocycles of interest are illustrated in Figure 47.

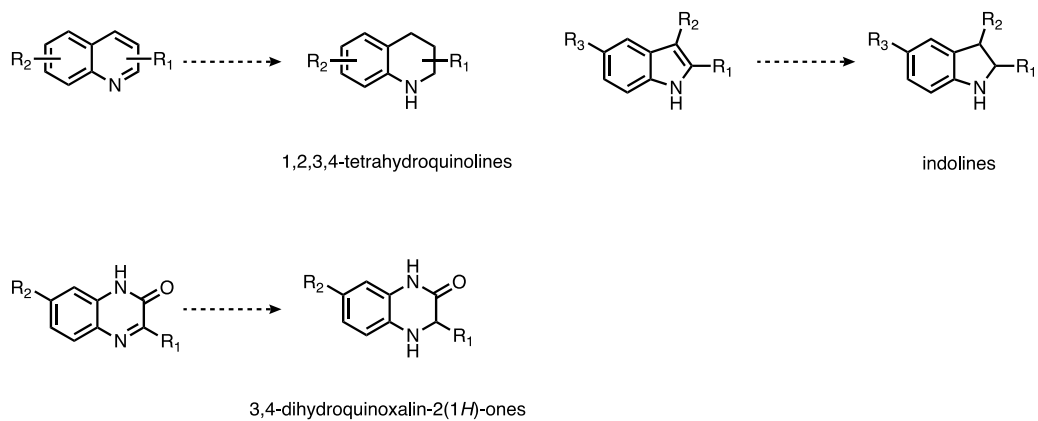


**Figure 47. Unsaturated N-heterocycles as future substrates for the catalytic transfer hydrogenation and the resulting hydrogenated products.**

## 5 Conclusion

---

This Master's thesis aimed at the generation of a heterogeneous CTF-supported rhodium catalyst to accelerate the transfer hydrogenation reaction of N-heterocycles. To this end, the thesis consisted of three parts.

In the first part, synthetic routes towards three nitrogen-containing building blocks were elaborated, i.e. the known building block 2,2'-bipyridine-5,5'-dicyanitrile **i**, and the two newly formed 2,2'-biquinoline-6,6'-dicyanitrile **ii** and quinoline-2,6-dicyanitrile **iii** (Figure 48).

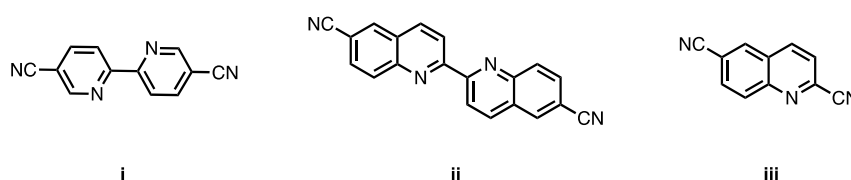


**Figure 48. Synthetized nitrogen-containing building blocks: 2,2'-bipyridine-5,5'-dicyanitrile **i**, 2,2'-biquinoline-6,6'-dicyanitrile **ii** and quinoline-2,6-dicyanitrile **iii**.**

Building block **i** was successfully synthesized by the nickel-catalyzed reductive homocoupling of 2-bromo-5-cyanopyridine. To achieve consistent reaction results without side-product formation, temperature control and zinc activation appeared to be important factors. Next, building block **ii** was synthesized by two distinct reaction pathways starting from 6-cyanoquinoline-*N*-oxide. The first pathway proceeded through the nickel-catalyzed reductive homocoupling of 2-chloroquinoline-6-carbonitrile which was synthesized through successive intermediates. However, the conversion was low and quinoline-6-carbonitrile was formed to a large extent. The second pathway provided a better alternative in terms of step economy as it evolved through the direct dimerization of 6-cyanoquinoline-*N*-oxide mediated by *tert*-butoxide. Several methods were examined, all leading to the formation of quinoline-6-carbonitrile and 6,6'-dicyano-2,2'-biquinoline-*N*-oxide in addition to building block **ii**. The method with LiOtBu was found to push the reaction to complete conversion towards 2,2'-biquinoline-6,6'-dicyanitrile, 6,6'-dicyano-2,2'-biquinoline-*N*-oxide and quinoline-6-carbonitrile. However, as NMR signals overlapped and MS signals were weak, this reaction

needs further investigation and optimization. Further, building block **iii** was synthesized by the selective cyanation of 6-cyanoquinoline-*N*-oxide with KCN. The reaction requires extra care as poisonous hydrogen cyanide may evolve. The use of acetyl chloride as activator was preferable to benzoyl chloride since the former was easier to handle and resulted in a clearer  $^1\text{H}$  NMR spectrum. Moreover, optimization of the reaction through the addition of KOtBu may result in faster conversion rates.

In the second part two CTFs, with distinct specific surface areas and porosities, were synthesized via the ionothermal method: the already described bipyCTF **iv** and the novel quinCTF **v** (Figure 49). The bipyCTF obtained through the conventional ionothermal method measured a BET specific surface area of  $654\text{ m}^2/\text{g}$  and a total pore volume of  $0.25\text{ cm}^3/\text{g}$ . The scale of the building block at which the synthesis was carried out, seemed to have an influence on the achieved specific surface area. The bipyCTF synthesized on a larger scale (500 mg) had a lower  $S_{\text{BET}}$ , i.e.  $531\text{ m}^2/\text{g}$ , compared to the bipyCTF synthesized on a smaller scale (180 mg) with a  $S_{\text{BET}}$  of  $654\text{ m}^2/\text{g}$ . The quinCTF yielded a remarkably higher specific surface area of  $1087\text{ m}^2/\text{g}$  and total pore volume of  $0.49\text{ cm}^3/\text{g}$ . Further, using the salt templated method with NaCl, a bipyCTF with  $S_{\text{BET}} 790\text{ m}^2/\text{g}$  and  $V_{\text{p,tot}} 0.31\text{ cm}^3/\text{g}$  was obtained. Hence, compared to the literature ( $S_{\text{BET}} 787\text{ m}^2/\text{g}$  and  $V_{\text{p,tot}} 0.40\text{ cm}^3/\text{g}$ ) a slight increase in specific surface area is obtained, although this is not significant. Both the bipyCTF as well as the quinCTF were obtained as black amorphous powders evidenced by PXRD and elemental analysis. Their non-crystalline nature leads to complicated characterization and structural uncertainties. Therefore, synthetic methods enabling crystalline yet porous CTFs are highly desired and should be the focus of future research.

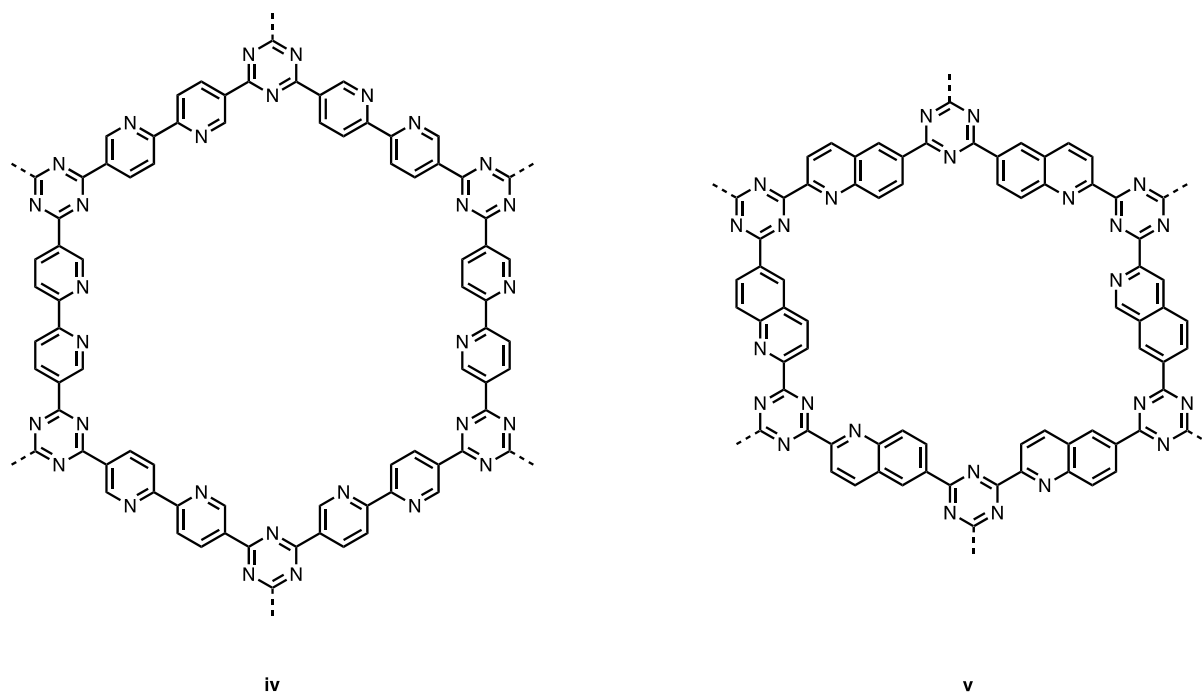


**Figure 49. Synthetized CTFs: bipyCTF iv and quinCTF v.**

Next, the bipyCTF, featuring bidentate coordination sites, was activated with a rhodium-Cp\* complex and had a metal loading of 22.9 g Rh/kg, as confirmed by ICP-OES analysis. In the final part, the obtained Rh@bipyCTF **vi** (Figure 50, left) was able to successfully catalyze the transfer hydrogenation reaction of 2-methylquinoxaline **vii** (Figure 50, right). The heterogeneous catalyst **vi** was air stable, and only 0.25 mol% Rh-catalyst was required to achieve a quantitative yield of 2-methyl-1,2,3,4-tetrahydroquinoxaline **viii** after about 2 hours reaction. Hence, the outcome is promising and opens new perspectives for future research such as the transfer hydrogenation of other industrially relevant N-heterocycles and the development of a catalytic system in a continuous flow setup.

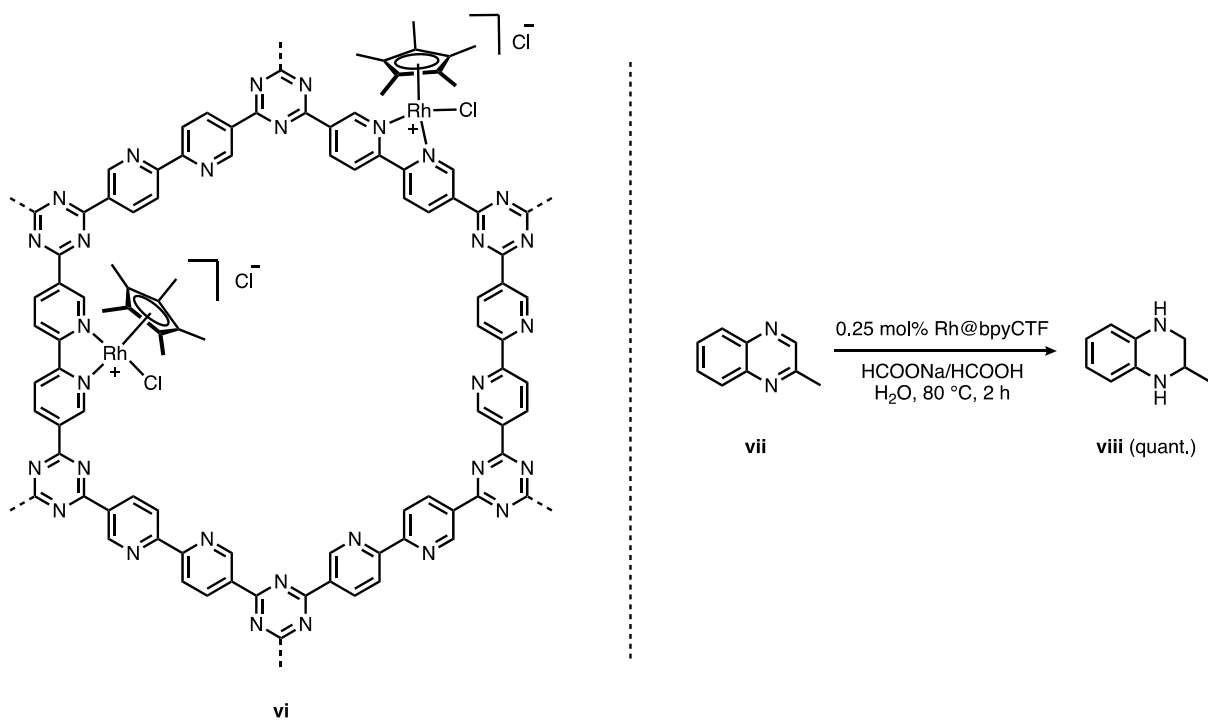


**Figure 50. Rh@bipyCTF vi (left) and Rh@bipyCTF catalyzed transfer hydrogenation of 2-methylquinoxaline vii (right).**

# 6 Materials and methods

---

## 6.1 General analytical methods and laboratory equipment

### **Thin Layer Chromatography (TLC)**

Thin layer chromatography was used to analyze crude reaction mixtures and to determine the retention factors ( $R_f$ ) for chromatographic purification. Therefore, the reaction mixtures were spotted on glass-backed silica plates (Merck, Silica gel 60 F<sub>254</sub>, precoated, thickness 0.25 mm) and subsequently put in a closed container with a mobile phase. The position of compounds on the plates were visualized by UV light (254 or 365 nm).

### **Preparative Thin Layer Chromatography (Prep. TLC)**

Preparative thin layer chromatography was used to separate and purify regioisomers in a crude reaction mixture. Therefore, the reaction mixtures were applied on Analtech silica plates GF (precoated, with a UV indicator (254 nm), dimensions 20 cm x 20 cm x 2 mm) and put in a closed container with a mobile phase. As for TLC, the compounds were visualized by UV light (254 nm).

### **Column chromatography**

A glass chromatographic column of appropriated size was provided with cotton wool at the bottom and covered with a thin layer of sand until the diameter was constant. Hereafter, the mobile phase, a specific solvent mixture determined by TLC, and silica powder (Davisil LC60A 70-200 micron, particle size 0.070-0.200 mm, pore size ca. 6.0 mm) were subsequently added. Next, the stationary phase was topped off with a thin layer of sand (approximately 0.5 cm). The crude product was coated on silica and added on top. To finish, a thin sand layer (approx. 1.0-1.5 cm) was applied again. The solvent mixture was then added to elute the different fractions.

### **Liquid Chromatography Mass Spectrometry (LC-MS)**

Liquid chromatography mass spectrometry was performed on an Agilent 1200 series device equipped with a Supelco Ascentis Express C18 HPLC column (4.6 mm x 3 cm, 2.7  $\mu$ m fused core particles with 90 Å pore size) and a UV detector. The HPLC is coupled to an Agilent 1100

Series mass spectrometer with electrospray ionization source (ESI, 70 eV) and a quadrupole detector. The mobile phase was a mixture of acetonitrile and water (5 mM NH<sub>4</sub>OAc).

### **Nuclear Magnetic Resonance Spectroscopy (NMR)**

The <sup>1</sup>H NMR and <sup>13</sup>C NMR spectra were obtained by means of a Bruker Avance Nanobay III NMR spectrometer at 400 MHz and 100.6 MHz respectively. The compounds were dissolved in a deuterated solvent (CDCl<sub>3</sub> or DMSO-d<sub>6</sub>) with tetramethylsilane (TMS) as reference compound. The NMR spectra were processed using TopSpin 4.0.8.

### **Fourier Transform Infrared Spectroscopy (FTIR)**

Infrared spectra from a sample in neat form were obtained by means of a Shimadzu IRAffinity-1S Fourier transformed infrared spectrometer equipped with a Quest ATR (Attenuated Total Reflectance) accessory with diamond crystal puck. The IR spectra were processed using LabSolutions IR software.

### **Melting point determination**

Melting points were obtained by means of a Kofler bench (type WME from Wagner & Munz) with a temperature range of 50-260 °C and an accuracy of ± 1 °C. Before the analysis, the melting bench is calibrated using compounds with a known melting temperature.

### **Nitrogen sorption analysis**

The nitrogen sorption analysis was carried out with a BELSORP mini II apparatus at 77 K. Prior to analysis, the samples were heated at 120 °C under vacuum for 24 h in order to remove residual solvent molecules. Specific surface areas were calculated based on the BET-equation (Appendix A). Total pore volumes were determined at P/P<sub>0</sub> = 0.99.

### **Powder X-Ray Diffraction (PXRD)**

Powder X-ray diffraction analysis was carried out by means of a Thermo Scientific ARL X'TRA Powder X-ray Diffractometer using Cu K $\alpha$  radiation ( $\lambda$  = 1.5406 Å) at 40 kV and 30 mA under ambient conditions. The spectra were measured at 1 °/min and processed by WinXRD software.



### **Induced Coupled Plasma Optical Emission Spectrometry (ICP-OES)**

The analysis, performed by professor Tack's research group (Ecochem, Department of Green Chemistry and Technology, Ghent University), was carried out by means of a Varian Vista-MPX™ CCD Simultaneous ICP-OES instrument (ICap7400 Duo). Prior to analysis, samples were digested using nitric acid according to the WAC/III/B/001 method. The wavelength for Rh was chosen as 343.489 nm. The analysis results were processed by the Thermo Scientific™ Qtegra™ Intelligent Scientific Data Solution™ (ISDS) software.

### **Elemental analysis**

Elemental composition was measured on a Thermo Scientific Flash 2000 CHNS-O analyzer equipped with a TCD detector, V<sub>2</sub>O<sub>5</sub> as catalyst and methionine as standard. The results from the elemental analysis were processed by the Thermo Scientific Eager Xperience software.

### **Dry solvents**

Dichloromethane and toluene were dried with a MBraun SPS-800 solvent purification system. These solvents were stored in Pure-Pac tanks of 17 L, pressurized by inert nitrogen gas and sent through two filtering/drying columns. These stainless-steel columns (1.4301 / US 304, internal volume of 4.8 L) possess molecular sieves adapted to the used solvent. The separate glass recipient was first put under vacuum with a membrane pump (type MPC 301 Zp) after which the dried solvents were collected under inert nitrogen gas. *N,N*-Dimethylformamide and 2-MeTHF were dried over 4 Å molecular sieves.

### **Reagents**

All chemicals were purchased from commercial suppliers and used without further purification.

## **6.2 Safety aspects**

Within the context of Green Chemistry, avoiding the use of hazardous chemicals and taking appropriate safety measures are important aspects.

To gain knowledge on specific risks and safety measures, three documents had to be read and signed at the start of this Master's thesis: 'Safety and hygiene in chemical laboratories', 'Safety

instructions: how to work with chemicals' and 'Welzijns- en Milieugids UGent'. Furthermore, a lab tour was given to point out the location and demonstrate the use of the safety equipment i.e. fire extinguishers, emergency showers, fire blankets, etc. Additionally, all students of the SynBioC Research Group had to pass an online safety test to be able to perform lab experiments. During the practical work in the lab, general personal protective equipment (PPE) such as a lab coat, safety goggles, was mandatory. In addition, nitrile gloves were available at all time.

In order to synthesize some of the chemical products, however, the use of hazardous substances could not be avoided. When handling these substances, understanding the hazards and taking appropriate precautions were crucial. To that end, the safety data sheets (SDS) of the used substances were consulted. The hazard statements of the most commonly used solvents and reagents are given in Table 7.<sup>145</sup> One must note that no toxicological study was performed on the newly synthesized products. Hence, these products were handled with caution.

**Table 7. Hazard statements from safety data sheets of most commonly used solvents and reagents.**

<b>Solvents</b>	
Chloroform-d ( $\text{CDCl}_3$ )	Harmful if swallowed. Causes skin irritation. Causes serious eye irritation. Toxic if inhaled. Suspected of causing cancer. Suspected of damaging the unborn child. Causes damage to organs (liver, kidney) through prolonged or repeated exposure.
Dichloromethane (DCM)	Causes skin irritation. Causes serious eye irritation. May cause drowsiness or dizziness. Suspected of causing cancer. Harmful to aquatic life.
<i>N,N</i> -Dimethylformamide (DMF)	Flammable liquid and vapor. Harmful in contact with skin. Causes serious eye irritation. May damage the unborn child.
Methanol (MeOH)	Highly flammable liquid and vapor. Toxic if swallowed, in contact with skin or if inhaled. Causes damage to organs.
Tetrahydrofuran (THF)	Highly flammable liquid and vapor. Harmful if swallowed. Causes serious eye irritation. May cause respiratory irritation. Suspected of causing cancer.
Toluene	Highly flammable liquid and vapor. May be fatal if swallowed and enters airways. Causes skin irritation. May cause drowsiness or dizziness. Suspected of damaging the unborn child. May cause damage to organs (central nervous system) through prolonged or repeated exposure. Harmful to aquatic life with long lasting effects.

---

## Reagents

---

Acetyl chloride (CH <sub>3</sub> COCl)	Highly flammable liquid and vapor. Causes severe skin burns and eye damage. Harmful to aquatic life.
Nickel(II) chloride hexahydrate (NiCl <sub>2</sub> ·6H <sub>2</sub> O)	Toxic if swallowed or if inhaled. Causes skin irritation. May cause an allergic skin reaction. May cause allergy or asthma symptoms or breathing difficulties if inhaled. Suspected of causing genetic defects. May cause cancer. May damage fertility or the unborn child. Causes damage to organs through prolonged or repeated exposure. Very toxic to aquatic life with long lasting effects.
Pentamethylcyclopentadienylrhodium(III) chloride dimer ([Cp*RhCl <sub>2</sub> ] <sub>2</sub> )	Harmful if swallowed, in contact with skin or if inhaled. Causes skin irritation. Causes serious eye irritation. May cause respiratory irritation.
Potassium cyanide (KCN)	May be corrosive to metals. Fatal if swallowed, in contact with skin or if inhaled. Causes damage to organs (thyroid) through prolonged or repeated exposure. Very toxic to aquatic life with long lasting effects.
Potassium <i>tert</i> -butoxide (KO <sup>t</sup> Bu)	Flammable solid. In contact with water releases flammable gases which may ignite spontaneously. Causes severe skin burns and eye damage.
Pyridine-2,6-dicarbonitrile	Harmful if swallowed. Harmful in contact with skin. Causes skin irritation. Causes serious eye irritation. Harmful if inhaled. May cause respiratory irritation.
Zinc(II) chloride (ZnCl <sub>2</sub> )	Harmful if swallowed. Causes severe skin burns and eye damage. Very toxic to aquatic life with long lasting effects.

---

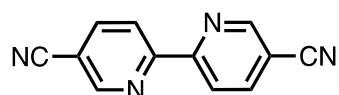
## 6.3 Synthesis procedures and characterization data

### 6.3.1 Synthesis of nitrogen-containing aromatic linkers

#### **2,2'-bipyridine-5,5'-dicarbonitrile (1)**

To a flame dried flask, 5 mol% NiCl<sub>2</sub>·6H<sub>2</sub>O (130 mg, 0.55 mmol) was dissolved in 26 mL anhydrous DMF under argon atmosphere. The resulting mixture was heated to 40 °C and 2-bromo-5-cyanopyridine **4** (2.00 g, 11 mmol, 1 eq), anhydrous LiCl (0.46 g, 11 mmol, 1 eq) and activated granular zinc (0.86 g, 13 mmol, 1.2 eq) were added. After raising the temperature to 50 °C, a grain of iodine and two drops of acetic acid were added into the mixture to initiate the reaction, which was then stirred for 1.5 hours to complete the conversion. Subsequently, the mixture was cooled to 0 °C before adding 1 M HCl (11 mL) and stirring it for an additional 30 min. Hereafter, aqueous ammonia (25 wt%) was added to make the mixture alkaline (pH

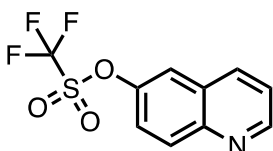
9), and the resulting product was extracted with ethyl acetate (3 x 40 mL). The combined organic fractions were dried over MgSO<sub>4</sub>, filtered and concentrated to a 20 mL-solution. Upon cooling the solution in an ice-bath a precipitate was formed, which was filtered off and washed with cold ethanol and diethyl ether. 2,2'-bipyridine-5,5'-dicarbonitrile **1** was obtained as a beige powder (1.11 g, 98%).



**<sup>1</sup>H NMR** (400 MHz, CDCl<sub>3</sub>): δ<sub>H</sub> 8.14 (2H, dxd, *J* = 8.3, 1.7 Hz, H<sup>4/4'</sup>), 8.64 (2H, d, *J* = 8.3 Hz, H<sup>3/3'</sup>), 8.97 (2H, s, H<sup>6/6'</sup>). **<sup>13</sup>C NMR** (100.6 MHz, CDCl<sub>3</sub>): δ<sub>C</sub> 110.7 (C<sup>5/5'</sup>), 116.5 (C≡N), 121.7 (C<sup>3/3'</sup>), 140.5 (C<sup>4/4'</sup>), 152.1 (C<sup>6/6'</sup>), 157.0 (C<sup>2/2'</sup>). **IR** (ATR, cm<sup>-1</sup>): ν<sub>max</sub> = 2234 (C≡N), 1587, 1462, 1371, 1238, 1028, 848. **MS** (ESI, 70 eV) *m/z* (%): 207.0 ([M + H]<sup>+</sup>, 100). **Mp** > 260 °C. Beige powder. Yield: 98%. The spectroscopic data are in agreement with the previously reported literature values.<sup>146</sup>

### Quinolin-6-yl trifluoromethanesulfonate (**6**)

A dropping funnel was sealed with a septum and attached to a 250 mL two-necked round bottomed flask. Quinolin-6-ol **5** (3.96 g, 27 mmol) was added to the flask, which was placed under argon. The dropping funnel was charged with 150 mL dry dichloromethane from which 100 mL was added to the flask. Next, analytical-grade pyridine (4.42 mL, 55 mmol, 2 eq) was added. The solution was cooled to 0 °C in an ice bath. Triflic anhydride (10 g, 35 mmol, 1.3 eq) was loaded in the dropping funnel and added dropwise with the remaining dichloromethane. The mixture was slowly brought to room temperature and stirred for 2 hours. At the end of the reaction (monitored by TLC), the reaction mixture was quenched with 1.0 M aq. HCl (20 mL) and washed with sat. NaHCO<sub>3</sub> and brine (40-50 mL). The organic phase was collected and treated again with NaHCO<sub>3</sub> and brine. The water phase was extracted two times with a 1:1 (v/v) mixture of DCM/Et<sub>2</sub>O. The combined organic phases were dried over anhydrous MgSO<sub>4</sub> and concentrated *in vacuo*. Crude quinolin-6-yl trifluoromethanesulfonate **6** was obtained as a brown viscous liquid (5.98 g, 79%).

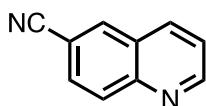


**<sup>1</sup>H NMR** (400 MHz, CDCl<sub>3</sub>): δ<sub>H</sub> 7.51 (1H, dxd, *J* = 8.4, 4.2 Hz, H<sup>3</sup>), 7.61 (1H, dxd, *J* = 9.3, 2.8 Hz, H<sup>7</sup>), 7.76 (1H, d, *J* = 2.6 Hz, H<sup>5</sup>), 8.20-8.22 (2H, m, H<sup>4/8</sup>), 9.01 (1H, dxd, *J* = 4.4, 1.6 Hz, H<sup>2</sup>). **<sup>13</sup>C NMR** (100.6 MHz, CDCl<sub>3</sub>): δ<sub>C</sub> 117.3 (C<sup>6</sup>), 119.4 (C<sup>5</sup>), 120.5 (CF<sub>3</sub>), 122.6 (C<sup>3</sup>), 123.3 (C<sup>7</sup>), 128.5 (C<sup>4a</sup>), 132.6 (C<sup>8</sup>), 136.3 (C<sup>4</sup>), 147.2 (C<sup>8a</sup>), 151.9 (C<sup>2</sup>). **<sup>19</sup>F NMR** (376 MHz, CDCl<sub>3</sub>): δ<sub>F</sub> -72.67 (3F, s). **MS**

(ESI, 70 eV)  $m/z$  (%): 278.0 ( $[M + H]^+$ , 100). Brown viscous liquid. Yield: 79%. The spectroscopic data are in agreement with the previously reported literature values.<sup>123</sup>

### Quinoline-6-carbonitrile (**7**)

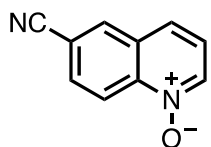
To a 250 mL flask containing quinolin-6-yl trifluoromethanesulfonate **6** (5.98 g, 22 mmol) was added  $Zn(CN)_2$  (3.04 g, 26 mmol, 1.2 eq) and  $Pd(PPh_3)_4$  (0.75 g, 0.65 mmol, 3 mol%). The mixture was purged with argon and degassed DMF was added (80 mL). The reaction was warmed to 120 °C and refluxed under argon for 3 hours. The resulting reaction mixture was evaporated *in vacuo* to remove approximately 70% of the DMF. After,  $NaHCO_3$  (33 mL) was added and the mixture was stirred for a while. Extraction was performed 2 times with  $Et_2O$  and 3 times with EtOAc. The turbidity was not collected together with the organic phase. The combined organic phases were dried over  $MgSO_4$ , filtered and evaporated *in vacuo*. The residue was purified by column chromatography ( $SiO_2$ , gradient hexane/EtOAc 60:40-55:45) to obtain quinoline-6-carbonitrile **7** as a white powder (2.57 g, 77%).



**$^1H$  NMR** (400 MHz,  $CDCl_3$ ):  $\delta_H$  7.54 (1H, dxd,  $J = 8.3, 4.2$  Hz,  $H^3$ ), 7.86 (1H, dxd,  $J = 8.7, 1.8$  Hz,  $H^7$ ), 8.20 (1H, d,  $J = 8.9$  Hz,  $H^8$ ), 8.21-8.24 (2H, m,  $H^4, H^5$ ), 9.06 (1H, dxd,  $J = 4.3, 1.7$  Hz,  $H^2$ ).  **$^{13}C$  NMR** (100.6 MHz,  $CDCl_3$ ):  $\delta_C$  110.5 ( $C^6$ ), 118.5 ( $C\equiv N$ ), 122.7 ( $C^3$ ), 127.6 ( $C^{4a}$ ), 130.2 ( $C^7$ ), 131.2 ( $C^8$ ), 134.1 ( $C^5$ ), 136.4 ( $C^4$ ), 149.2 ( $C^{8a}$ ), 153.3 ( $C^2$ ). **IR** (ATR,  $cm^{-1}$ ):  $\nu_{max} = 2228$  ( $C\equiv N$ ), 1582, 1366, 1306, 1273, 1246, 1200, 849, 831. **MS** (ESI, 70 eV)  $m/z$  (%): 155.1 ( $[M + H]^+$ , 100). White powder.  $R_f = 0.40$  (hexane/EtOAc 55:45). Yield: 77%. The spectroscopic data are in agreement with the previously reported literature values.<sup>123</sup>

### 6-cyanoquinoline-*N*-oxide (**8**)

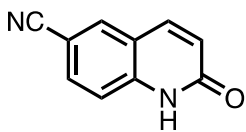
To a 0.2 M solution of quinoline-6-carbonitrile **7** (1.50 g, 9.73 mmol) in DCM (49 mL) *m*-chloroperbenzoic acid (70 wt%, 2.08 g, 12 mmol) was added at 0 °C in four portions over 10 min. The reaction mixture was stirred at room temperature for 7 hours (monitored by LC-MS). Next, 1 M NaOH (19 mL) was added to the resulting reaction mixture. After separation of the organic phase, extraction of the aqueous phase was performed with a 1:4 (v/v) mixture of *i*PrOH/ $CHCl_3$ . The organic phases were combined, dried over anhydrous  $MgSO_4$ , filtered and concentrated *in vacuo*. 6-cyanoquinoline-*N*-oxide **8** was obtained as a yellow powder (1.41 g, 85%).



**<sup>1</sup>H NMR** (400 MHz, CDCl<sub>3</sub>): δ<sub>H</sub> 7.44 (1H, dxd, *J* = 8.5, 6.3 Hz, H<sup>3</sup>), 7.77 (1H, d, *J* = 8.5 Hz, H<sup>7</sup>), 7.90 (1H, d, *J* = 9.1 Hz, H<sup>4</sup>), 8.28 (1H, s, H<sup>5</sup>), 8.61 (1H, d, *J* = 6.1 Hz, H<sup>2</sup>), 8.87 (1H, d, *J* = 9.1 Hz, H<sup>8</sup>). **<sup>13</sup>C NMR** (100.6 MHz, CDCl<sub>3</sub>): δ<sub>C</sub> 113.2 (C<sup>6</sup>), 117.5 (C≡N), 121.8 (C<sup>8</sup>), 123.0 (C<sup>3</sup>), 125.1 (C<sup>7</sup>), 130.0 (C<sup>4a</sup>), 131.0 (C<sup>4</sup>), 134.1 (C<sup>5</sup>), 137.6 (C<sup>2</sup>), 142.7 (C<sup>8a</sup>). **IR** (ATR, cm<sup>-1</sup>): ν<sub>max</sub> = 2228 (C≡N), 2156, 2029, 1535, 1368, 1306, 1273, 1200, 849, 833, 787, 733. **MS** (ESI, 70 eV) *m/z* (%): 171.1 ([M + H]<sup>+</sup>, 100). Yellow powder. Yield: 85%.

### 2-oxo-1,2-dihydroquinoline-6-carbonitrile (**10**)

In a round bottomed flask, 6-cyanoquinoline-*N*-oxide **8** (1.0 g, 5.88 mmol), H<sub>2</sub>O (60 mL) and methanesulfonyl chloride (1.35 g, 11.75 mmol) were subsequently added. The mixture was stirred at room temperature for 5-12 min (monitored by LC-MS). The resulting reaction mixture was filtered, and the solid product left on the filter was rinsed with water and dried *in vacuo*. 2-oxo-1,2-dihydroquinoline-6-carbonitrile **10** was obtained as a white solid (802 mg, 80%).

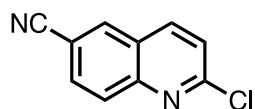


**<sup>1</sup>H NMR** (400 MHz, DMSO-*d*<sub>6</sub>): δ<sub>H</sub> 6.62 (1H, dxd, *J* = 9.6, 1.1 Hz, H<sup>3</sup>), 7.40 (1H, d, *J* = 8.6 Hz, H<sup>8</sup>), 7.87 (1H, dxd, *J* = 8.6, 1.4 Hz, H<sup>7</sup>), 7.94 (1H, d, *J* = 9.6 Hz, H<sup>4</sup>), 8.24 (1H, d, *J* = 1.4 Hz, H<sup>5</sup>), 12.13 (1H, s, H<sup>1</sup>). **<sup>13</sup>C NMR** (100.6 MHz, DMSO-*d*<sub>6</sub>): δ<sub>C</sub> 104.3 (C<sup>6</sup>), 116.7 (C<sup>8</sup>), 119.3 (C≡N), 119.6 (C<sup>4a</sup>), 124.1 (C<sup>3</sup>), 133.3 (C<sup>7</sup>), 133.5 (C<sup>5</sup>), 139.9 (C<sup>4</sup>), 142.2 (C<sup>8a</sup>), 162.3 (C=O). **MS** (ESI, 70 eV) *m/z* (%): 171.1 ([M + H]<sup>+</sup>, 100). White solid. Yield: 80%. Remark: only the <sup>1</sup>H NMR signals of the major tautomer were assigned and belong to the lactam form according to the literature.<sup>126</sup> The smaller <sup>1</sup>H NMR signals can be possibly assigned to the minor tautomer, 2-hydroxyquinoline-6-carbonitrile, or to 4-hydroxyquinoline-6-carbonitrile. However, additional NMR analyses are needed to assign these signals. These could not be taken due to the stop of the laboratory activities (SARS-CoV-2 measures).

### 2-chloroquinoline-6-carbonitrile (**9**)

A solution of 2-oxo-1,2-dihydroquinoline-6-carbonitrile **10** (747 mg, 4.39 mmol) in phosphoryl trichloride (6 mL) was refluxed for 30 min. After, the mixture was cooled to room temperature, poured slowly in ice water with HCl (38 mL, pH = 1) and neutralized with aqueous NaOH until the product precipitated. The aqueous suspension was extracted with DCM (4 x 5 mL). The organic phases were combined, dried over anhydrous MgSO<sub>4</sub>, filtered through a plug of SiO<sub>2</sub>

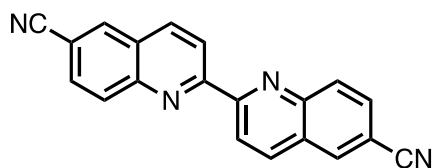
in a glass frit and concentrated *in vacuo*. 2-chloroquinoline-6-carbonitrile **9** was obtained as a light yellow powder (605 mg, 73%).



**<sup>1</sup>H NMR** (400 MHz, CDCl<sub>3</sub>): δ<sub>H</sub> 7.53 (1H, d, *J* = 8.8 Hz, H<sup>3</sup>), 7.89 (1H, dxd, *J* = 8.8, 1.6 Hz, H<sup>7</sup>), 8.11 (1H, d, *J* = 8.7 Hz, H<sup>8</sup>), 8.17 (1H, d, *J* = 8.6 Hz, H<sup>4</sup>), 8.23 (1H, s, H<sup>5</sup>). **<sup>13</sup>C NMR** (100.6 MHz, CDCl<sub>3</sub>): δ<sub>C</sub> 111.0 (C<sup>6</sup>), 118.3 (C≡N), 124.5 (C<sup>3</sup>), 126.3 (C<sup>4a</sup>), 130.3 (C<sup>8</sup>), 131.6 (C<sup>7</sup>), 133.8 (C<sup>5</sup>), 139.1 (C<sup>4</sup>), 148.9 (C<sup>8a</sup>), 154.1 (C<sup>2</sup>). **MS** (ESI, 70 eV) *m/z* (%): 189/191 ([M + H]<sup>+</sup>, 100). Light yellow powder. Yield: 73%.

### 2,2'-biquinoline-6,6'-dicarbonitrile (**2**)

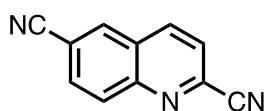
To a flame-dried flask 6-cyanoquinoline-*N*-oxide **8** (400 mg, 2.34 mmol) and anhydrous toluene (21 mL) were added. After heating to 90 °C, **8** was dissolved and a light-yellow color was observed. Under the atmosphere of nitrogen, 1 M lithium *tert*-butoxide in THF (4.69 mL, 4.69 mmol) was slowly added dropwise. The color changed to black. The mixture was then stirred for 12 hours at 90 °C. Next, the resulting reaction mixture was filtered, at which a brown residue was left on the filter. Subsequent washing with cold MeOH was done until the brown residue was dissolved in the filtrate. A yellow residue (50 mg) remained on the filter, corresponding to the product **2**. The filtrate was concentrated under reduced pressure, washed with DCM and stirred for 1 h. Afterwards, the mixture was filtered off and the filtrate was concentrated under reduced pressure to give a residue corresponding to the product **2** (13 mg). 2,2'-biquinoline-6,6'-dicarbonitrile **2** was obtained as a yellow powder (63 mg, 18%).



**<sup>1</sup>H NMR** (400 MHz, CDCl<sub>3</sub>): δ<sub>H</sub> 7.92 (2H, d, *J* = 8.7 Hz, H<sup>7/7'</sup>), 8.31 (2H, s, H<sup>5/5'</sup>), 8.32 (2H, d, *J* = 8.8 Hz, H<sup>4/4'</sup>), 8.42 (2H, d, *J* = 8.6 Hz, H<sup>8/8'</sup>), 9.00 (2H, d, *J* = 9.0 Hz, H<sup>3/3'</sup>). **<sup>13</sup>C NMR**: Due to the poor solubility of the compound in CDCl<sub>3</sub>, DMSO-*d*<sub>6</sub> or AcOD-*d*<sub>4</sub>, no adequate <sup>13</sup>C NMR spectrum could be recorded for peak assignment. **IR** (ATR, cm<sup>-1</sup>): ν<sub>max</sub> = 2228 (C≡N), 1618, 1589, 1481, 1452, 1375, 1331, 1213, 899, 848, 828. **MS** (ESI, 70 eV) *m/z* (%): 307.0 ([M + H]<sup>+</sup>, 100). **Mp** > 260 °C. Yellow powder. Yield: 18%.

### Quinoline-2,6-dicarbonitrile (**3**)

To a suspension of KCN (1.15 g, 17.64 mmol) in MeOH (21 mL) was added 6-cyanoquinoline-*N*-oxide **8** (1 g, 5.88 mmol). The flask was placed under a flow of nitrogen gas, flushing liberated HCN through two consecutive gas washing bottles containing a 1 M KOH (3.37 g in 60 mL) and a 1 M Na<sub>2</sub>S<sub>2</sub>O<sub>3</sub> (9.49 g in 60 mL) aqueous solution. Acetyl chloride (1.25 mL, 1.38 g, 17.64 mmol) was added over 5 minutes. The mixture was stirred for 29 h at room temperature under a continuous gas flow of N<sub>2</sub>. A color change from yellow to light pink at the end of the reaction was observed. Afterwards, upon addition of approximately 30 mL of water, the product precipitated as a light pink solid. The precipitate was filtered off, washed with cold MeOH and Et<sub>2</sub>O and subsequently dried *in vacuo*. Quinoline-2,6-dicarbonitrile **3** was obtained as a light pink powder (606 mg, 58%).



<sup>1</sup>H NMR (400 MHz, CDCl<sub>3</sub>): δ<sub>H</sub> 7.84 (1H, d, *J* = 8.5 Hz, H<sup>3</sup>), 7.99 (1H, d, *J* = 9.0 Hz, H<sup>7</sup>), 8.30 (1H, d, *J* = 9.0 Hz, H<sup>8</sup>), 8.32 (1H, s, H<sup>5</sup>), 8.41 (1H, d, *J* = 8.5 Hz, H<sup>4</sup>). <sup>13</sup>C NMR (100.6 MHz, CDCl<sub>3</sub>): δ<sub>C</sub> 113.3 (C<sup>6</sup>), 116.7 (C<sup>2</sup>C<sup>9</sup>≡N), 117.6 (C<sup>6</sup>C<sup>10</sup>≡N), 124.9 (C<sup>3</sup>), 127.8 (C<sup>4a</sup>), 131.66 (C<sup>8</sup>), 131.73 (C<sup>7</sup>), 133.9 (C<sup>5</sup>), 136.5 (C<sup>2</sup>), 138.1 (C<sup>4</sup>), 148.8 (C<sup>8a</sup>). IR (ATR, cm<sup>-1</sup>): ν<sub>max</sub> = 2054 (C≡N), 1586, 1483, 1327, 1312, 1217, 907, 848. MS (ESI, 70 eV) *m/z* (%): 180.1 ([M + H]<sup>+</sup>, 100). *Mp* = 255.5 °C. Light pink powder. Yield: 58%.

### 6.3.2 Synthesis of CTFs and post-synthetic metalation

#### Conventional ionothermal procedure for the synthesis of CTFs

2,2'-bipyridine-5,5'-dicarbonitrile-based CTF **21** (bipyCTF) and quinoline-2,6-dicarbonitrile-based CTF **22** (quinCTF) were synthesized according to the ionothermal procedure reported by Hug *et al.*<sup>140</sup> First, a glass ampoule was filled with 1 equivalent of the building block of interest (max 500 mg per ampoule) and 5 equivalents dried ZnCl<sub>2</sub>. Next, the ampoule was flame-sealed under vacuum and heated in a Naberthem muffle furnace with a heating rate of 100 °C/h towards 400 °C (bipyCTF) or 450 °C (quinCTF), and held at this temperature for 48 h. After cooling down to room temperature, the resulting black colored lump was ground well with a mortar and a pestle and stirred in distilled water (250 mL for 100 mg CTF) for 4 h. Afterwards, the solid was filtered and washed with water and diethyl ether. The CTF was then refluxed in 1 M HCl overnight (250 mL for 100 mg CTF) at 100 °C and filtered. Hereafter, the CTF was washed successively with water, THF, ethanol and diethyl ether using 3 times 100 mL



for every washing solvent. Finally, the purified CTF was dried under vacuum overnight at 150 °C for activation prior to use. The obtained yields were between 80-87%.

### **Salt-templated ionothermal procedure for the synthesis of 2,2'-bipyridine-5,5'-dicarbonitrile-based CTF 21**

The salt templated method according to Troschke *et al.*<sup>52</sup> was performed in a similar manner as the conventional ionothermal synthesis method. During the first step, a glass ampoule was filled with 1 equivalent of 2,2'-bipyridine-5,5'-dicarbonitrile **1** (max 500 mg per ampoule), 5 equivalents dried ZnCl<sub>2</sub> and 2.1 equivalents of an alkali salt (NaCl or KCl). Next, the ampoule was flame sealed under vacuum and heated in a Naberthem muffle furnace first at 350 °C with a heating rate of 60 °C/h for 48 hours and subsequently at 450 °C with a heating rate of 100 °C/h for 15 hours. Again, a black colored lump was obtained. The workup was analogous to the one described for the conventional ionothermal synthesis method.

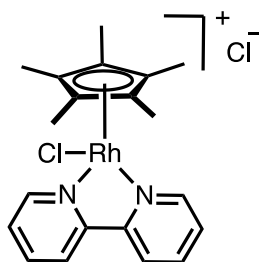
### **Post-synthetic metalation of bipyCTF with [Cp\*RhCl<sub>2</sub>]<sub>2</sub>**

To obtain the Rh@bipyCTF catalyst, an oven dried flask was charged with bipyCTF (300 mg), [Cp\*RhCl<sub>2</sub>]<sub>2</sub> (22.47 mg, 0.04 mmol) and a 1:1 mixture (v/v) of dry MeOH and CHCl<sub>3</sub> (115 mL). The mixture was refluxed at 70 °C for 24 hours under argon. There was no color change, the solid remained black. Next, the solid was filtered and rinsed with MeOH (3 x 25 mL), CHCl<sub>3</sub> (2 x 25 mL) and Et<sub>2</sub>O (2 x 25 mL) to remove the weakly bonded Rh complex. The resulting Rh@bipyCTF was dried under vacuum prior to use.

## 6.3.3 Catalytic transfer hydrogenation of N-heterocycles

### **General procedure for the synthesis of the homogeneous catalyst (pentamethylcyclopentadienyl)rhodium(III)-2,2'-bipyridine chloride ([Cp\*Rh(bpy)Cl]Cl)**

To an oven dried flask, [Cp\*RhCl<sub>2</sub>]<sub>2</sub> (30 mg, 0.05 mmol) and dry MeOH (5 mL) were added and formed a red colored suspension. Next, 2,2'-bipyridine was added (15.16 mg, 0.1 mmol) after which the suspension cleared up and formed a yellowish solution. The mixture was stirred for 1 hour at room temperature. Hereafter, the flask was placed in an ice bath and 5 mL cold Et<sub>2</sub>O was added in 5 portions over 20 min. As no crystallization occurred, the flask was placed in the freezer at -20 °C for 2 days. The crystals were filtered off and dried under vacuum. The [Cp\*Rh(bpy)Cl]Cl catalyst was obtained as orange powder (38 mg, 84 %).



**$^1\text{H}$  NMR** (400 MHz,  $\text{CDCl}_3$ ):  $\delta_{\text{H}}$  1.73 (15H, s,  $\text{C}_5(\text{CH}_3)_5$ ), 7.83 (2H,  $\sim\text{t}$ ,  $J = 6.4$  Hz,  $\text{C}_{10}\text{H}^{5/5'}\text{N}_2$ ), 8.24 (2H,  $\sim\text{t}$ ,  $J = 7.7$  Hz,  $\text{C}_{10}\text{H}^{4/4'}\text{N}_2$ ), 8.86 (2H, d,  $J = 5.4$  Hz,  $\text{C}_{10}\text{H}^{3/3'}\text{N}_2$ ), 9.04 (2H, d,  $J = 8.1$  Hz,  $\text{C}_{10}\text{H}^{6/6'}\text{N}_2$ ).  **$^{13}\text{C}$  NMR** (100.6 MHz,  $\text{CDCl}_3$ ):  $\delta_{\text{C}}$  9.4 ( $\text{C}_5(\text{CH}_3)_5$ ), 97.3 (d,  $J_{\text{Rh-C}} = 8.07$  Hz,  $\text{C}_5(\text{CH}_3)_5$ ), 125.7 ( $\text{C}^{3/3'}$ ), 128.6 ( $\text{C}^{5/5'}$ ), 140.9 ( $\text{C}^{4/4'}$ ), 151.4 ( $\text{C}^{6/6'}$ ), 154.7 ( $\text{C}^{2/2'}$ ). **IR** (ATR,  $\text{cm}^{-1}$ ):  $\nu_{\text{max}} = 3541, 3283, 1603, 1443, 1302, 1024, 766$ .

**MS** (ESI, 70 eV)  $m/z$  (%): 429.0/430.0 ( $[\text{M}-\text{Cl}]^+$ , 100). Orange powder. Yield: 84%. The spectroscopic data are in agreement with the previously reported literature values.<sup>147</sup>

### General procedure for the rhodium-catalyzed transfer hydrogenation of 2-methylquinoxaline in batch

This procedure was used for both the homogeneous and heterogeneous rhodium-catalyzed transfer hydrogenation of 2-methylquinoxaline. A tube was charged with the rhodium catalyst (0.25 mol% Rh). Then, 2 M  $\text{HCOONa}/\text{HCOOH}$  solution (9.0 mL, pH 4.4) and 2-methylquinoxaline (100 mg, 0.69 mmol) were sequentially added, forming an emulsion. The tube was closed and heated to 80 °C, and the mixture was stirred vigorously for the appropriate reaction time in the oil bath (2 h for homogeneous and 2 h 15 min for the heterogeneous catalysis). After the reaction, the tube was allowed to cool down to room temperature.

The heterogeneous transfer hydrogenation reaction with Rh@bipyCTF was analyzed at different time intervals (15 min - 30 min - 1 h - 1.5 h - 2 h - 2 h 15 min - 3 h - 18 h). Hereby, 0.2 mL of the reaction mixture was taken with a needle and syringe, moved to a 10 mL flask and dried *in vacuo*. Some CTF stuck to the needle and was put back into the reaction mixture.  $\text{CDCl}_3$  was added to the residue and the solution was filtered using a syringe filter upon transferring the solution into an NMR tube. At each time interval, the conversion was determined by  $^1\text{H}$  NMR (400 MHz,  $\text{CDCl}_3$ ) through the integration of the methyl protons of both the substrate, 2-methylquinoxaline **24** ( $\delta_{\text{H}}$  2.79 ppm, s,  $\text{CH}_3$ ), and the product, 2-methyl-1,2,3,4-tetrahydroquinoxaline **25** ( $\delta_{\text{H}}$  1.19 ppm, d,  $J = 6.3$  Hz,  $\text{CH}_3$ ).

## 7 Appendix

---

**Appendix A:** Multiple point BET plots resulting from the nitrogen sorption analysis of the synthesized CTFs.

Based on the BET equation (Equation 1) the specific surface areas of the CTFs were calculated (Equation 2):

$$\frac{1}{V_{STP} \cdot \left(\frac{P_0}{P} - 1\right)} = \frac{1}{V_{m,STP} \cdot C} + \frac{C-1}{V_{m,STP} \cdot C} \cdot \frac{P_0}{P} \quad (\text{Equation 1})$$

$$S_{BET} = \frac{V_{m,STP} \cdot 10^{-6}}{0.0224} \cdot N_A \cdot p a_1 \quad (\text{Equation 2})$$

with  $P_0$  = saturation pressure of the  $N_2$  gas at the temperature of adsorption (in Pa);

$P$  = equilibrium pressure of the  $N_2$  gas at the temperature of adsorption (in Pa);

$C$  = BET constant;

$V_{STP}$  = volume of  $N_2$  gas adsorbed under standard temperature and pressure (STP) (in  $\text{mL g}^{-1}$ );

$V_{m,STP}$  = volume of  $N_2$  gas needed to form a monolayer under standard temperature and pressure (STP) (in  $\text{mL g}^{-1}$ );

$S_{BET}$  = BET specific surface area (in  $\text{m}^2 \text{g}^{-1}$ );

$N_A$  = Avogadro's number ( $6.022 \cdot 10^{23} \text{ mol}^{-1}$ );

$p a_1$  = cross section of an adsorbed  $N_2$  gas molecule ( $0.162 \cdot 10^{-18} \text{ m}^2$ )

In order to validate the obtained value for the specific surface area, the multiple point BET plot is given. Herein, a straight line between relative pressure values ( $P/P_0$ ) of 0.05 to 0.3 and a coefficient of determination ( $R^2$ ) of  $\geq 0.999$  must be obtained.

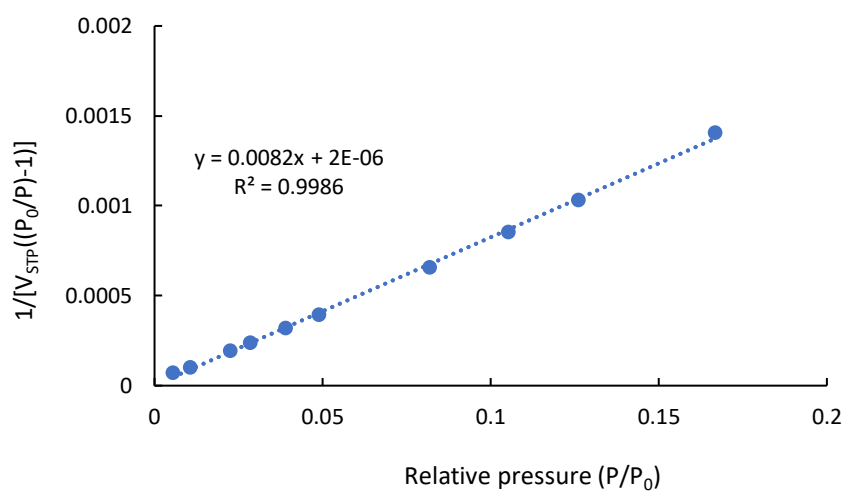


**Figure 51. Multiple point BET plot of bipyCTF 21 (500 mg sample) resulting in a specific surface area of 531 m<sup>2</sup>/g. The obtained coefficient of determination  $R^2 = 0.9986$  and BET constant  $C = 4101$ .**

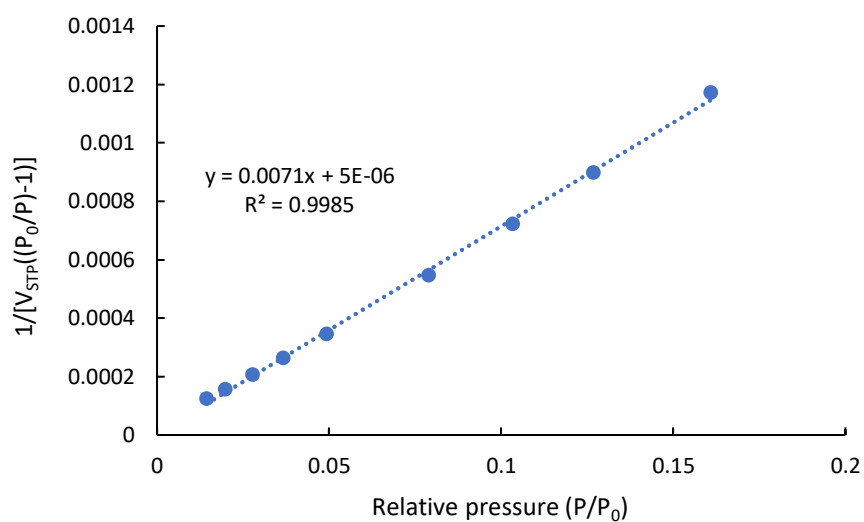


**Figure 52. Multiple point BET plot of bipyCTF 21 (180 mg sample) resulting in a specific surface area of 654 m<sup>2</sup>/g. The obtained coefficient of determination  $R^2 = 0.9985$  and BET constant  $C = 1443$ .**

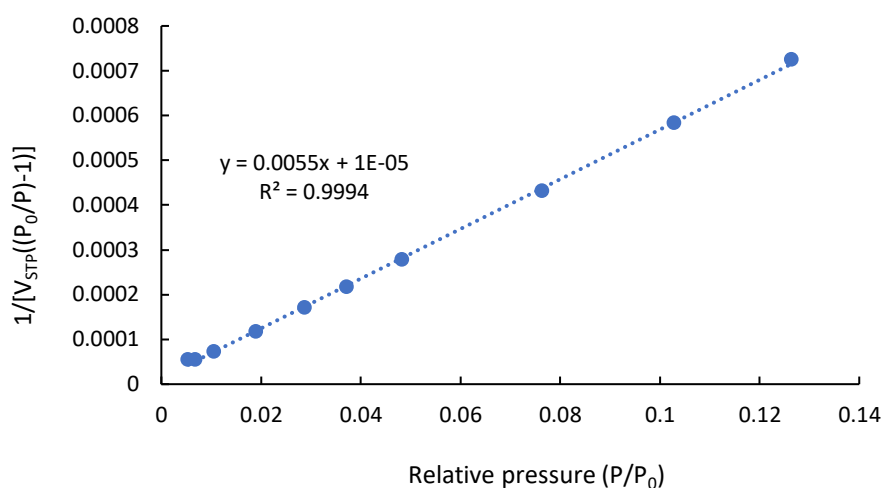


**Figure 53. Multiple point BET plot of bipyCTF 21 for entry A resulting in a specific surface area of 790 m<sup>2</sup>/g. The obtained coefficient of determination  $R^2 = 0.9994$  and BET constant  $C = 551$ .**

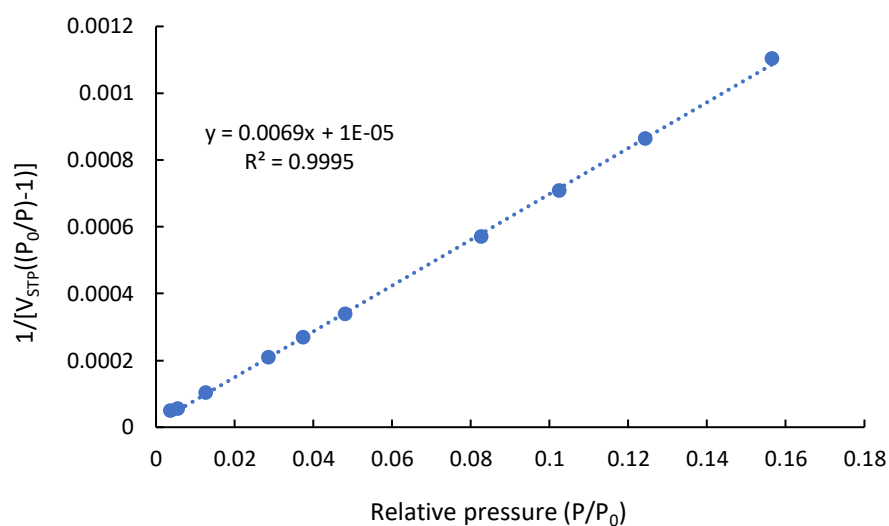


**Figure 54. Multiple point BET plot of bipyCTF 21 for entry B resulting in a specific surface area of 630 m<sup>2</sup>/g. The obtained coefficient of determination  $R^2 = 0.9995$  and BET constant  $C = 174$ .**

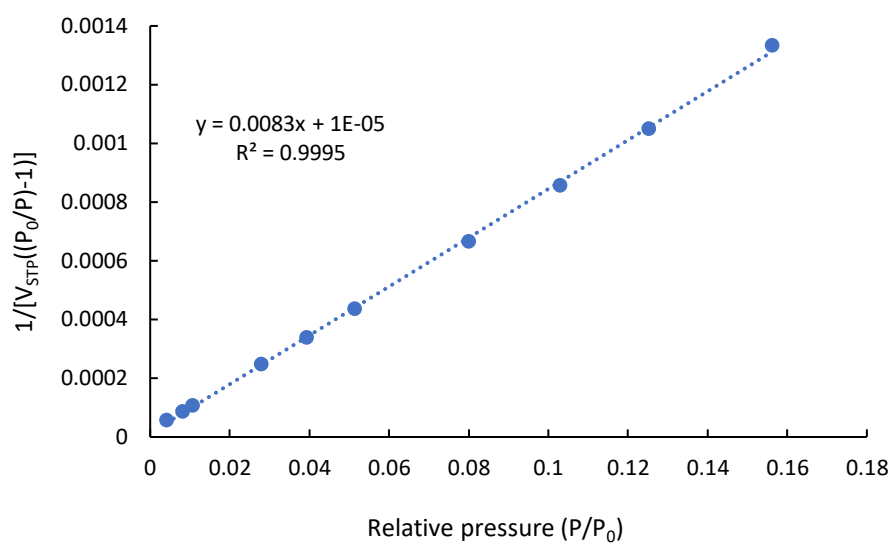


**Figure 55. Multiple point BET plot of bipyCTF 21 for entry C resulting in a specific surface area of 524 m<sup>2</sup>/g. The obtained coefficient of determination  $R^2 = 0.9995$  and BET constant  $C = 831$ .**

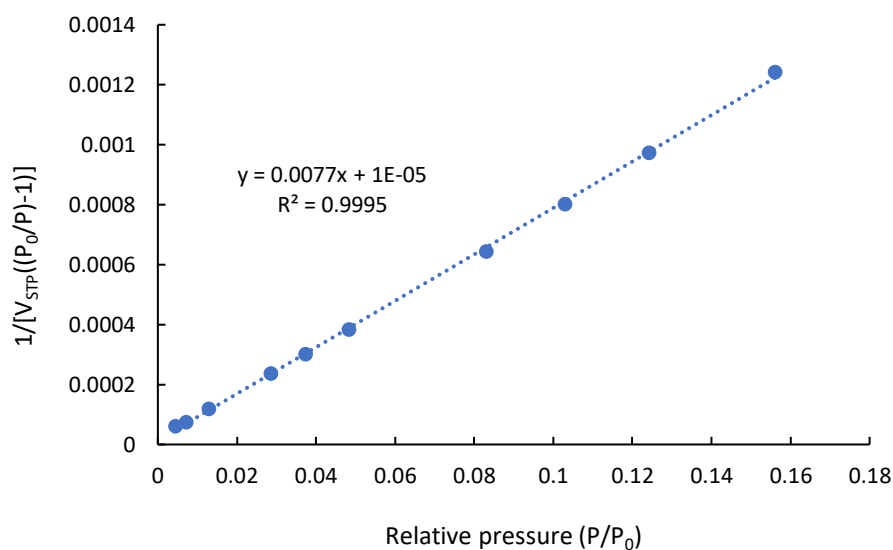


**Figure 56. Multiple point BET plot of bipyCTF 21 for entry D resulting in a specific surface area of 565 m<sup>2</sup>/g. The obtained coefficient of determination  $R^2 = 0.9995$  and BET constant  $C = 771$ .**

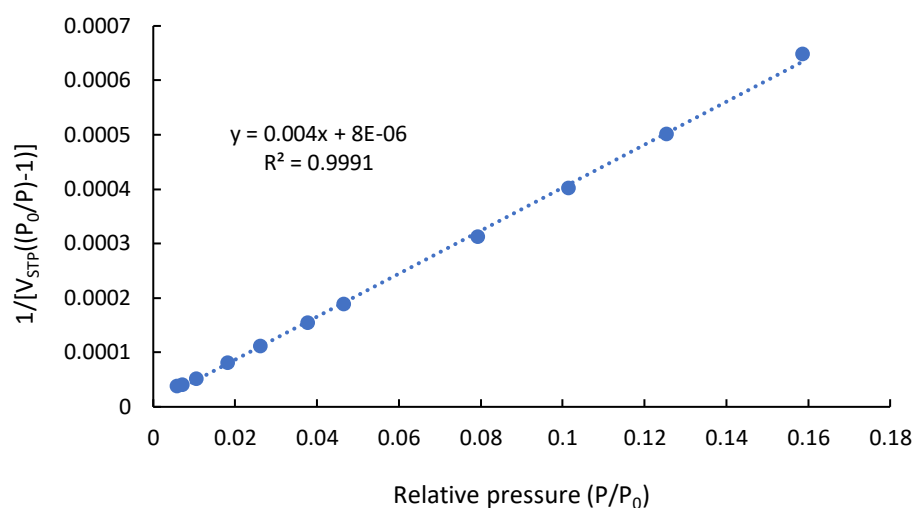


**Figure 57. Multiple point BET plot of quinCTF 22 resulting in a specific surface area of 1087 m<sup>2</sup>/g.** The obtained coefficient of determination  $R^2 = 0.9991$  and BET constant  $C = 501$ .

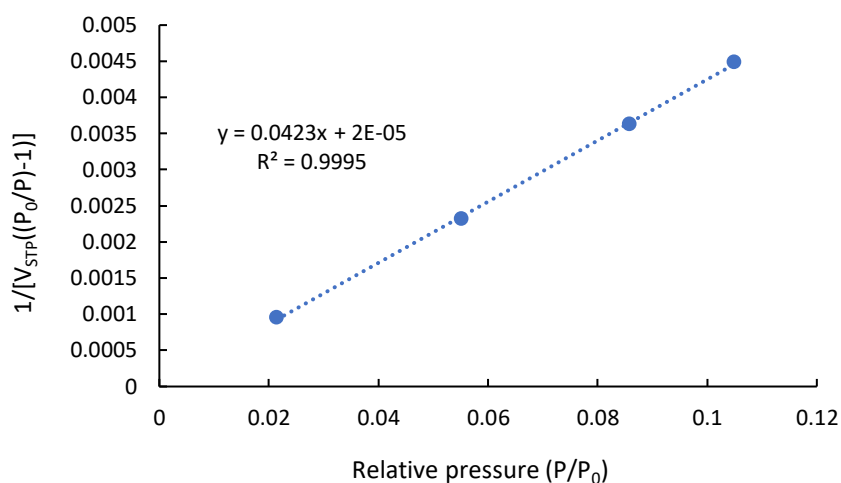


**Figure 58. Multiple point BET plot of Rh@bipyCTF 23 resulting in a specific surface area of 103 m<sup>2</sup>/g.** The obtained coefficient of determination  $R^2 = 0.9995$  and BET constant  $C = 2116$ .

## 8 References

---

1. Sheldon, R. A.; Arends, I. W. C. E.; Hanefeld, U. In *Green Chemistry and Catalysis*; WILEY-VCH, **2007**; pp 1–47.
2. Anastas, P. T.; Williamson, T. C. In *Green Chemistry: Designing Chemistry for the Environment*; American Chemical Society, **1996**; pp 1–17.
3. American Chemical Society. 12 Principles of Green Chemistry <https://www.acs.org/content/acs/en/greenchemistry/principles/12-principles-of-green-chemistry.html> (accessed Sep 7, 2019).
4. Armor, J. N. *Catal. Today* **2011**, *163*, 3–9.
5. De Vries, J. G.; Jackson, S. D. *Catal. Sci. Technol.* **2012**, *2*, 2009–2009.
6. Heveling, J. *J. Chem. Educ.* **2012**, *89*, 1530–1536.
7. Chorkendorff, I.; Niemantsverdriet, J. W. In *Concepts of Modern Catalysis and Kinetics*; WILEY-VCH, **2003**; pp 1–21.
8. Lefferts, L.; Hensen, E.; Niemantsverdriet, H. In *Catalysis: An Integrated Textbook for Students.*; WILEY-VCH, **2018**; pp 15–62.
9. Duan, S.; Wang, R.; Liu, J. *Nanotechnology* **2018**, *29*.
10. Thomas, J. M.; Raja, R.; Lewis, D. W. *Angew. Chemie - Int. Ed.* **2005**, *44*, 6456–6482.
11. Yang, X. F.; Wang, A.; Qiao, B.; Li, J.; Liu, J.; Zhang, T. *Acc. Chem. Res.* **2013**, *46*, 1740–1748.
12. Samantaray, M. K.; D’Elia, V.; Pump, E.; Falivene, L.; Harb, M.; Ould Chikh, S.; Cavallo, L.; Basset, J. M. *Chem. Rev.* **2020**, *120*, 734–813.
13. Liang, J.; Liang, Z.; Zou, R.; Zhao, Y. *Adv. Mater.* **2017**, *29*.
14. Čejka, J.; Corma, A.; Zones, S. In *Zeolites and Catalysis: Synthesis, Reactions and Applications*; WILEY-VCH, **2010**; pp 171–207.
15. Yaghi, O. M.; Richardson, D. A.; Li, G.; Davis, C. E.; Groy, T. L. *Mater. Res. Soc. Symp. - Proc.* **1995**, *371*, 15.
16. Yaghi, O. M.; O’Keeffe, M.; Ockwig, N. W.; Chae, H. K.; Eddaoudi, M.; Kim, J. *Nature* **2003**, *423*, 705–714.
17. Tranchemontagne, D. J.; Mendoza-Cortés, J. L.; O’Keeffe, M.; Yaghi, O. M. *Chem. Soc. Rev.* **2009**, *38*, 1257–1283.
18. Côté, A. P.; Benin, A. I.; Ockwig, N. W.; O’Keeffe, M.; Matzger, A. J.; Yaghi, O. M. *Science (80-. )*. **2005**, *310*, 1166–1170.
19. Diercks, C. S.; Yaghi, O. M. *Science (80-. )*. **2017**, *355*, eaal1585.
20. Lyle, S. J.; Waller, P. J.; Yaghi, O. M. *Trends Chem.* **2019**, *1*, 172–184.
21. Bojdys, M. J.; Jeromenok, J.; Thomas, A.; Antonietti, M. *Adv. Mater.* **2010**, *22*, 2202–2205.
22. Kuhn, P.; Forget, A.; Su, D.; Thomas, A.; Antonietti, M. *J. Am. Chem. Soc.* **2008**, *130*, 13333–13337.
23. Feng, X.; Ding, X.; Jiang, D. *Chem. Soc. Rev.* **2012**, *41*, 6010–6022.
24. Mooibroek, T. J.; Gamez, P. *Inorganica Chim. Acta* **2007**, *360*, 381–404.



25. Liu, M.; Guo, L.; Jin, S.; Tan, B. *J. Mater. Chem. A* **2019**, *7*, 5153–5172.
26. Furukawa, H.; Yaghi, O. M. *J. Am. Chem. Soc.* **2009**, *131*, 8875–8883.
27. Doonan, C. J.; Tranchemontagne, D. J.; Glover, T. G.; Hunt, J. R.; Yaghi, O. M. *Nat. Chem.* **2010**, *2*, 235–238.
28. Alahakoon, S. B.; Thompson, C. M.; Occhialini, G.; Smaldone, R. A. *ChemSusChem* **2017**, *10*, 2116–2129.
29. Hu, H.; Yan, Q.; Ge, R.; Gao, Y. *Chinese J. Catal.* **2018**, *39*, 1167–1179.
30. Das, G.; Biswal, B. P.; Kandambeth, S.; Venkatesh, V.; Kaur, G.; Addicoat, M.; Heine, T.; Verma, S.; Banerjee, R. *Chem. Sci.* **2015**, *6*, 3931–3939.
31. Kaczmarek, A. M.; Liu, Y. Y.; Kaczmarek, M. K.; Liu, H.; Artizzu, F.; Carlos, L. D.; Van Der Voort, P. *Angew. Chemie - Int. Ed.* **2020**, *59*, 1932–1940.
32. El-Kaderi, H. M.; Hunt, J. R.; Mendoza-Cortés, J. L.; Côté, A. P.; Taylor, R. E.; O’Keeffe, M.; Yaghi, O. M. *Science (80-. )*. **2007**, *316*, 268–272.
33. Ding, S. Y.; Wang, W. *Chem. Soc. Rev.* **2013**, *42*, 548–568.
34. Waller, P. J.; Gándara, F.; Yaghi, O. M. *Acc. Chem. Res.* **2015**, *48*, 3053–3063.
35. Pang, Z. F.; Zhou, T. Y.; Liang, R. R.; Qi, Q. Y.; Zhao, X. *Chem. Sci.* **2017**, *8*, 3866–3870.
36. Dalapati, S.; Addicoat, M.; Jin, S.; Sakurai, T.; Gao, J.; Xu, H.; Irle, S.; Seki, S.; Jiang, D. *Nat. Commun.* **2015**, *6*, 7786.
37. Ding, X.; Guo, J.; Feng, X.; Honsho, Y.; Guo, J.; Seki, S.; Maitarad, P.; Saeki, A.; Nagase, S.; Jiang, D. *Angew. Chemie - Int. Ed.* **2011**, *50*, 1289–1293.
38. Rowan, S. J.; Cantrill, S. J.; Cousins, G. R. L.; Sanders, J. K. M.; Stoddart, J. F. *Angew. Chemie Int. Ed.* **2002**, *41*, 898–952.
39. Jin, Y.; Yu, C.; Denman, R. J.; Zhang, W. *Chem. Soc. Rev.* **2013**, *42*, 6634–6654.
40. Kandambeth, S.; Dey, K.; Banerjee, R. *J. Am. Chem. Soc.* **2019**, *141*, 1807–1822.
41. Yaghi, O. M.; Kalmutzki, M. J.; Diercks, C. S. In *Introduction to Reticular Chemistry*; WILEY-VCH, **2019**; pp 197–223.
42. Kuhn, P.; Antonietti, M.; Thomas, A. *Angew. Chemie - Int. Ed.* **2008**, *47*, 3450–3453.
43. Ren, S.; Bojdys, M. J.; Dawson, R.; Laybourn, A.; Khimyak, Y. Z.; Adams, D. J.; Cooper, A. I. *Adv. Mater.* **2012**, *24*, 2357–2361.
44. Wang, K.; Yang, L. M.; Wang, X.; Guo, L.; Cheng, G.; Zhang, C.; Jin, S.; Tan, B.; Cooper, A. *Angew. Chemie - Int. Ed.* **2017**, *56*, 14149–14153.
45. Yu, S. Y.; Mahmood, J.; Noh, H. J.; Seo, J. M.; Jung, S. M.; Shin, S. H.; Im, Y. K.; Jeon, I. Y.; Baek, J. B. *Angew. Chemie - Int. Ed.* **2018**, *57*, 8438–8442.
46. Puthiaraj, P.; Cho, S. M.; Lee, Y. R.; Ahn, W. S. *J. Mater. Chem. A* **2015**, *3*, 6792–6797.
47. Xiang, Z.; Cao, D. *Macromol. Rapid Commun.* **2012**, *33*, 1184–1190.
48. Tahir, N.; Krishnaraj, C.; Leus, K.; Van Der Voort, P. *Polymers (Basel)*. **2019**, *11*, 1326.
49. Kuhn, P.; Thomas, A.; Antonietti, M. *Macromolecules* **2009**, *42*, 319–326.
50. Schwinghammer, K.; Hug, S.; Mesch, M. B.; Senker, J.; Lotsch, B. V. *Energy Environ. Sci.* **2015**, *8*, 3345–3353.
51. Zhang, W.; Li, C.; Yuan, Y. P.; Qiu, L. G.; Xie, A. J.; Shen, Y. H.; Zhu, J. F. *J. Mater. Chem.* **2010**, *20*, 6413–6415.
52. Troschke, E.; Grätz, S.; Borchardt, L.; Haubold, D.; Senkovska, I.; Eychmueller, A.; Kaskel, S. *Microporous Mesoporous Mater.* **2017**, *239*, 190–194.

53. Liu, M.; Huang, Q.; Wang, S.; Li, Z.; Li, B.; Jin, S.; Tan, B. *Angew. Chemie - Int. Ed.* **2018**, *57*, 11968–11972.
54. Rengaraj, A.; Puthiaraj, P.; Haldorai, Y.; Heo, N. S.; Hwang, S. K.; Han, Y. K.; Kwon, S.; Ahn, W. S.; Huh, Y. S. *ACS Appl. Mater. Interfaces* **2016**, *8*, 8947–8955.
55. Chan-Thaw, C. E.; Villa, A.; Katekomol, P.; Su, D.; Thomas, A.; Prati, L. *Nano Lett.* **2010**, *10*, 537–541.
56. Chan-Thaw, C. E.; Villa, A.; Prati, L.; Thomas, A. *Chem. - A Eur. J.* **2011**, *17*, 1052–1057.
57. He, T.; Liu, L.; Wu, G.; Chen, P. *J. Mater. Chem. A* **2015**, *3*, 16235–16241.
58. Wang, Z.; Liu, C.; Huang, Y.; Hu, Y.; Zhang, B. *Chem. Commun.* **2016**, *52*, 2960–2963.
59. Artz, J.; Palkovits, R. *ChemSusChem* **2015**, *8*, 3832–3838.
60. Beine, A. K.; Krüger, A. J. D.; Artz, J.; Weidenthaler, C.; Glotzbach, C.; Hausoul, P. J. C.; Palkovits, R. *Green Chem.* **2018**, *20*, 1316–1322.
61. Pilaski, M.; Artz, J.; Islam, H. U.; Beale, A. M.; Palkovits, R. *Microporous Mesoporous Mater.* **2016**, *227*, 219–227.
62. Park, K.; Gunasekar, G. H.; Prakash, N.; Jung, K. D.; Yoon, S. *ChemSusChem* **2015**, *8*, 3410–3413.
63. Gunasekar, G. H.; Shin, J.; Jung, K. D.; Park, K.; Yoon, S. *ACS Catal.* **2018**, *8*, 4346–4353.
64. Gunasekar, G. H.; Jung, K. D.; Yoon, S. *Inorg. Chem.* **2019**, *58*, 3717–3723.
65. Sudakar, P.; Gunasekar, G. H.; Baek, I. H.; Yoon, S. *Green Chem.* **2016**, *18*, 6456–6461.
66. Rajendiran, S.; Natarajan, P.; Yoon, S. *RSC Adv.* **2017**, *7*, 4635–4638.
67. Tahir, N.; Muniz-Miranda, F.; Everaert, J.; Tack, P.; Heugebaert, T.; Leus, K.; Vincze, L.; Stevens, C. V.; Van Speybroeck, V.; Van Der Voort, P. *J. Catal.* **2019**, *371*, 135–143.
68. Bavykina, A. V.; Mautscke, H. H.; Makkee, M.; Kapteijn, F.; Gascon, J.; Llabrés Xamena, F. X. *CrystEngComm* **2017**, *19*, 4166–4170.
69. Palkovits, R.; Antonietti, M.; Kuhn, P.; Thomas, A.; Schüth, F. *Angew. Chemie - Int. Ed.* **2009**, *48*, 6909–6912.
70. Bavykina, A. V.; Goesten, M. G.; Kapteijn, F.; Makkee, M.; Gascon, J. *ChemSusChem* **2015**, *8*, 809–812.
71. Bavykina, A. V.; Olivos-Suarez, A. I.; Osadchii, D.; Valecha, R.; Franz, R.; Makkee, M.; Kapteijn, F.; Gascon, J. *ACS Appl. Mater. Interfaces* **2017**, *9*, 26060–26065.
72. Bavykina, A. V.; Rozhko, E.; Goesten, M. G.; Wezendonk, T.; Seoane, B.; Kapteijn, F.; Makkee, M.; Gascon, J. *ChemCatChem* **2016**, *8*, 2173–2173.
73. Dang, Q. Q.; Liu, C. Y.; Wang, X. M.; Zhang, X. M. *ACS Appl. Mater. Interfaces* **2018**, *10*, 27972–27978.
74. Park, K.; Lim, S.; Baik, J. H.; Kim, H.; Jung, K. D.; Yoon, S. *Catal. Sci. Technol.* **2018**, *8*, 2894–2900.
75. Rajendiran, S.; Park, K.; Lee, K.; Yoon, S. *Inorg. Chem.* **2017**, *56*, 7270–7277.
76. Gunasekar, G. H.; Park, K.; Ganesan, V.; Lee, K.; Kim, N. K.; Jung, K. D.; Yoon, S. *Chem. Mater.* **2017**, *29*, 6740–6748.
77. Jena, H. S.; Krishnaraj, C.; Wang, G.; Leus, K.; Schmidt, J.; Chaoui, N.; Van Der Voort, P. *Chem. Mater.* **2018**, *30*, 4102–4111.
78. Andersson, P. G.; Munslow, I. J. *Modern Reduction Methods*; WILEY-VCH, **2008**.
79. Johnstone, R. A. W.; Wilby, A. H.; Entwistle, I. D. *Chem. Rev.* **1985**, *85*, 129–170.

80. Wang, C.; Wu, X.; Xiao, J. *Chem. - An Asian J.* **2008**, *3*, 1750–1770.
81. Brieger, G.; Nestrick, T. J. *Chem. Rev.* **1974**, *74*, 567–580.
82. Wang, D.; Astruc, D. *Chem. Rev.* **2015**, *115*, 6621–6686.
83. Gladiali, S.; Alberico, E. *Chem. Soc. Rev.* **2006**, *35*, 226–236.
84. Ikariya, T.; Blacker, A. J. *Acc. Chem. Res.* **2007**, *40*, 1300–1308.
85. Noyori, R.; Hashiguchi, S. *Acc. Chem. Res.* **1997**, *30*, 97–102.
86. Gladiali, S.; Mestroni, G. In *Transition Metals for Organic Synthesis: Building Blocks and Fine Chemicals*; WILEY-VCH, **2008**; pp 97–119.
87. Bäckvall, J. E. *J. Organomet. Chem.* **2002**, *652*, 105–111.
88. Clapham, S. E.; Hadzovic, A.; Morris, R. H. *Coord. Chem. Rev.* **2004**, *248*, 2201–2237.
89. Pàmies, O.; Bäckvall, J. E. *Chem. - A Eur. J.* **2001**, *7*, 5052–5058.
90. Samec, J. S. M.; Bäckvall, J. E.; Andersson, P. G.; Brandt, P. *Chem. Soc. Rev.* **2006**, *35*, 237–248.
91. Hashiguchi, S.; Fujii, A.; Takehara, J.; Ikariya, T.; Noyori, R. *J. Am. Chem. Soc.* **1995**, *117*, 7562–7563.
92. Haack, K. J.; Hashiguchi, S.; Fujii, A.; Ikariya, T.; Noyori, R. *Angew. Chemie (International Ed. English)* **1997**, *36*, 285–288.
93. Vitaku, E.; Smith, D. T.; Njardarson, J. T. *J. Med. Chem.* **2014**, *57*, 10257–10274.
94. Sridharan, V.; Suryavanshi, P. A.; Menéndez, J. C. *Chem. Rev.* **2011**, *111*, 7157–7259.
95. Silva, T. S.; Rodrigues, M. T.; Santos, H.; Zeoly, L. A.; Almeida, W. P.; Barcelos, R. C.; Gomes, R. C.; Fernandes, F. S.; Coelho, F. *Tetrahedron* **2019**, *75*, 2063–2097.
96. Rueping, M.; Tato, F.; Schoepke, F. R. *Chem. - A Eur. J.* **2010**, *16*, 2688–2691.
97. Borrok, M. J.; Kiessling, L. L. *J. Am. Chem. Soc.* **2007**, *129*, 12780–12785.
98. Wei, Z.; Shao, F.; Wang, J. *Chinese J. Catal.* **2019**, *40*, 980–1002.
99. Grasmann, M.; Laurenczy, G. *Energy Environ. Sci.* **2012**, *5*, 8171–8181.
100. Liu, X.; Li, S.; Liu, Y.; Cao, Y. *Cuihua Xuebao/Chinese J. Catal.* **2015**, *36*, 1461–1475.
101. Robertson, A.; Matsumoto, T.; Ogo, S. *Dalt. Trans.* **2011**, *40*, 10304–10310.
102. Ogo, S.; Makihara, N.; Watanabe, Y. *Organometallics* **1999**, *18*, 5470–5474.
103. Ogo, S.; Makihara, N.; Kaneko, Y.; Watanabe, Y. *Organometallics* **2001**, *20*, 4903–4910.
104. Ogo, S.; Abura, T.; Watanabe, Y. *Organometallics* **2002**, *21*, 2964–2969.
105. Romain, C.; Gaillard, S.; Elmkkadem, M. K.; Toupet, L.; Fischmeister, C.; Thomas, C. M.; Renaud, J. L. *Organometallics* **2010**, *29*, 1992–1995.
106. Nieto, I.; Livings, M. S.; Sacci, J. B.; Reuther, L. E.; Zeller, M.; Papish, E. T. *Organometallics* **2011**, *30*, 6339–6342.
107. Zhang, L.; Qiu, R.; Xue, X.; Pan, Y.; Xu, C.; Li, H.; Xu, L. *Adv. Synth. Catal.* **2015**, *357*, 3529–3537.
108. Matsui, K.; Maegawa, Y.; Waki, M.; Inagaki, S.; Yamamoto, Y. *Catal. Sci. Technol.* **2018**, *8*, 534–539.
109. Pitman, C. L.; Finster, O. N. L.; Miller, A. J. M. *Chem. Commun.* **2016**, *52*, 9105–9108.
110. Quintana, L. M. A.; Johnson, S. I.; Corona, S. L.; Villatoro, W.; Iii, W. A. G.; Takase, M. K.; Vandervelde, D. G.; Winkler, J. R.; Gray, H. B.; Blakemore, J. D. *Proc. Natl. Acad. Sci. U. S. A.* **2016**, *113*, 6409–6414.
111. Wu, X.; Wang, C.; Xiao, J. *Chem. Rec.* **2016**, *16*, 2772–2786.

112. Kaes, C.; Katz, A.; Hosseini, M. W. *Chem. Rev.* **2000**, *100*, 3553–3590.
113. Liao, L. Y.; Kong, X. R.; Duan, X. F. *J. Org. Chem.* **2014**, *79*, 777–782.
114. Huang, L.; Ackerman, L. K. G.; Kang, K.; Parsons, A. M.; Weix, D. J. *J. Am. Chem. Soc.* **2019**, *141*, 10978–10983.
115. Sämann, C.; Schade, M. A.; Yamada, S.; Knochel, P. *Angew. Chemie - Int. Ed.* **2013**, *52*, 9495–9499.
116. Phapale, V. B.; Guisán-Ceinos, M.; Buñuel, E.; Cárdenas, D. J. *Chem. - A Eur. J.* **2009**, *15*, 12681–12688.
117. Everson, D. A.; Jones, B. A.; Weix, D. J. *J. Am. Chem. Soc.* **2012**, *134*, 6146–6159.
118. Sengmany, S.; Léonel, E.; Polissaint, F.; Nédélec, J. Y.; Pipelier, M.; Thobie-Gautier, C.; Dubreuil, D. *J. Org. Chem.* **2007**, *72*, 5631–5636.
119. Moore, L. R.; Vicic, D. A. *Chem. - An Asian J.* **2008**, *3*, 1046–1049.
120. Smith, C. R. *Synlett* **2009**, 1522–1523.
121. Arcadi, A.; Cacchi, S.; Marinelli, F.; Morera, E.; Ortar, G. *Tetrahedron* **1990**, *46*, 7151–7164.
122. Thompson, A. L. S.; Kabalka, G. W.; Akula, M. R.; Huffman, J. W. *Synthesis (Stuttg.)* **2005**, *4*, 547–550.
123. Yu, P.; Morandi, B. *Angew. Chemie - Int. Ed.* **2017**, *56*, 15693–15697.
124. Srivastava, R. R.; Zych, A. J.; Jenkins, D. M.; Wang, H. J.; Chen, Z. J.; Fairfax, D. J. *Synth. Commun.* **2007**, *37*, 431–438.
125. Biswas, A.; Karmakar, U.; Pal, A.; Samanta, R. *Chem. - A Eur. J.* **2016**, *22*, 13826–13830.
126. Xie, L. Y.; Duan, Y.; Lu, L. H.; Li, Y. J.; Peng, S.; Wu, C.; Liu, K. J.; Wang, Z.; He, W. M. *ACS Sustain. Chem. Eng.* **2017**, *5*, 10407–10412.
127. Zhao, J.; Li, P.; Xia, C.; Li, F. *RSC Adv.* **2015**, *5*, 32835–32838.
128. Wang, D.; Jia, H.; Wang, W.; Wang, Z. *Tetrahedron Lett.* **2014**, *55*, 7130–7132.
129. Todorov, A. R.; Wirtanen, T.; Helaja, J. *J. Org. Chem.* **2017**, *82*, 13756–13767.
130. Stumpf, T. D. J.; Steinbach, M.; Höltnke, M.; Heuger, G.; Grasemann, F.; Fröhlich, R.; Schindler, S.; Göttlich, R. *European J. Org. Chem.* **2018**, *2018*, 5538–5547.
131. Stephens, D. E.; Lakey-Beitia, J.; Burch, J. E.; Arman, H. D.; Larionov, O. V. *Chem. Commun.* **2016**, *52*, 9945–9948.
132. Wang, H.; Pei, Y.; Bai, J.; Zhang, J.; Wu, Y.; Cui, X. *RSC Adv.* **2014**, *4*, 26244–26246.
133. Evoniuk, C. J.; Gomes, G. D. P.; Hill, S. P.; Fujita, S.; Hanson, K.; Alabugin, I. V. *J. Am. Chem. Soc.* **2017**, *139*, 16210–16221.
134. Ma, W.; Zhang, J.; Xu, C.; Chen, F.; He, Y. M.; Fan, Q. H. *Angew. Chemie - Int. Ed.* **2016**, *55*, 12891–12894.
135. Annesley, T. M. *Clin. Chem.* **2003**, *49*, 1041–1044.
136. Furey, A.; Moriarty, M.; Bane, V.; Kinsella, B.; Lehane, M. *Talanta* **2013**, *115*, 104–122.
137. Wei, C.; He, Y.; Shi, X.; Song, Z. *Coord. Chem. Rev.* **2019**, *385*, 1–19.
138. Quinn, J. R.; Zimmerman, S. C. *J. Org. Chem.* **2005**, *70*, 7459–7467.
139. Abednatanzi, S.; Gohari Derakhshandeh, P.; Tack, P.; Muniz-Miranda, F.; Liu, Y. Y.; Everaert, J.; Meledina, M.; Vanden Bussche, F.; Vincze, L.; Stevens, C. V.; Van Speybroeck, V.; Vrielinck, H.; Callens, F.; Leus, K.; Van Der Voort, P. *Appl. Catal. B Environ.* **2020**, *269*, 118769.

140. Hug, S.; Tauchert, M. E.; Li, S.; Pachmayr, U. E.; Lotsch, B. V. *J. Mater. Chem.* **2012**, *22*, 13956–13964.
141. Himiyama, T.; Waki, M.; Maegawa, Y.; Inagaki, S. *Angew. Chemie - Int. Ed.* **2019**, *58*, 9150–9154.
142. Rahman, M.; Kundu, D.; Hajra, A.; Majee, A. *Tetrahedron Lett.* **2010**, *51*, 2896–2899.
143. Fang, W. Y.; Qin, H. L. *J. Org. Chem.* **2019**, *84*, 5803–5812.
144. Krishnaraj, C.; Jena, H. S.; Leus, K.; Van Der Voort, P. *Green Chem.* **2020**, *22*, 1038–1071.
145. Sigma-Aldrich. Material Safety Data Sheet (MSDS) <https://www.sigmaaldrich.com> (accessed Aug 14, 2020).
146. Veauthier, J. M.; Carlson, C. N.; Collis, G. E.; Kiplinger, J. L.; John, K. D. *Synthesis (Stuttg.)*. **2005**, *16*, 2683–2686.
147. Blakemore, J. D.; Hernandez, E. S.; Sattler, W.; Hunter, B. M.; Henling, L. M.; Brunschwig, B. S.; Gray, H. B. *Polyhedron* **2014**, *84*, 14–18.